Dynamics of surge-type glaciers in Yukon, Canada, revealed by multi-satellite images

（人工衛星画像で捉えたカナダ・ユーコン地域における

サージ型氷河の動態）

Takahiro Abe

Department of Natural History Sciences, Graduate School of Science,

Hokkaido University

Submitted for the degree of Doctor of Philosophy

March 2017

Table of Contents

Chapter 3: Data and methodology

Chapter 4: Winter speed-up of quiescent surge-type glaciers in Yukon, Canada

Chapter 5: Basal condition in winter using numerical glacier hydrology model

Chapter 6: Twelve-year cyclic surging episodes at Donjek Glacier in Yukon, Canada

Chapter 7: Surge dynamics of Steele Glacier in Yukon, Canada, revealed by multi-satellite images

Abstract

Surge-type glaciers repeatedly oscillate between a short active phase characterized by order-of-magnitude speed-up and a long quiescent phase. During the active phase, a significantly large volume of ice is transported downstream, causing surface elevation changes and terminus advance, as well as forming heavily-damaged crevasses and looped moraines. On the other hands, in the quiescent phase, they flow slowly or become stagnant in the downstream area, leading to ice thickening in the reservoir area. The imbalanced flow results in retreat and thinning in the receiving area. Surge-type glaciers are distributed in specific areas, and one of highly concentrated zones is near the border of Alaska and Yukon, Canada. In this area, glacier surge often initiates in winter, but the triggering mechanism remains unclear. An extensive ground-based observation on the 1982-83 Variegated Glacier's surge has brought a fundamental idea of surge generation mechanism. However, there remains a question as to how basal water pressure increase and subsequent speed-up can be maintained without further input of meltwater from the surface. Moreover, it remains uncertain what controls the surge cycle, and generates the pre-condition before surging. To answer these questions, we used multi-satellite images to reveal dynamics of surge-type glaciers in Yukon, Canada. The detailed spatial and temporal changes in ice speed can tell us new insight into behaviors of surge-type glaciers during both quiescent and active phases. Surface elevation change data can show the place where surge initiates and how the surge front propagates downstream. Spatial patterns of looped moraines can reveal how the tributaries affects the trunk before and during surge.

This thesis includes the following four topics; 1) Winter speed-up of quiescent

surge-type glaciers in Yukon, Canada; 2) Basal condition in winter using numerical glacier hydrological model; 3) Twelve-year cyclic surging episodes at Donjek Glacier in Yukon, Canada; 4) Surge dynamics of Steele Glacier in Yukon, Canada, revealed by multi-satellite images. All these results have significant implications for better understanding the dynamics of not only surge-type glaciers but also glaciers and ice sheets in general.

1) Winter speed-up of quiescent surge-type glaciers in Yukon, Canada

Glacier surge often initiates in winter but the reason remains unclear, while melt-induced summer speed-up is well-known and the mechanism has been generally understood. Examining spatial and temporal changes in ice velocity at many surge-type glaciers near the border of Alaska and Yukon, Canada, we found winter speed-up of quiescent surge-type glaciers. Moreover, the fast-flowing region propagated from upstream to downglacier at Anderson Glacier. In the absence of surface meltwater in winter, we suggest the presence of englacial water storage that does not directly connect the surface but can promote basal sliding as water pressure increases by creep closure.

2) Basal condition in winter using numerical glacier hydrology model

Whereas the summer speed-up signal and its hydrological mechanism have been actively discussed in many papers, basal condition in winter has been poorly understood. In chapter 4, we showed the significant acceleration in the upper reaches and the propagation downstream in winter at several quiescent surge-type glaciers in Yukon, Canada. In order to examine the mechanism of the winter acceleration, we used numerical glacier hydrology model. Although we reproduced effective pressure decrease immediately after water input, we could not reproduce any decreases of the effective pressure in winter. Additional water upstream in winter was able to decrease the effective pressure, but the change rate was rapid and not continuous. These results indicate that an alternative interpretation is needed for explaining the winter speed-up.

3) Twelve-year cyclic surging episodes at Donjek Glacier in Yukon, Canada

There are numerous surge-type glaciers in Yukon, but the complete surge cycles had been examined at only a few glaciers. Here we used Landsat-series optical images to examine long-term evolution of Donjek Glacier, at which no recent surges were reported. We found twelve-year cyclic surging episodes in 1989, 2001, and 2013. The changes in the terminal area was consistent with the speed data, and the 1978 event was confirmed. Moreover, the surging area was limited to a place where the valley width significantly narrows. With the data of slope angle at the area, we suggest the valley constriction strongly controls the surge dynamics at Donjek Glacier.

4) Surge dynamics of Steele Glacier in Yukon, Canada, revealed by multi-satellite images

To reveal the surge generation and maintenance mechanisms, we used multi-satellite images to derive ice speed, ice thickness change, spatial patterns of moraine, focusing a recent surge at Steele Glacier in Yukon, Canada. The detailed evolution of ice speed showed that the acceleration initiated in 2011, and that the speed reached the peak greater than 20 m/d, followed by the rapid decrease. The seasonal speed-ups were observed in the active phase. This shows the seasonal surface meltwater reaches the bed, which enhances the basal sliding. The ice thickness change data revealed the location of dynamic balance line (the border between upstream thickening area and downstream thinning area), which is located at the confluence between Steele and Hodgson Glaciers. The present looped moraine indicates that the ice flow on Steele Glacier has been disturbed by that on Hodgson Glacier. The calculated driving stress changes show that the ice thickening and steepening at the confluence increased the driving stress in the quiescent phase. However, the driving stress itself is insufficient to cause the acceleration. We speculate that the increase of creep closure due to the ice thickening in the quiescent phase generates high basal water pressure, which reduces the yield stress and the till deforms at a critical value. After the surge initiation, the affected area is gradually expanding downstream as the speed increases. The ice transport from upstream generated the high driving stress in the middle part in 2015, and in the downstream part in 2016. The relatively high stress may assist to maintain the distributed hydrological system at the base and the seasonal water input from the surface can keep higher speed during the active phase. The rapid decrease after the peak speed in 2015, in spite of the relatively high driving stress in 2015-16, can be explained by the water discharge from the margin of Steele Glacier, which filled Hazard Lake in 2016. Surging glaciers are classified into Alaskan and Svalbard types, which imply the surging characteristics may arise from the differences of thermal structure, size of glacier.

Acknowledgement

This dissertation concludes five years of my study in Graduate School of Science, Hokkaido University. I would thank all people that helped and encouraged me in my graduate course.

First and foremost, I would like to express my sincere gratitude to my supervisor, Prof. Masato Furuya, for everything that he gave me valuable advices during my doctoral course. He gave me a lot of opportunities to participate many academic conferences, which have encouraged my curiosity for Earth science. His warm, patient, and valuable guidance enabled me to grow up as a scientist. Additionally, I also would like to thank Prof. Kosuke Heki, Dr. Shin Sugiyama, and Dr. Youichiro Takada for their constructive comments as the members of the doctoral degree supervisory committee. Dr. Shin Sugiyama often gave me valuable advice about my study as a professional glaciologist, which encouraged me and progress my study. I would like to appreciate Dr. Daiki Sakakibara at Arctic Research Center in Hokkaido University for the collaboration of the study in Chapter 6 and 7.

I also would like to appreciate Prof. Martin Funk at the glacier group in the Laboratory of Hydraulic, Hydrology and Glaciology, Swiss Federal Institute of Technology in Zurich, Switzerland. I stayed there between October 2015 and March 2016, and received his advice. He gave me a warm welcome and every support for my stay in Zurich. Dr. Mauro Werder taught me the fundamental of glacier hydrology and how to run GlaDS glacier hydrological model. His advices and collaboration for my research in Chapter 5 are extremely valuable. The members in the glacier group always helped me for my daily life, language, and study in Zurich. I had a priceless experience in Switzerland during Christmas season in 2015.

I appreciate Emeritus Prof. Junji Koyama, Prof. Kiyoshi Yomogida, Dr. Kei Katsumata, and Dr. Kazunori Yoshizawa for their constructive comments in Solid Seminar. Finally, I express my gratitude to my family and colleagues. I would like to thank JSPS fellowship (15J01952) and KEKENHI (24651001) for a grant that allowed me to complete this study. During my stay in Switzerland, I was supported by Japanese-Swiss Science and Technology Program: Young Researcher Exchange Program between Japan and Switzerland 2015. I really appreciate JSPS and ETH-Zurich.

The ALOS/PALSAR L1.0 and ALOS-2/PALSAR-2 L1.1 data were partially shared among the PALSAR Interferometry Consortium to Study our Evolving Land surface (PIXEL) under a cooperative research contract between the Earthquake Research Institute, the university of Tokyo, and JAXA. They were also provided by the contract under the ALOS-PI4 (No. 538) and ALOS-2-PI6 (No. 3021). The ownership of ALOS/PALSAR belongs to JAXA and the Ministry of Economy, Trade and Industry (METI). The ownership of ALOS-2/PALSAR-2 belongs to JAXA. Landsat optical images are downloaded from the USGS HP. Sentinel-1A data were downloaded from ESA Scientific Data Hub site. Glacier outlines were downloaded from the Randolph Glacier Inventory version 4.0 http://www.glims.org/RGI/rgi40_dl.html. ASTER DEMs were downloaded from MADAS.

Chapter 1

General introduction

1.1 What is Glacier Surge?

Glacier surge is a quasi-cyclic event with orders-of-magnitude speed-up during a shorter active phase, accompanying terminus advance, followed by a much longer quiescent phase (Meier and Post 1969; Raymond, 1987; Harrison and Post, 2003). The ice near terminus gradually thins and retreats during the long quiescent phase, whereas it thickens in upstream. Meanwhile, the glacier suddenly accelerates in the active phase, causing the ice thickening downstream and the terminus advance (Fig. 1-1). These phases repeat every several decades.

The magnitude of the ice speed is a few to a few hundred times faster than quiescent phase. There is no strict definition of surge, and the diversity of spectrum of speed-up behaviors. For example, Herreid and Truffer (2016) developed a new method that automatically detects glaciers with flow instabilities, and succeeded in detecting various speed-up episodes in Alaska Range. The behaviors also have differences depending on the area, thus the physical mechanisms of the surge generation have been thought to be different. The details are described in the later section.

Some characteristic features are often observed on surge-type glaciers in the active phase. First, it is extraordinary speed-up mentioned above, which often causes km-scale terminus advance. Second, it is heavily crevasses. Due to the sudden speed-up, the shear stress near the glacier side margins become larger, which makes crevasses open. Moreover, rapid looped-moraine movement can be observed on the glacier. The looped moraines themselves are taken as an evidence of the past surge. Reminding that surge is a cyclic event, the spatial patterns of the moraines can tell us where and how a sudden speed-up occurs.

A surge-type glacier in the quiescent phase needs much caution because those features are also observed at non-surge-type glaciers. Thereby, we have to distinguish surge-type glaciers from non-surge-type glaciers with multiple criteria (e.g., Copland et al., 2003, Yasuda and Furuya, 2015). In particular, in regards to some glaciers that have been slightly advancing due to mass gain, it is difficult to recognize it as surge or not. This condition applies to high concentration zone of surge-type glaciers such as Karakorum (Paul, 2015).

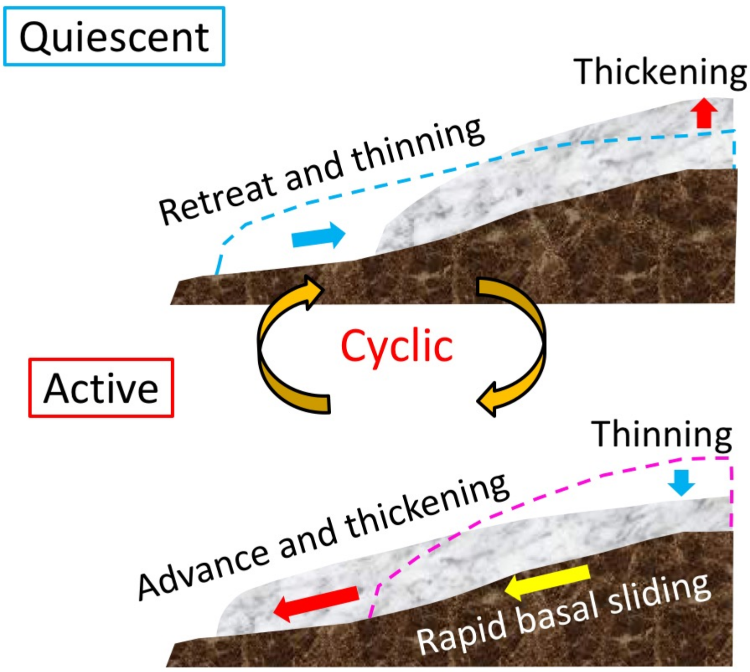

Figure 1-1: Schematic diagrams showing the quiescent and active phases of glacier surge

1.2 St. Elias Mountains –Near the border between Alaska and Yukon, Canada-

Surge-type glaciers are distributed in specific areas such as Alaska-Yukon, Svalbard, Iceland, Karakorum (Post, 1969; Sevestre and Benn, 2015, Fig. 1-2), and the number of them is about 1 % of all glaciers in the world (Jiskoot et al., 1998). However, we should note that the there are various sizes of glaciers, and that indicates that the longer glaciers are less. Indeed, Machguth and Huss (2014) reported that glaciers longer than 10 km are only 1.5 % of ~200,000 glaciers in the world, and the number of those longer than 40 km are less than 250. In Alaska-Yukon area, there are much longer glaciers than other regions (Machguth and Huss, 2014). Therefore, surge-type glaciers are significant in terms of ice volume. Moreover, Clarke et al. (1986) performed statistical analysis of surge-type glaciers, and found that surge-type glaciers are likely to be longer than normal glaciers.

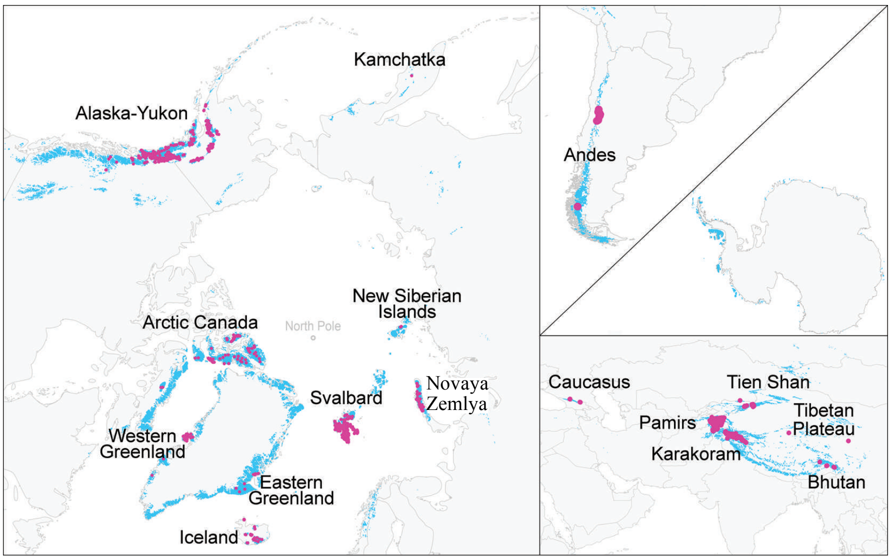

Figure 1-2: Distribution of surge-type glaciers in the world (modified from Sevestre and Benn, 2015). The blue colors represent normal glaciers, and the pink dots are surge-type glaciers.

One of highly concentrated zones is near the border of Alaska and Yukon, Canada (Fig. 1-3). There are numerous glaciers in this region, and ice-covered area is 45905 km^2 (including Wrangell Mountains, Bertheir et al., 2010). Recent satellite gravimetry and airborne altimetry have revealed the total mass loss rate (Luthcke et al., 2013; Larsen et al., 2015) and the contribution to global sea level rise from Alaskan Glaciers is 0.026 ± 0.007 m, which is one of the largest contributors as well as Arctic Canada and Antarctica excluding ice sheets (Radić and Hock, 2011). Ice loss of glaciers is caused mainly by two processes; surface mass balance and ice discharge. The former is the balance of surface melting and accumulation. The latter is the ice mass dissipated by calving to ocean/lake. Recent studies have reported that the effect from calving is relatively large. Many outlet glaciers in Greenland have been accelerating (e.g., Joughin et al., 2004; Moon et al., 2012), which has caused dynamic thinning (e.g., Pritchard et al., 2009). Dynamic thinning is thinning of ice thickness caused by a longitudinally stretching flow regime due to flow acceleration, and also takes place during glacier surge. Thinning due to this effect should be distinguished from that due to surface melting. In Greenland, the rate of ice loss estimated from various observation and simulation data show that the dynamic thinning accounts for one third to roughly half of total ice loss (van den Broeke et al., 2009; Endelin et al., 2014). Thus, it is important to examine spatial and temporal change in ice speed in order to understand the dynamics and to estimate appropriately future states of glaciers and ice sheets in the world.

Post (1969) described the first distribution map of surge-type glaciers in Alaska-Yukon, mainly from aerial photogrammetry. He identified 204 glaciers as surge-type in this area, and the behaviors have received much scientific attention (Meier and Post, 1969), but there are many questions about the dynamics due to the lack of quantitative observation data. In general, surge-type glaciers locate in remote and harsh environment, and it is hard to perform in-situ and continuous observations. In the next section, I introduce the history of observations on surge-type glaciers and describe some unsolved problems in the surge mechanism.

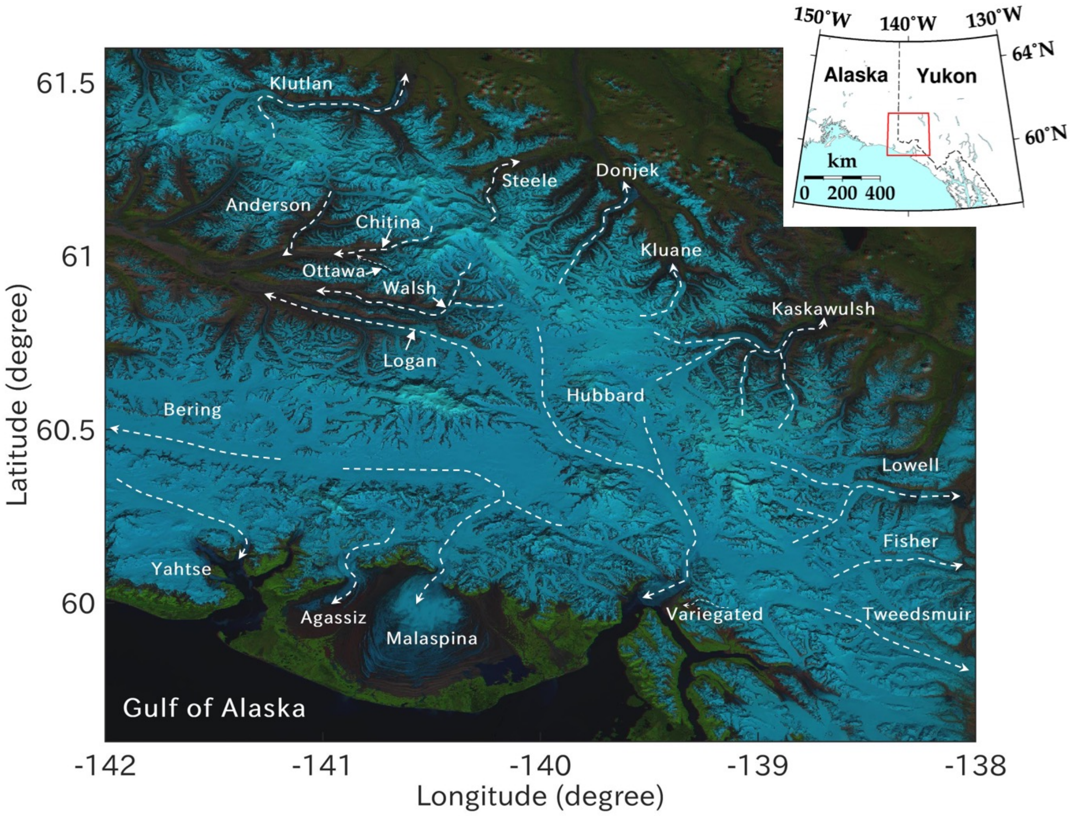

Figure 1-3 Distribution of major mountain glaciers in Alaska-Yukon, and their names. The white line and arrows show the directions of main flows. Back ground is false color composite images acquired by Landsat 8 on 15 May 2015, 9 and 17 June 2016.

1.3 Observations of surge-type glaciers in Yukon and unsolved problems on the surge mechanism

Among many surge-type glaciers in Yukon, the surge history of Variegated glacier has been well-documented. Variegated Glacier is located in southeast Alaska (Fig.1-3), and extensive field observations were performed prior to and during the 1982-1983 surge. This is because the relatively constant surge cycle has been known (Post, 1969). The various observed data showed that surge was induced by rapid basal sliding, not by ice deformation, and basal water pressure reached up to ice overburden pressure in the active phase. Based on these data, fundamental theory of surge generation mechanism has been proposed (Kamb et al., 1985; Kamb, 1987; Raymond, 1987). In-situ observations have also been extensively performed on Trapridge Glacier, and Black Rapid Glacier (e.g., Clarke et al., 1984; Truffer et al., 2000).

To date, three review papers on glacier surge have been published (Meier and Post, 1969; Raymond, 1987; Harrison and Post, 2003). These papers have brought us to know previous studies of glacier surge, and problems on surge generation/maintenance mechanisms. Meier and Post (1969) first suggested the problems of glacier surge, and Raymond (1987) summarized the latest knowledge at that time and the problems on surge generation mechanisms based on the observations of Variegated Glacier's surge on 1982-1983. The observation activities were so vigorous, and collected various data. However, the surge occurs every several decades and surge-type glaciers are located in remote area. Thus, there are insufficient numbers of observation data associated with surge.

Because glacier surge has been considered as a result of high basal water pressure, ice flow is closely related to glacial hydrology. Thus, we should understand how water flows through glaciers, and how it affects ice speed. Generally, ice speed consists of ice deformation, and basal sliding (Cuffey and Paterson, 2010). Here, till deformation is included in basal sliding. Seasonal changes in ice speed have been well-known, and many observations have been reported (Iken and Bindshadler, 1986; Zwally et al., 2002). This mechanism is considered as follows; when surface melting occurs, the meltwater goes into ice and reaches the bed. It develops linked-cavity system (Kamb, 1987). This system can establish a slow drainage, and raise basal water pressure as water input increase. Thus, glacier can accelerate in a short term, which is called summer speed-up. However, an excess of meltwater input can develop efficient drainage system, R-channel (Röthlisberger, 1972). In this system, the decrease of basal water pressure can occur as the increase of water input, due to the balance between wall melting and creep closure. This can cause late-summer slow-down of ice speed. However, the relation between meltwater variability and ice speed has been poorly understood because it is hard to observe directly the bottom of glacier. In order to examine how meltwater can develop drainage system and affect ice speed more realistically, numerical glacier hydrological model has been recently developed in two dimensions (Schoof, 2010; Hewitt, 2013; Werder et al., 2013). The detail of glacier hydrological model is described in Chapter 5.

On the contrary to summer speed-up, glacier surge often initiates in winter (Raymond, 1987; Harrison and Post, 2003). This seems that snow accumulation is responsible for it. However, the contribution of seasonal snow accumulation to ice speed is very little, thus we do not know the exact reason of winter initiation. Based on the idea by Kamb et al. (1985), an efficient channel-like drainage system developed in summer is destructed by creep closure toward winter, subsequently changing an inefficient linked-cavity drainage system, which can cause high basal water pressure and lead to initiate surge. However, there remain some questions about this theory. Because surge do not occur every winter, it remains unclear what triggers surge every several decades. Moreover, what is the source of how to supply such an amount of water at base during winter? While summer speed-up can be clearly driven by surface meltwater input, the origin of water to enhance basal sliding in winter remains unclear. To answer this questions, we need to measure ice speed evolution prior to and during surge.

Recent advances of remote sensing technique have enabled us to derive spatial and temporal ice speed variations of surge-type glaciers without ground observations, which gave us new insight to surge dynamics. In particular, satellite-based Synthetic Aperture Radar has brought us much more scientific data to better understand glacier dynamics including non-surge-type glaciers (e.g., Joughin et al., 2010; Abe and Furuya, 2016). The detail of SAR systems and the application history to glacier dynamics are described in Chapter 2. Fatland and Lingle (1998) examined velocity changes in ice speed of Bering Glacier's surge in 1993-1995, using ERS-1 ice-mode data, and they found bull's eye-like signals with a diameter of a few kilometers. They interpreted them as local vertical movements of a few to tens centimeters following the meltwater movement from the inside to the base because. Based on these observations, Lingle and Fatland (2003) proposed englacial water storage hypothesis. They suggest that a transfer of englacial water to the bed might be the initial trigger of temperate glacier surges. Although this idea can be applied to both surge-type and non-surge type glaciers, the hypothesis is important for many discussions about surge mechanisms in this thesis. Thus, the studies of dynamics of surge-type glaciers using SAR data has many contributions on revealing surge generation mechanisms, in terms of detecting the 2D velocity fields.

There are also many surge-type glaciers in Svalbard. Monacobreen, one of major surge-type glaciers in Svalbard, showed glacier surge in 1990s. ERS-1, and -2, C-band SAR satellite operated by European Satellite Agency, observed spatial and temporal changes in ice speed due to the surge (Luckman et al., 2002; Murray et al., 2003). They showed that the acceleration and deceleration was much smaller than that of Variegated Glacier's surge, and the phase was much longer than Alaskan type surge. Murray et al. (2003) categorized glacier surge mechanisms into two groups based on these behaviors. One is Alaskan temperate-type; a hydrological transition from efficient tunnel-like drainage to inefficient linked-cavity drainage with a corresponding increase in water pressure (Kamb et al., 1985; Harrison and Post, 2003). The other is Svalbard polythermal-type; thermal regulation that pressure-melting at the base and keeping subglacial water by ice flow and friction (Fowler et al., 2001; Murray et al., 2003). However, a recent study has shown seasonal modulation of faster speed in winter during the active phase at West Kunlun Shan in Northern Tibet (Yasuda and Furuya, 2015). They suggest the importance of englacially stored water from surface melting in Svalbard-type surge. Thus, the generation and maintenance mechanism of glacier surge has not been fully understood.

To understand surge mechanism is indispensable to find out subglacial hydrology and its relation to ice flow. Although it is very hard to observe interior of a glacier directly, glacier surface velocity is affected by the hydrological change. This understanding contributes to the understanding of multi time-scale ice dynamics. Second, it is necessary to reveal surge dynamics in order to assess the responses of glaciers to recent climate change. Although the behavior of surge-type glaciers is very complex, it has been considered as a result from internal regulation. Thereby, the onset of active phase is not related to summer temperature and occurs at different times from glacier to glacier (Meier and Post, 1969). However, recent global warming has some impacts on surge-type glaciers, which may induce, for example, reduction in the period of surge-cycle. Indeed, Lowell Glacier, in Yukon, has experienced five surges during the last 50 years, and the surge interval has decreased (Bevington and Copland, 2014). This has been caused by strongly negative surface mass balance since 1970s. To date, the influence of climate change on surge-type glaciers has been poorly understood (e.g., Harrison and Post, 2003; Frappé and Clarke, 2007). The interval of surge cycle may be partly regulated by climatic factors such as temperature and precipitation. Moreover, it is very difficult for us to distinguish normal-glaciers' retreat under the condition of global warming from surge-type glaciers' retreat during their quiescent phases. To distinguish those behaviors, we need to better understand the dynamics of surge-type glaciers.

Glaciers are abundant in the world's high elevation and polar areas, and they are sensitive to changing climatic conditions. However, the responses of glaciers to climatic change is very complex, and thus we have to know the dynamics. In order to understand the dynamics of surge-type glaciers, we have to collect various data by examining much more cases of surging episodes. This can lead to precise estimation of future state of glaciers.

1.4 Objective and outline of this study

In this thesis, we examined dynamics of surge-type glaciers in Yukon, Canada, using multi-satellite images. The primary objectives of this study are 1) to reveal the spatial and temporal changes in ice speed in Yukon, and 2) to discuss surge generation and maintenance mechanism, comparing with previous theory. This study has significant contribution to better understanding of glacier dynamics including normal glaciers and ice sheets. Chapter 2 refers to synthetic aperture radar system and its history of the application to glacier dynamics. Chapter 3 introduces general information about satellite data, and fundamental methodology I used in this study. Chapter 4, 5, 6, and 7 describes the main studies of my doctoral thesis. Chapter 8 presents the conclusion of this thesis. They are summarized as follows.

Chapter 4: We derived spatial and temporal velocity changes of quiescent surge-type glaciers. We analyzed ALOS/PALSAR images between 2006 and 2011 to derive seasonal changes in ice speed, in particular winter season. This is the first study for revealing the detailed seasonal evolutions of ice speed at surge-type glaciers in the region. The detailed velocity changes data show that some surge-type glaciers in their quiescent phases speed-up from fall to winter in upstream regions, whereas they speed-up during summer in downstream portions. We discuss the mechanism of the winter speed-up based on englacial water storage hypothesis proposed by Lingle and Fatland (2003).

Chapter 5: We explored basal condition of the surge-type glaciers in winter using numerical glacier hydrology model in order to examine the winter speed-up in the quiescent phase that we found in Chapter 4. It is clear that present models are developed to explain summer speed-up, and we cannot reproduce any winter acceleration signals in Chapter 4 by only changing parameters. This indicates that a new theory needs to integrate for reproducing the winter speed-up.

Chapter 6: We found twelve-year cyclic surging episodes at Donjek Glacier by Landsat-series optical images. There were no previous reports about the short-term and constant interval surge cycle in this area. I derived spatial and temporal velocity changes from 1986 to 2016, and terminus area changes from 1973 to 2016. We discuss the relation between the constant surge cycle and the role of valley constriction in the surge.

Chapter 7: We examined a recent surge at Steele Glacier using multi-satellite images to reveal the temporal evolution of ice speed, ice thickness, and looped moraines. We captured the high temporal velocity evolutions due to the surging. Based on the ice speed and ice thickness changes data, we discuss the surge initiation and the maintenance mechanism.

Chapter 8: We conclude this study comprehensively, and propose future works.

Chapter 2

Synthetic Aperture Radar system and its application to glacier observations

2.1 Synthetic Aperture Radar system

Synthetic Aperture Radar (SAR) obtains surface information in terms of phase and intensity. The phase data include information about distance between satellite and ground, and the intensity data include backscatter strength. SAR can acquire data regardless of weather and time because it uses microwaves. The high spatial resolution has been achieved by pulse compression and synthetic aperture technique (Fig. 2-1). In real aperture radar, the resolution of beam transmitting direction (range) and satellite direction (azimuth) depends on pulse width and the antenna size, respectively. In this case, very powerful electricity that can generate such a wide pulse, and huge antenna are needed to distinguish targets with order of tens meter. This is unrealistic to mount and operate on a satellite. In synthetic aperture radar, the spatial resolutions of range (R_r) and azimuth (R_a) direction are determined in the following equations.

$$R_r = \frac{c}{2B_R}$$

$$R_a = \frac{D_A}{2}$$

Where c is the speed of light, B_R is the frequency bandwidth of the microwave pulse and D_A is the size of antenna. These equations mean that the resolutions are only dependent on the bandwidth for range, and the antenna size for azimuth, which are notable features in SAR system. In the case of recent Japanese SAR satellite ALOS-2/PALSAR-2 (D_A = 10 m, B_R = 84 MHz in the strip map mode SM1), range and azimuth resolution can theoretically reach up to 1.8 × 5.0 m. Thus, SAR obtains surface information with high spatial resolution, and we can obtain the data over the entire region. Because of this reason, many researchers use SAR images for various purposes such as crustal deformation due to earthquakes and volcanic eruptions, landslides, glaciers and ice sheet dynamics (e.g., Abe, 2013)

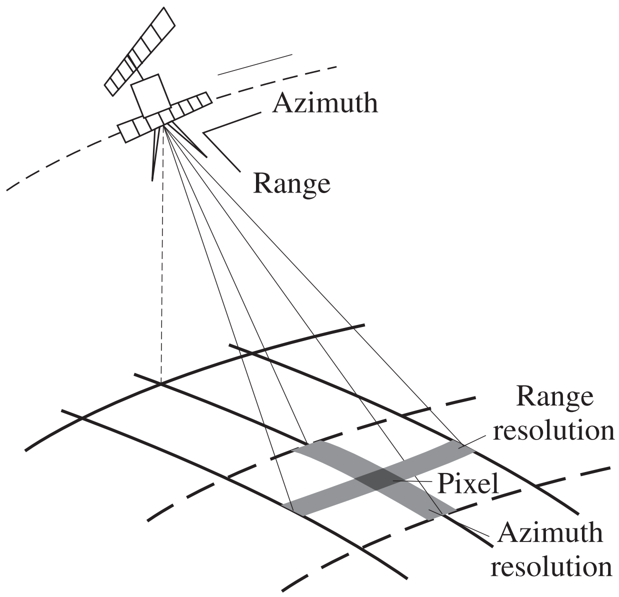

Figure 2-1: Basic principle of SAR (Seeber, 2003).

However, there are some disadvantages of satellite SAR. First, it is temporal resolution. Comparing GNSS F3 solution with an interval of ~1 day, SAR can get surface information every a few days to tens of days. This depends on revisit days of SAR satellite, and sometimes on the observation scenario. This problem is strongly concerned about coherence between two images. Thereby, the temporal interval of the two images is better to be shortened. Second, SAR sensor transmits a pulse diagonally downward (i.e. side looking), which sometimes cause geometric effect (Fig. 2-2). They are composed of three effects. The first is layover. It occurs when the radar beam reaches the top of a tall feature like mountains (B) before it reaches the base (A). The return signal from the top of the feature will be received before the signal from the bottom. As a result, the top of the feature is displaced towards the radar from its true position on the ground, and lays over the base of the feature (B to A) on the SAR image. The second is foreshortening. It occurs when the radar beam reaches the base of a tall feature tilted towards the radar before it reaches the top. Because the radar measures distance in slant-range, the slope (from point D to point E) will appear compressed and the length of the slope will be represented incorrectly (D to E) on the SAR image plane. The third is shadow effect. This effect increases with greater incident angle, just as our shadows lengthen as the sun sets (a dotted-line in Fig. 2-2).

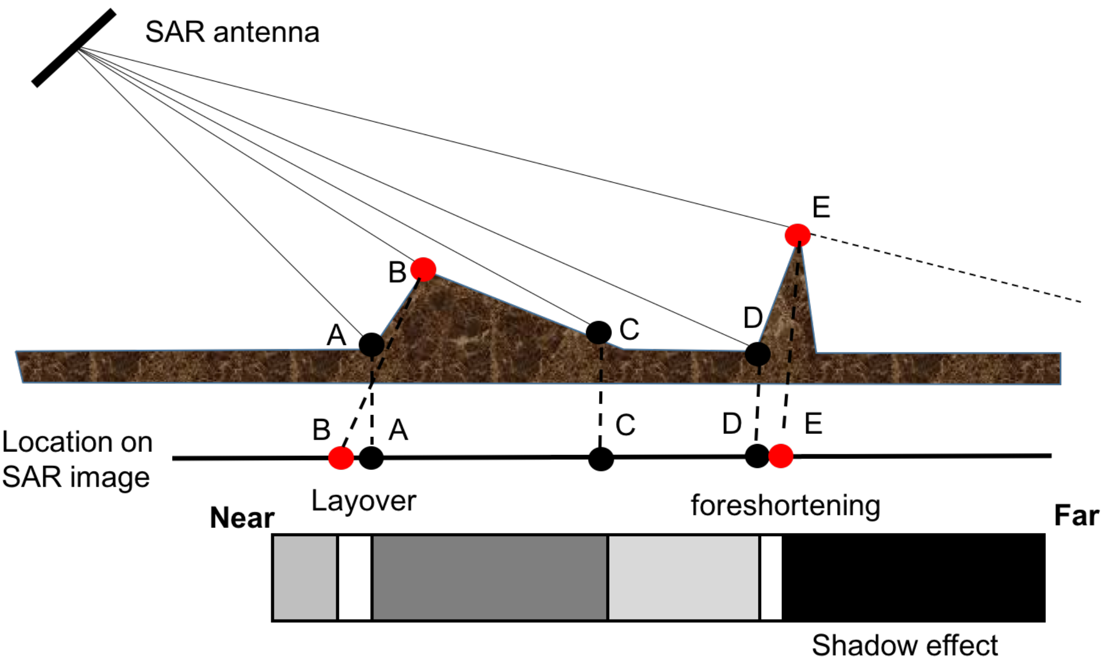

Figure 2-2: Schematic image of foreshortening, layover, and shadow effect. Modified from Ouchi (2009).

Moreover, SAR is often affected by conditions of troposphere, and ionosphere. These are shown as a phase propagation delay on SAR image. The tropospheric delay is due to water vapor, which is highly variable in space and time. Thus, we cannot easily separate it from other signals such as real surface deformation, and errors from orbit uncertainty and DEM. In ionospheric zone, microwave can be phase-delayed due to density of electron. The tendency of affecting ionospheric noise depends on the length of microwave. For this reason, Japan SAR satellites are in particular likely to be affected because they use longer microwave length. In GNSS, the effect can be ignored because of two distinct frequency microwaves. However, SAR systems only use one frequency microwave so that we cannot remove it easily. Although many studies have been undergoing to remove the ionospheric effect (e.g., Kobayashi et al., 2009; Gomba et al., 2016), there has been no revolutionary solution to date. This is one of unsolved problems about SAR-based studies, especially for research subject to small displacement with a few centimeters. In other words, we can know tropospheric and ionospheric condition over the entire area because SAR images include such information with high spatial resolution (e.g. Kinoshita et al., 2013).

2.2 SAR application to glacier observations

In 1993, two papers about SAR-based study were published. One of them is Massonnet et al. (1993), which revealed crustal deformation due to the 1993 Landers earthquake in California, USA. The other is Goldstein et al. (1993), which revealed the ice velocity field of Ruth ice steam on Antarctica. Both papers have demonstrated that SAR could detect detail surface displacement without any equipment on ground. Since 1993, especially in these twenty years, SAR-based studies about glacier dynamics have been rapidly developed (Joughin et al., 2010). In 1990s, Interferometric SAR (InSAR) has been widely used to detect ice speed. InSAR is a technique to derive ground displacement or digital elevation model from a pair of SAR phase data. Using InSAR, we can measure surface deformation with the precision of a few centimeters. Many studies about ice flow detection using SAR interferometry had been reported in the 1990s (e.g., Rignot et al., 1995; Joughin et al., 1999). Japanese SAR satellite, JERS-1 data interferometry were also used to detect to surface movement on Antarctic ice sheet (Ozawa et al., 2000).

However, only relatively large glaciers had been studied because of low spatial resolution of satellite images and lack of global DEM in those days. Moreover, InSAR is not adequate to detect meter-order displacement because of difficulty in unwrapping process especially for fast-moving glaciers such as ice streams in Antarctica. Instead of InSAR, pixel offset technique was introduced to detect surface velocity in the latter half of the 1990s (Gray et al., 1998). Pixel offset (or feature tracking) is a robust algorithm to regard localized offsets after co-registration between two images as surface displacement with the precision on the order of tens centimeters. The advantage of this technique is to use intensity data, not to use phase data, which means it can detect meter-order displacements without unwrapping. Although the spatial resolution of analyzed results is less than that of InSAR, we can obtain two components; range and azimuth offset fields. This technique has been widely used for detecting ice speed using SAR data acquired by satellite whose revisit days are relatively long (Joughin et al., 2010).

Since 2000s, both image quality and analysis method have been improved, and different institutions have launched many SAR satellites with different bands. In 2006, Japanese SAR Satellite, Advanced Land Observing Satellite (ALOS) was launched. Phased Array type L-band Synthetic Aperture Radar (PALSAR) onboard ALOS has advantage for detecting ice flow because longer microwave like L-band can penetrate into ice (Rignot et al., 2001) and temporal decorrelation caused by surface melting is small. Thus, we can derive ice velocity fields using image-pair whose temporal separation is tens of days. Using high-quality ALOS/PALSAR data, not only the entire velocity map of Antarctic (Rignot et al., 2011) and Greenland (Rignot and Mouginot, 2012) has been developed (Fig. 2-3), but also spatial and temporal changes in ice velocity has been examined in mountain glaciers such as Alaska-Yukon (Burgess et al., 2013a; Abe and Furuya, 2015), Karakorum (Quincey et al., 2011), Patagonia (Muto and Furuya, 2013; Mouginot and Rignot, 2015), Northwest Tibet (Yasuda and Furuya, 2013).

In 2014, two new SAR satellite ALOS-2 and Sentinel-1A have started to be operated. These satellites have more sophisticated sensors, and some applications have been reported (e.g. Kobayashi et al., 2015; Nagler et al., 2015). In terms of next SAR satellites, Tandem-L/ALOS-NEXT project operated by Germany and Japan, and NISAR project operated by United States and India have been undergoing to aim launch in 2020 (e.g., Moreira et al., 2015). Glacier monitoring from SAR satellite will become more active.

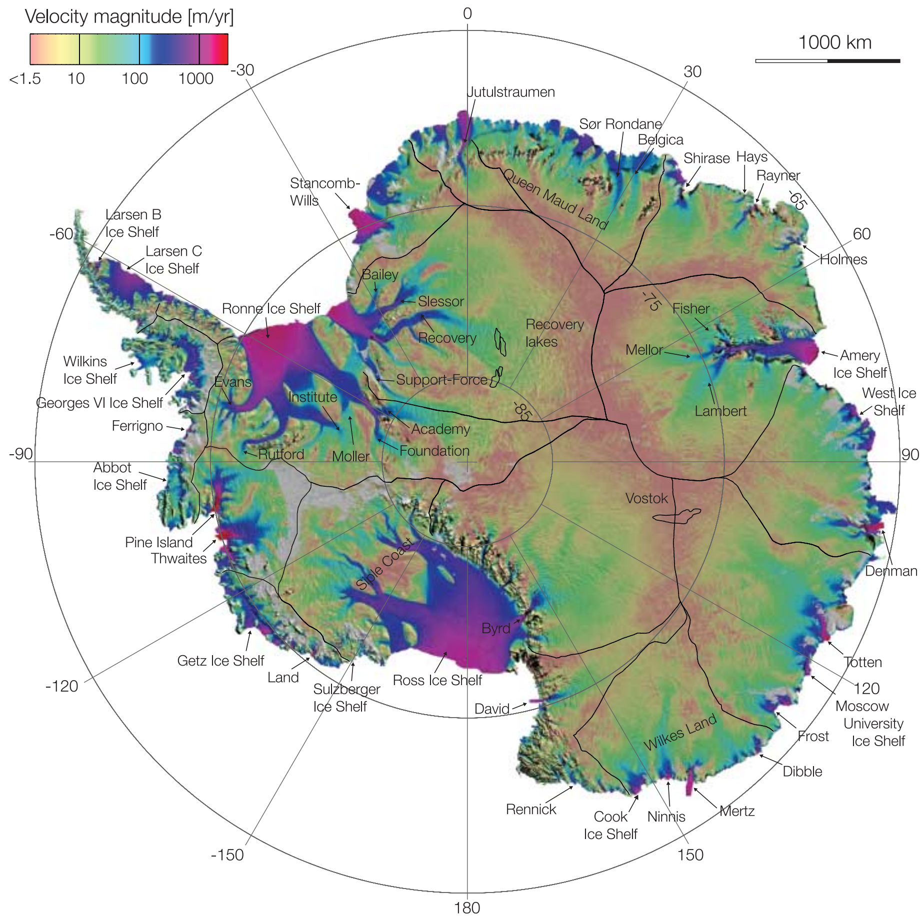

Figure 2-3: Velocity map over entire Antarctic Ice sheet (Rignot et al., 2011).

Chapter 3

Data and methodology

3.1 Satellite images

3.1.1 SAR data and image processing

In this study, we used ALOS/PALSAR level 1.0 raw data to derive surface displacement on glaciers using Gamma software (Wegmüller and Werner, 1997). First, we generated Single Look Complex image (SLC) from raw data. Each pixel in the image has phase and intensity data with a complex structure. Then, we processed high co-registration of two SLC data using affine transformation and ASTER GDEM version 2. This procedure is much more significant to derive precise displacement in performing offset tracking technique in 3.2.1. We confirmed there was no entire mis-registration on each pair before performing offset tracking below.

3.1.2 Landsat optical images

Landsat is a long-term series satellite operated by the United States Geological Survey (USGS). The first satellite Landsat-1 was launched in 1972, and the following satellites (Landsat-2, -3, -4, and -6) had been operated. Nowadays, the two satellites (Landsat-7 and -8) are under operation to observe earth system. The latest satellite Landsat-8 has a new sensor, Operational Land imager (OLI). Owing to this sensor, glacier velocity monitoring from space has been getting more active (Rosenau et al. 2015; Fahnestock et al., 2016). Here we used Landsat images band 8 images (spatial resolution is 15 m for Landsat 7 and 8) and band 4 (spatial resolution is 30 m for Landsat 4 and 5) acquired from 1973 to 2016 in order to study long-term evolution of Donjek Glacier in Chapter 6, and from 2007 to 2016 for Steele Glacier in Chapter 7.

3.1.3 Terra/ASTER images

Terra is a multi-national scientific satellite equipped with multi high-performance sensors. It was launched in 1999, and has been under operation. One of the sensors onboard is ASTER (Advanced Spaceborne Thermal Emission and Reflection Radiometer), developed by Ministry of Economy, Trade and Industry (MEXI) and National Aeronautics and Space Administration (NASA). It has an along-track stereoscopic capability using its near infrared spectral band and its nadir-viewing and backward-viewing telescopes to acquire stereo image data. The spatial resolution is 15 m in the horizontal plane.

On June 1, 2016, the National Institute of Advanced Industrial Science and Technology (AIST) has released new ASTER product, ASTER-VA, adding digital elevation data in order to promote the utilization of the Terra data. ASTER-VA is a free product and we can download the ASTER image from MADAS (METI AIST Data Archive System). We selected and downloaded the data which were not affected by cloud cover.

3.2 Data processing

3.2.1 Offset tracking technique using SAR data

In deriving surface velocity field in Yukon, Canada, we applied offset tracking technique to precisely co-registrated two SLC images (Strozzi et al., 2002). Offset tracking (or Feature tracking) is well-established technique to detect large displacements, and has been widely used in glaciology (e.g., Joughin et al., 2010). We divided one single-look complex (SLC) image into a number of patches (window) and derived their offsets from the corresponding patches in the other SLC image with a subpixel-level precision. These offsets were calculated by cross-correlating backscatter intensity samples from a master image (the older image) with those from a slave image (the newer image). The accuracy of the pixel-offset technique is on the order of 10–20 cm for ALOS data with ~300 m (Kobayashi et al., 2009).

Elevation differences, in particular mountain areas, could cause large artifacts in the pixel offsets due to a slight difference in satellite positions before and after image acquisition (stereoscopic effect; Michel et al., 1999; Kobayashi et al., 2009). We removed this artifact by using elevation-dependent coregistration fully incorporating the ASTER GDEM version 2.

After performing this technique, we can obtain range and azimuth offset. Both stands for linear combination of west-east, south-north, and vertical components, and thus we cannot derive three-dimensional velocity field. According to this, assuming no vertical movement of glaciers or parallel flow assumption (Joughin et al., 1998), we derived surface velocity field.

3.2.2 Feature tracking for optical images

Similar tracking techniques have been often applied to Landsat optical images to derive surface velocity field (e.g., Heid and Kääb, 2012). Here we used Landsat-series L1T data distributed from USGS. These products have been already processed for ortho- and radiometric correction. They were downloaded from USGS HP.

We used matlab-based algorithm developed by Sakakibara (2016) to derive ice speed. This code adapts frequency-domain cross-correlation on orientation images (CCF-O, Fitch et al., 2002; Haug et al., 2010). The orientation images (F_o and G_o) from the first (f) and second images (g) are derived from calculating space derivative as follows.

$$F_o = sgn\left(\frac{\partial f}{\partial x} + i\,\frac{\partial f}{\partial y}\right)$$

$$G_o = sgn\left(\frac{\partial g}{\partial x} + i\,\frac{\partial g}{\partial y}\right)$$

$$\text{where } sgn\,(x) = \begin{cases} 0\; if\; |x| = 0 \\ \frac{x}{|x|}\; otherwise \end{cases}$$

where sgn is the signum function and i is the complex imaginary unit. The advantages of creating these orientation images are to reduce the effect of image contrast between the two images (Heid and Kääb, 2012). This scheme also works well for the striped Landsat images that occurred after SLC failure. Although there are several methods to derive ice speed, the CCF-O algorithm performs better than the other methods in case of Alaskan glaciers case (Heid and Kääb, 2012).

After performing the calculation, the median filters about magnitude and flow direction were performed in each result within areas of 3×3 or 5×5 pixels to reject the outliers and to smooth the results. The errors of ice speed were estimated by the mean speed of non-glacial area clipped by the Randolph Glacier Inventory version 4.0 glacial masks (Pfeffer et al., 2014). We confirmed that the orientations of the displacement vectors were identical to the flow direction of the glacier.

3.2.3 Surface elevation changes using ASTER DEM

ASTER VA products released from AIST include surface elevation data (DEM), and we can derive surface elevation changes. Although it is better for us to use some field observation data (e.g. GPS) as ground control point to confirm the quality, we used

ALOS PRISM-derived DEM, ALOS World 3D – 30m (hereafter AW3D30) provided by JAXA to calibrate the scene bias. Here is a general procedure. First, we removed some outliers whose differences are larger than 100 or 250 m compared to AW3D30. Second, we estimated the scene offset of height between ALOS and each DEM in non-glacial area. The difference was subtracted from each DEM to decrease the scene offset. After performing the procedure, we derived surface elevation changes using multi ASTER DEMs.

Chapter 4

Winter speed-up of quiescent surge-type glaciers in Yukon, Canada

Paper was published in *The Cryosphere*

Abe, T., and M. Furuya, Winter speed-up of quiescent surge-type glaciers in Yukon, Canada, *The Cryosphere*, 9(3), 1183-1190, 2015.

4.1 Introduction

Ice flow on mountain glaciers and ice sheets typically shows greatest acceleration from spring to early summer, followed by deceleration in mid-summer to fall (e.g., Iken and Bindschadler, 1986; MacGregor et al., 2005; Sundal et al., 2011). These speed changes are attributed to subglacial slip associated with water pressure changes, and these changes arise from seasonal variability of meltwater input and the evolution of the subglacial hydraulic system (Schoof, 2010; Bartholomaus et al., 2011; Hewitt, 2013; Werder et al., 2013). From spring to early summer, meltwater from the surface reaches the bed, and develops an "inefficient" drainage system, in which water flow channels are not well developed, producing a high basal water pressure. The high water pressure increases basal slip, which increases the surface velocity. As the amount of meltwater increases, the basal drainage system becomes "efficient" due to the enlarging channels (Röthlisberger, 1972). The larger channels allow a higher meltwater flux with lower water pressure causing to a gradual decrease in the surface velocity. In late summer to fall, when the meltwater input terminates, the surface velocity has its yearly minimum. Meltwater input and subsequent evolution of the drainage system apparently influence surface ice speeds from spring to fall.

Several studies reported that surface ice speeds in winter were in between the early summer maximum and early fall minimum (e.g., Iken and Truffer, 1997; Sundal et al., 2011; Burgess et al., 2013a). Some recent studies also indicate that the amount of surface meltwater in summer can influence the velocity evolution in winter, in a way that reduces the annual ice flow (Burgess et al., 2013b; Sole et al., 2013). However, there have been relatively few comprehensive velocity measurements throughout wintertime particularly in the middle-to-upstream regions of mountain glaciers. Although the first velocity map over entire Alaska and the Yukon glaciers was shown by Burgess et al. (2013a), they didn't show the spatial and temporal changes in ice velocity. Nevertheless, it is well-known that glacier surges often initiate in winter, exhibiting orders-of-magnitude speed-up and resulting in km-scale terminus advance (Meier and Post, 1969; Raymond, 1987). In order to interpret both the wintertime surge initiation and the intermediate values of winter speed, cavity closure and subsequent water pressure increase are often envisaged, starting with the surge mechanism proposed for the 1982-83 surge at the Variegated Glacier by Kamb et al. (1985). Even in winter, there may be some remnants of summer meltwater that can increase the water pressure (Iken and Truffer, 1997). However, in the absence of meltwater input, the subglacial cavities are increasingly disconnected in winter, resulting in a 'stickier' bed even if the water pressure in each cavity becomes locally high (Bartholomaus et al., 2011). Hence, it remains an open question why and how the water pressure increase and subsequent speed-up can be maintained without further input of meltwater from the surface. Do the surface velocities monotonously increase from later summer to the next spring? Such an increase is often assumed, but the process would require some extra sources of water to maintain the higher water pressure. The wintertime dynamics of sub- and englacial water are thus yet to be fully understood. Reaching an understanding requires new continuous measurements.

The St. Elias Mountains near the border of Alaska, USA, and the Yukon, Canada (Fig. 4-1) contain numerous surge-type glaciers (Meier and Post, 1969). But only a few of these have been studied and reported in the literature (e.g., Clarke et al., 1984; Truffer et al., 2000; Flowers et al., 2011; Burgess et al., 2012). Our understanding of surge-type glacier dynamics is still limited (Raymond, 1987; Harrison and Post, 2003; Cuffey and Paterson, 2010), because few detailed observations have been performed over a complete surge-cycle.

Recent advances in remote sensing techniques allow us to survey the ice-velocity distribution over the entire St. Elias Mountains. Here we present the spatial and temporal changes in the ice velocity for the surge-type glaciers, focusing particularly on the seasonal cycle during the quiescent phases to better understand the wintertime behavior. The three glaciers (Chitina, Anderson, and Walsh) are examined in detail to reveal the speed changes at the upper and the lower regions. On the other hand, the active surging occurred at four glaciers (Lowell, Tweedsmuir, Ottawa, and Logan) in the analysis period, and the details of these glaciers are described in the supplementary material.

Understanding the dynamics of surge-type glaciers is also important to better simulate future ice dynamics in the St. Elias Mountains. Significant contributions of the Alaskan glaciers' retreat to the possible sea-level rise due to global warming have been estimated (Radić and Hock, 2011), but projections of glacier mass balance assume non-surge type glaciers whose dynamics are only affected by long-term climate changes. Although the dynamics of surge-type glaciers itself is not directly related to the climate change, there have been several pieces of evidence for the impact of climate change on surge cycle (e.g., Harrison and Post, 2003; Frappé and Clarke, 2007).

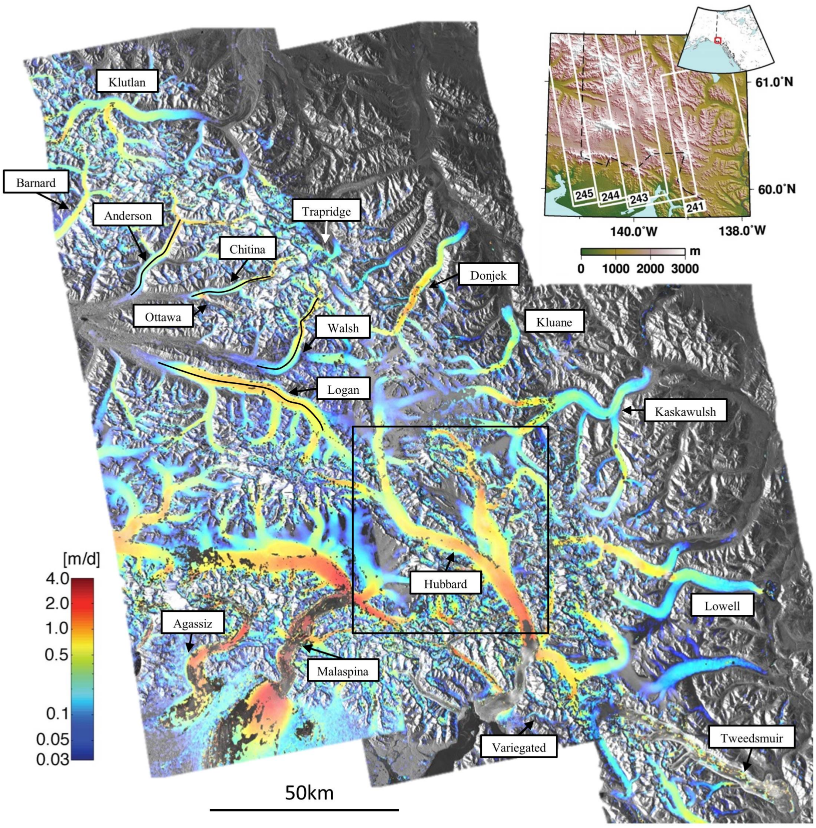

Figure 4-1: Composite ice-speed map of the study area. The individual maps for the study area were derived by intensity tracking between two PALSAR images. The left, middle and right velocity maps are derived from images pairs from 10 February 2010 and 28 March 2010 of Path 245, 30 December 2006 and 14 February 2007 of Path 243, 14 January 2008 and 29 February 2008 of Path 241, respectively. The square region around Hubbard Glacier is shown in Fig. 4-3. Black lines in some glaciers show the flow line. The upper right panel indicates the location and topography of the study area as well as the satellite's imaging areas.

4.2 Data sets and method

4.2.1 ALOS/PALSAR data

We processed phased array-type L-band (wavelength 23.6 cm) synthetic aperture radar (PALSAR) images from the Advanced Land Observation Satellite (ALOS) operated by the Japan Aerospace Exploration Agency (JAXA). Scenes were acquired along multiple paths (Fig. 1, Table 1). ALOS was launched on January 2006, and its operation was terminated on May 2011. Thus, the datasets for the study area were acquired only from December 2006 to March 2011. The details of the datasets are listed in Table 1. Only the FBS (fine-beam single-polarization mode) and FBD (fine-beam dual-polarization mode) data were used in this study because their higher spatial resolutions allowed us to reliably measure the flow velocities. We used Gamma software to process level 1.0 data to generate single look complex images (Wegmüller and Werner, 1997) and ran pixel-offset tracking analyses. See Table 1 for more detail of the datasets.

Table 4-1: Data list of the ALOS/PALSAR

Sensor/Path	Frame	Master	Slave	Mode	#Bperp (m)	Span (day)
PALSAR/241	1190-1210	20070829	20071014	FBD-FBD	597	46
		20080114	20080229	FBS-FBS	796	46
		20090116	20090303	FBS-FBS	529	46
		20100119	20100306	FBS-FBS	756	46
		20100306	20100421	FBS-FBS	353	46
		20100421	20100606	FBS-FBD	104	46
		20100606	20100722	FBD-FBD	122	46
		20100722	20100906	FBD-FBD	332	46
PALSAR/243	1200 -1220	20061230	20070214	FBS-FBS	1342	46

		20070817	20071002	FBD-FBD	425	46
		20071002	20080102	FBD-FBS	627	92
		20080102	20080217	FBS-FBS	1041	46
		20080819	20090104	FBD-FBS	1779	138
		20090104	20090219	FBS-FBS	652	46
		20090822	20091007	FBD-FBD	566	46
		20091007	20100107	FBD-FBS	726	92
		20100107	20100222	FBS-FBS	794	46
		20100825	20101010	FBD-FBD	505	46
PALSAR/244	1200-1220	20070116	20070303	FBS-FBS	1554	46
		20070903	20071019	FBD-FBD	474	46
		20071019	20080119	FBD-FBS	799	92
		20080905	20081021	FBD-FBD	672	46
		20081021	20090121	FBD-FBS	874	92
		20090908	20091024	FBD-FBD	419	46
		20091024	20100124	FBD-FBS	960	92
		20100124	20100311	FBS-FBS	722	46
		20100911	20101027	FBD-FBD	504	46
		20101027	20110127	FBD-FBS	997	92
		20110127	20110314	FBS-FBS	840	46
PALSAR/245	1200-1220	20070920	20071105	FBD-FBS	655	46
		20071105	20071221	FBS-FBS	86	46
		20071221	20080205	FBS-FBS	884	46
		20080807	20080922	FBD-FBD	1027	46
		20080922	20081223	FBD-FBS	596	92
		20090810	20090925	FBD-FBD	671	46
		20090925	20091226	FBD-FBS	776	92
		20091226	20100210	FBS-FBS	690	46
		20100210	20100328	FBS-FBS	532	46
		20100328	20100513	FBS-FBD	169	46
		20100513	20100628	FBD-FBD	122	46
		20100628	20100813	FBD-FBD	486	46
		20100813	20100928	FBD-FBD	470	46
		20100928	20101229	FBD-FBS	614	92
		20101229	20110213	FBS-FBS	790	46

Bperp stands for the orbit separation distance perpendicular to the radar line of sight.

4.2.2 Pixel offset tracking

The pixel-offset tracking (or feature or speckle tracking) algorithms used in this study are based on maximizing the cross-correlation of intensity image patches. The method closely follows that used by Strozzi et al. (2002) and Yasuda and Furuya (2013). We used a search patch of 64 × 192 pixels (range × azimuth) with a sampling interval of 4 × 12 pixels for most glaciers. But, due to its larger size for Hubbard Glacier, we used a search patch of 128 × 384 pixels. We set 4.0 as the threshold of the signal-to-noise ratio and patches below this level were treated as missing data. The FBD data were oversampled in the range direction (i.e., satellite to ground direction) due to the difference of the range dimension so that it is the same as that of the FBS data.

In the pixel-offset tracking, we corrected for a stereoscopic effect known as an artifact offset over rugged terrain (Strozzi et al., 2002). This is caused by the separation between satellite orbital paths, and the effect of foreshortening also generates the offsets. We reduced the artifact by applying an elevation-dependent correction, incorporating the Advanced Spaceborne Thermal Emission and Reflection Radiometer (ASTER) global digital elevation model (GDEM) version 2 data with 30-m resolution. We applied the same method described by Kobayashi et al. (2009) and confirmed that there remained few topography-correlated artifact offsets.

Using both range and azimuth offset data, we derived the surface velocity data (Fig. 4-1) by assuming no vertical displacements. The studied glaciers are gently sloped at approximately 1-2 degrees, and thus, the vertical component was much smaller than the horizontal component. In addition, we derived the velocity map using image pairs that were temporally separated by at most 138 days. The glaciers' surface elevation change during this period should be negligibly small in comparison to the horizontal movement of the glaciers. To examine the spatial and temporal changes, we first set a flow line at each glacier, and then averaged the velocity pixel data over the ~350 × 350-m^2 area with its center at the flow line. We estimated the measurement error to be below 0.1 m/d, from the standard deviation at each area.

The uncertainties of offset tracking have been estimated to be ~0.3-0.4 m in the rugged terrain, using two images with ALOS/PALSAR's 46-day interval at non-deforming area (Kobayashi et al., 2009). Assuming linear temporal evolution, the errors in the velocity estimate were inferred to be below 0.1 m/d.

4.3 Observation results

Here we focus on winter speed-up signals at surge-type glaciers that were in their quiescent phase during the analysis period. The Chitina, Anderson, and Walsh Glaciers are the major surge-type glaciers of the Chitina River valley system (Clarke and Holdsworth, 2002), and could be examined with the highest temporal resolution because of the overlap of multiple satellite tracks. The names of major 17 glaciers in the region are shown in Figure 4-1.

Figures 4-2a, 2c, and 2e show the spatial-temporal evolution of ice velocity at the three glaciers (Anderson, Chitina and Walsh) along their flow lines shown in Figure 4-1. At the 20-km point on Anderson Glacier (Fig. 4-2a), the winter speed is more than double the fall speed. At Chitina Glacier (Fig. 4-2c), the winter velocities at the 20-km point exceed 0.5 m/d, which is significantly greater than the fall velocities of ~0.3 m/d regardless of the surge signal at Ottawa glacier in 2010 (Black circle in Fig. 4-2c). At the 20-km point on Walsh Glacier (Fig. 4-2e), the winter speed is more than 50% greater than the fall speed.

Figure 4-2b, 2d, and 2f are time-series plots averaged over the downstream (blue) and upstream (red) section in Figs. 4-2a, 4-2c, and 4-2e, respectively. We can recognize the distinct seasonal trends in the upstream and downstream. Although the downstream speeds (blue) in early summer are faster than those in winter, the upstream speeds (red) in winter are comparable to, and sometimes faster than those in early summer (Fig. 4-2b, 2d, and 2f). For instance, over the 18-21 km section on Anderson Glacier, the velocity is ~0.5 m/d in early summer 2010 but exceeds 0.7 m/d in winter of 2009/2010 and 2010/2011 (Fig. 4-2b). Over the 18-21 km section on Chitina Glacier, the velocity is ~0.5 m/d in early summer 2010 but is also in winter of 2009/2010 and 2010/2011 (Fig. 4-2d). Similarly, over the 21-24 km section on Walsh Glacier, the velocity is 0.4 m/d in early summer 2010 but 0.6 m/d in winter (Fig. 4-2f). Moreover, in contrast to the propagation toward upstream region of the summer speed-up observed in Greenland outlet glacier (Bartholomew et al., 2010), the higher-velocity area expands from upstream in fall to downstream section in winter. This propagation toward downstream is most clearly observed at Anderson Glacier (Fig. 4-2a).

We could not obtain quality and much summer velocity data for each year due to large intensity changes associated with surface melting and due to the data availability problem except the year 2010. Figure 4-2 shows summer speed-up signals in 2010 in the lower middle reaches at each glacier. In addition, compared to the gradual propagation of the winter speed-up toward downglacier noted above, the summer speed-up in the lower reaches appears to occur primarily over a shorter period. The glacier dynamics at lower reaches thus seems to be consistent with previous findings.

For Hubbard Glacier, the only tidewater glacier in the study area, the ~15 km-length section in the midstream region has velocities in January and February that are ~33-60%

greater than the velocities of the previous August to October (Figs. 4-3a, d, e, and h). The significant speed-up during the 2009 winter may be associated with a small surge in the upper tributary (Fig. 4-3e). The much smaller tributary in the upper reach of Malaspina Glacier (Fig. 4-1) also exhibits greater velocities in winter, suggesting that the winter speed-up mechanism is independent of the glacier's size.

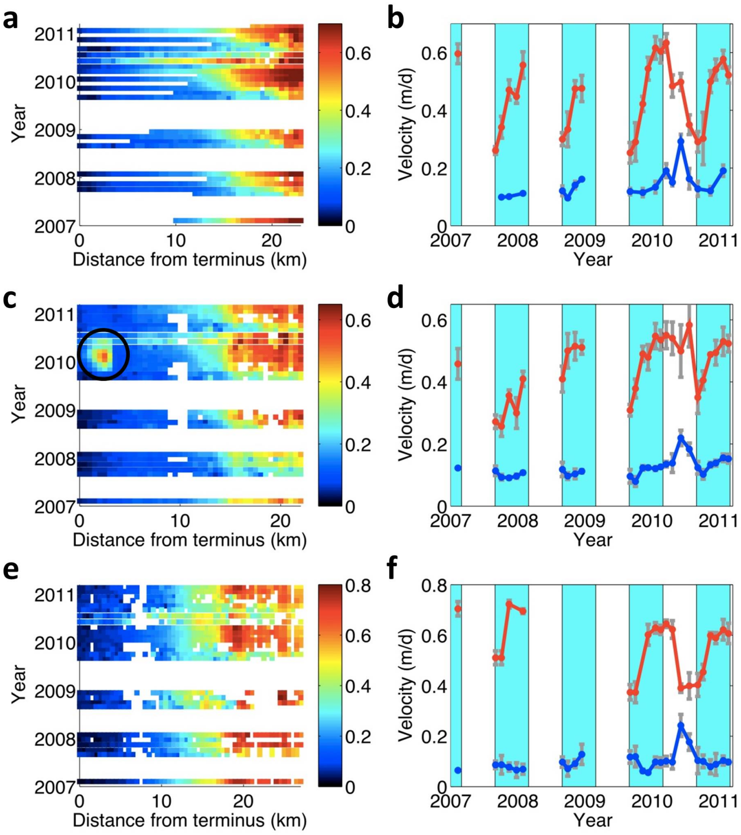

Figure 4-2: Left panels: Spatial and temporal changes in ice velocity along the flow lines of (a) Anderson, (c) Chitina, and (e) Walsh Glaciers. The profiles are plotted with 500 m intervals along the flow lines shown in Fig. 1. Black circle indicates the speed-up signal caused by Ottawa Glacier (a tributary of Chitina Glacier, and here is the confluence.). Right panels: Averaged time-series plots at two distinct sections derived from Fig. 4-2a, c, and e, respectively. Red line shows upper region (b: 18-21 km of, d: 18-21 km, f: 21-24 km) and blue line do lower region (b: 5-8 km, d: 5-8 km, f: 4-7 km). Cyan shades stand for winter season (Sep - Feb).

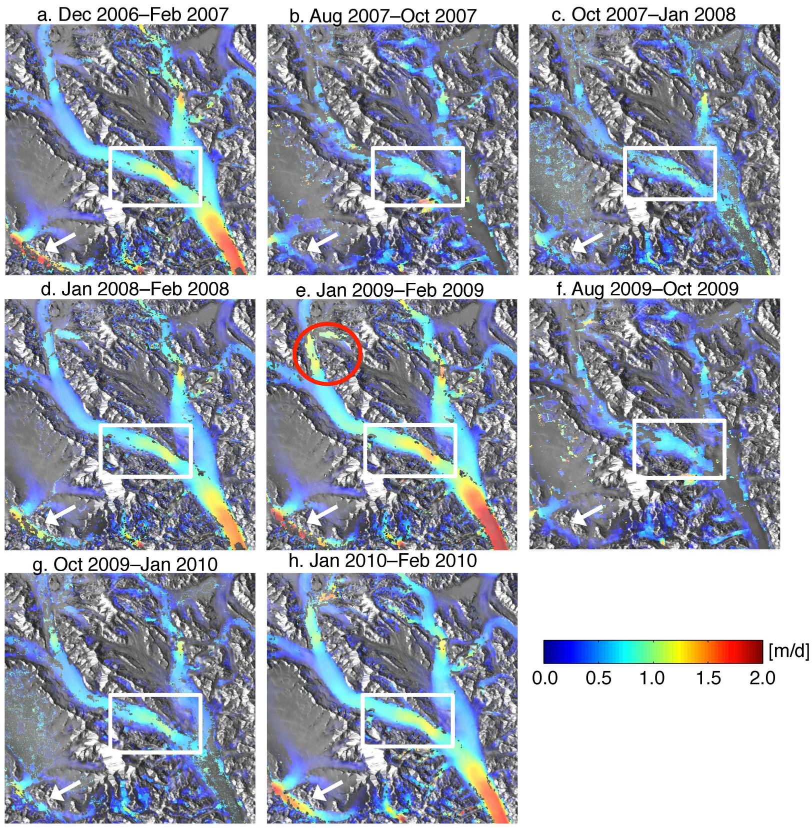

Figure 4-3: Spatial-temporal evolution of ice velocity at Hubbard Glacier and an upper tributary of Malaspina Glacier. The flow direction of Hubbard Glacier is from north to south. The white square marks a region in which the velocity in winter (a, d, e, h) exceeds that of late summer and fall (b, c, f, g). The red circle in (e) marks a "mini-surge-like" signal in the upstream region during January-February 2009. The white arrow in that image shows a winter speed-up of an upper tributary of Malaspina Glacier.

4.4 Discussion

According to the average air temperature at Yakutat Airport provided by The Alaska Climate Research Center data (http://akclimate.org), the monthly average temperature from 2006-2011 is about 0.2 ℃ in November, and about -2 ℃ for December, January, and February. Almost all of our study area is above 1000 m a.s.l. Thus, the wintertime temperature is significantly below freezing, so there should be little surface meltwater during winter. Under such circumstances, it is likely that the mechanisms of winter speed-up and its downglacier propagation are different from those of the summer speed-up that usually propagates upglacier. Also, the detected annual winter speed-up in the upstream is up to 100% too high to be explained by snow accumulation, considering that the ice thickness in the area is a few hundred meters or more

The observed winter speed-up in the upstream region may be regarded as a "mini-surge" (Kamb and Engelhardt, 1987; Humphrey and Raymond, 1994). However, not all previously reported mini-surges occurred in winter. For instance, the mini-surges prior to the 1982-1983 surge at Variegated Glacier occurred in summer (Kamb et al., 1985; Kamb and Engelhardt, 1987). A mini-surge defined in Kamb and Engelhardt's paper indicates dramatically accelerated motion for a roughly 1-day period, which occurred repeatedly during June and July in 1978-81. Although Kamb et al. (1985) noted an anomalous increase in wintertime velocities since 1978, the measurements were done only once in September and once in June (Raymond and Harrison, 1988), and thus they may include the spring speed-up signals as pointed out by Harrison and Post (2003). To the best of our knowledge, no comprehensive wintertime velocity observations have been done in upstream regions. However, even if sporadic speed-up events repeatedly occur from fall to winter, we cannot distinguish them from gradual seasonal speed-up because of the present coarse temporal resolution. Nevertheless, it is important that our results clearly revealed flow velocity evolution from fall to winter, indicating the increase is not monotonously toward next summer.

We now compare our findings to previous studies. Iken and Truffer (1997) found a gradual speed-up from fall to winter at the ~2-km-long downstream section of the temperate Findelengletcher in Switzerland, where the speed continues to increase, reaching a maximum in summer. In contrast, our observed winter speed-up occurs in the upstream region, and speed does not continue to increase after winter. Sundal et al. (2011) examined how ice speed-up and meltwater runoff are related at land-terminating glaciers in Greenland. The ice speed-up is affected by the amount of surface runoff each year, which differs between high and low melting years. The results indicate that the ice speed in a high melting year gradually increases from fall to winter. However, the ice speed does not accelerate in low melting years. Moreover, they did not report the spatial distribution of speed during winter, and the maximum speed is apparently observed in early spring to summer. Our velocity data do not simply indicate the gradual speed-up from fall to next spring. The winter speed-up initiates upstream, and the maximum speed in winter is comparable to that in early summer. As some of the glaciers could not be examined with a high temporal resolution, it is likely that there are other winter speed-up glaciers.

How can we explain the observed winter speed-up signals? First, we argue that the mechanism proposed by Kamb et al. (1985) for the Variegated Glacier does not apply here. In that mechanism, the efficient tunnel-shaped drainage system, which is present in summer, may provide a less efficient distributed system in early winter due to depletion of surface meltwater and the destruction of conduits by creep closure. Thus, the subglacial water pressure may greatly increase. For our observed winter speed-up to be explained by this mechanism, there would have to be an efficient drainage system. Although such an efficient drainage system is often observed near the terminus (Raymond et al., 1995; Werder et al., 2013), the winter speed-up is observed upstream, far from the terminus. In addition, even if there exist meltwater remnants in the upstream region, it is unclear how the subsequent speed-up can be maintained without further input of meltwater from the surface. In the absence of meltwater input, subglacial cavities will be increasingly disconnected (Bartholomaus et al., 2011). Thus, we need to consider a mechanism that can trap water in the upstream in winter so that the subglacial water pressure can be maintained high enough to generate basal slip.

One such mechanism was proposed by Lingle and Fatland (2003). In that study, using the few ERS1/2 tandem radar interferometry data with the 1-3 day's observation interval, they similarly detected a faster speed in winter than in fall at the non-surging Seward Glacier in the St. Elias Mountains. They also found localized circular motion anomalies at both surging and non-surging glaciers that indicated local uplifting and/or subsidence caused by transient subglacial hydraulic phenomena. Combining their observations with earlier glacier hydrological studies, they proposed a model of englacial water storage and gravity-driven water flow toward the bed in winter that applies to both surge-type and non-surge-type glaciers. Lingle and Fatland (2003) suggested that the size of englacial water storage would determine if a given glacier is surge-type or not.

Few winter speed-up observations have been made since Lingle and Fatland (2003), but our data suggests that winter speed-up may not be a rare phenomenon. Each local uplift and/or subsidence event in the Lingle and Fatland study must be a transient short-term process, episodically occurring in places. We could not observe such localized signals in our offset-tracking displacements because our observation interval, at least 46 days, is much longer than the 1-3 days in Lingle and Fatland (2003). Nevertheless, we propose that both Lingle and Fatland's and our observations are caused by the same physical processes. This is because the locally increased basal water pressure could increase basal sliding and contribute to larger horizontal displacements. Following Lingle and Fatland's hypothesis, our finding of winter speed-up signals at the quiescent surge-type glaciers seems to indicate the presence of sizable englacial water storage whose water volume will not only change seasonally but also evolve secularly until the next active surging phase. Considering that the observed glaciers are surge-type but during their quiescent phase, we speculate that total englacial water volume may not yet be large enough to generate the active surging phase.

Till deformation is another mechanism to cause glacier surge (e.g., Cuffey and Paterson, 2010), and some glaciers in Alaska and the Yukon have till layers. For example, Truffer et al. (2000) examined surface velocity and basal motion at the ice-till interface at Black Rapid Glacier in the Alaska Range, finding that the large-scale mobilization of subglacial sediments plays a dominant role in the surge mechanism. However, based on Coulomb-plastic rheology for the till deformation (e.g., Clarke, 2005), substantial till deformation requires a high basal water pressure. So, regardless of the presence of till layer, the mechanism for winter speed-up should include a process in which a high basal water pressure can be kept during wintertime.

Schoof et al. (2014) recently reported wintertime water pressure oscillations at a surge-type glacier in Yukon, and interpreted them as spontaneous oscillations driven by water input from englacial sources or ground-water flow. But without flow velocity data, they could not correlate the wintertime drainage phenomenon to glacial dynamics. The present observations though are consistent with the englacial water storage model of Lingle and Fatland, and thus may help explain our observed upstream glacier speed-ups in winter.

Although the englacial water storage model may explain the winter speed-up, the specific water-storage system remains unknown (Fountain and Walder, 1998). One plausible form of englacial water storage is the basal crevasses observed by Harper et al. (2010) at Bench Glacier, Alaska. Such crevasses have no direct route to the surface, yet can store significant volumes of water near the bed. Thus, water in the basal crevasses may generate high pressure when they become constricted due to creep closure in winter.

The formation of basal crevasses in grounded glaciers requires a high basal-water pressure that may approach the ice overburden pressure and/or longitudinally extending ice flow (van der Veen, 1998). Although such crevasses have not been detected in this area, their restrictive conditions might explain our observations of uncommon winter speed-up signals and the distribution of surge-type glaciers in the area.

4.5 Concluding remarks

In this study, we applied offset tracking to ALOS/PALSAR data on glaciers near the border of Alaska and the Yukon to show their spatial and temporal velocity changes in 2006-2011. For many of the quiescent surge-type glaciers around the St. Elias Mountains, upstream accelerations occurred from fall to winter and then propagated toward downstream. The winter speeds in the upstream regions were comparable to, and sometimes faster than those in spring to summer. Combining the absence of upstream surface meltwater input in winter with insights from some previous studies, we speculate that sizable water storage may be present near the bottom of glaciers, not directly connected to the surface, yet can enhance basal sliding by increased water pressure as they constrict in winter. Further observational and theoretical studies are necessary to decipher the winter speed-up mechanisms and determine if such water storage systems exist.

Chapter 5

Basal condition in winter using numerical glacier hydrology model

5.1 Introduction

Meltwater movement within a glacier develops a drainage system, which closely links to basal sliding and glacial erosions. The arrival of water at the bed results in lubrication at the interface between ice and bed. This process enhances basal sliding. Thus, seasonal meltwater production on glacier surface is relevant to ice dynamics. Iken and Bindshadler (1986) first observed the seasonal speed-up on Findelengletscher in Switzerland. Zwally et al. (2002) also performed ground GPS observation of summer ice-speed acceleration in the ablation area of Greenland, and proposed that summer meltwater drains into ice and lubricates the interface between ice and bed, enhancing basal sliding. Recent synthetic aperture radar measurements have revealed seasonal speed-up of many outlet glaciers and its complex diversity in Greenland (Joughin et al., 2008; Sundal et al., 2011; Moon et al., 2014; Moon et al., 2015).

The basic theory of seasonal change in ice speed is as follows; During winter, without water input from the surface, drainage pathways are partly closed, which is a weakly connected system. When surface melt water reaches the bed in summer, it develops distributed linked-cavity system. This bed condition generates high water pressures which reduces basal resistance and increases ice velocity. On the other hand, an increase in the capacity of the drainage system, aided by the melting of well-connected channels, may subsequently reduce water pressures and allow for slower ice velocities even with a larger quantity of melt water. As meltwater decreases in fall, the speed further decreases.

In recent years, the relation between summer meltwater production and winter or annual ice speed has been argued. Sole et al. (2013) showed that amount of surface meltwater in summer can influence the velocity evolution in winter, in a way that reduces the annual ice flow. Tedstone et al (2015) found a correlation between a few-year-averaged past runoff with ice speed. They proposed that ice flow may respond to past runoff integrated over a multiyear timescale through a cumulative reduction of stored water in the unchannelized portions of the subglacial hydrologic system, which reduces basal lubrication and slows ice velocities. Stevens et al. (2016) derived the similar negative correlation between multiyear net runoff and annual speed. The seasonal and inter-annual responses of glacier dynamics to runoff variability are so complicated.

Abe and Furuya (2015) examined spatial and temporal changes in ice speed of surge-type glaciers in Yukon, Canada, derived from ALOS/PALSAR radar images between 2006 and 2011. They found winter speed-up of some quiescent surge-type glaciers. Although glacier surge often initiates in winter (Raymond, 1987; Harrison and Post, 2003), the reason remains unclear. Their findings show new insight into basal hydrology and glacier dynamics in winter. In order to reveal how it occurs, we explored basal condition in winter using a numerical glacier hydrology model.

5.2 Numerical glacier hydrology model

In order to examine how a drainage system evolves under a glacier, Numerical Glacier Hydrology Model (hereafter NGHM) has been used. NGHM is to calculate a development of subglacial water pathways and subsequent water pressure, based on physical principles. Meltwater in NGHM flows along hydraulic potential, which is the sum of potential energy and water pressure. The history of NGHM are briefly summarized as follows;

Clarke (1996) developed zero-dimensional box model which combined both distributed and channelized systems. Kessler and Anderson (2004) described discrete drainage pathways of mixture of cavities and channels, allowing a transition between distributed and channelized modes. They converted subglacial water pressure to sliding velocity and compared the results with spring speed-up event and speed-up due to glacial outburst floods. The model is one dimensional along the glacier center line, which is the same dimension as developed by Flowers et al. (2004).

Recently, two-dimensional NGHMs have been developed. Schoof (2010) first described a 2D network of discrete conduits that can be both distributed and channelized flow into a single equation in terms of the cross-sectional area. He adopted arborescent channel system when the discharge is sufficiently large. However, the computations were done only on a rectangular grid of individual conduits, which strongly affects the topography of the arborescent drainage system that emerges. Hewitt (2013) integrated a linked-cavity sheet with a structured channel network to investigate the coupling with ice dynamics. Although there have been only a few models which couple hydrology with ice speed (Kessler and Anderson, 2004; Hewitt, 2013; Hoffman and Price, 2014), these kinds of models were developed to explain how drainage system evolves as surface meltwater is produced, and thus there is no model used to explore winter drainage system.

In this study, we used a two-dimensional Glacier Drainage System model (GlaDS) that couples channelized and distributed subglacial water flow (Werder et al., 2013). In this model, distributed flow occurs through linked cavities that are represented as a continuous water sheet of variable thickness. Channelized flow occurs through Röthlisberger channels that can form on any of edges of a prescribed, unstructured network of potential channels (Fig. 5-1). One of the novelty compared with Schoof's model is greater freedom in the arrangement of the channel segments on an unstructured network, while its geometry is constrained by the particular random mesh arrangement. GlaDS is not able to calculate surface ice speed, but two-way coupling of this model to an ice flow model is possible as performed by Hewitt (2013); the effective pressure modulates the sliding speed which in turn affects the cavity opening rate.

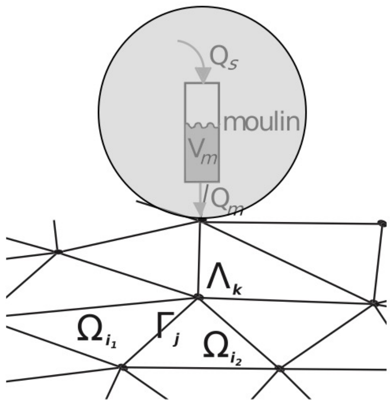

Figure 5-1 A view of part of a network Γ with nodes. The network has edges Γ_j and nodes Λ_k, partitioning the domain Ω into subdomains Ω_i. The channels are constrained to lie on the edges and the sheet occupies the subdomains. The gray-shaded circle represents moulin system and its connection to the network, but it is not set in this study. Modified from Werder et al. (2013).

5.3 Model setting

In order to examine basal condition in winter as much as simple, we assumed an ideal shape of valley glacier (Fig. 5-2). The surface topography is proportional to square-root of the glacier length. The bed topography is represented by a parabola, and the basal slope is inclined. The width and length of the glacier in the model is about 2 km and 25 km, which mimics Anderson Glacier in Yukon (Abe and Furuya, 2015). We divided the glacier surface area into 1093 triangle nodes.

In the setting, meltwater production was only induced by basal melting with a constant and seasonal forcing. In reality, surface meltwater input causes diurnal and seasonal evolution of the channel development and the extent, which means that we should take this effect into account. Werder et al (2013) described moulins input a Voronoi tessellation of randomly chosen points, and the moulins are chosen to sit at the lowest node contained within each Voronoi cell. This approach crudely mimics the surface and englacial routing that occurs in reality. However, the aim of my work is to examine subglacial condition in winter, assuming that there is no surface meltwater in winter. Therefore, we did not set any moulins and the water inputs in the model (Figure 5-1).

We calculated time evolution of cross-sections at each node with default setting as described in Werder et al. (2013), and solved subglacial water pressure. Then, we calculated the effective pressure (ice overburden pressure minus basal water pressure).

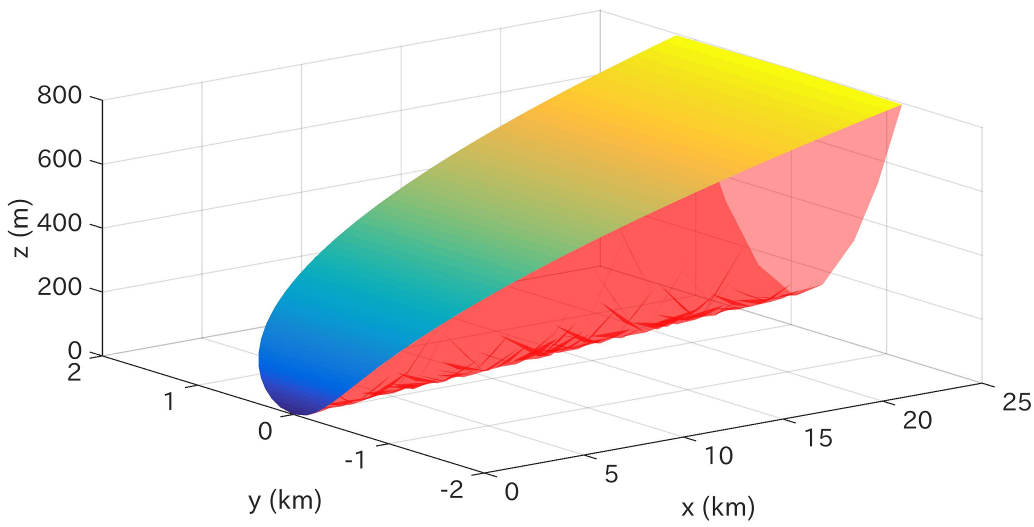

Figure 5-2 The shape of a glacier used in this model.

5.4 Results and Discussion

First, we examined seasonal evolution of channel extents with default settings. Figure 5-3 shows some snapshots of the development of the channels with different epochs. We ran the model for 2 years and confirmed similar seasonal evolutions in both years. The channels were represented by the black lines and the volume as the thickness of the lines. Immediately after the initiation of water production, the effective pressure N dropped down, which indicates the distributed inefficient drainage is dominant (Fig. 5-3a). Followed by the N drop, the channelized efficient drainage is developed (Fig. 5-3b). As time goes by, the channels disappear due to meltwater decrease (Fig. 5-3c), and the N goes again high value (Fig. 5-3d), indicating the surface speed slow-down. The time evolution of spatial-averaged N at two areas with default setting results in

Figure 5-4. When water input suddenly increases (130 days), the N also rapidly decreases. This drives spring/summer speed-up. After the decrease, sufficient amount of subglacial water causes initiation of channel development (150 days). The channelized system causes the reduction in N by further collecting net water input. After the peak of seasonal forcing of water production, the N continues to rise in autumn and winter. In next year, the same behaviors are repeated.

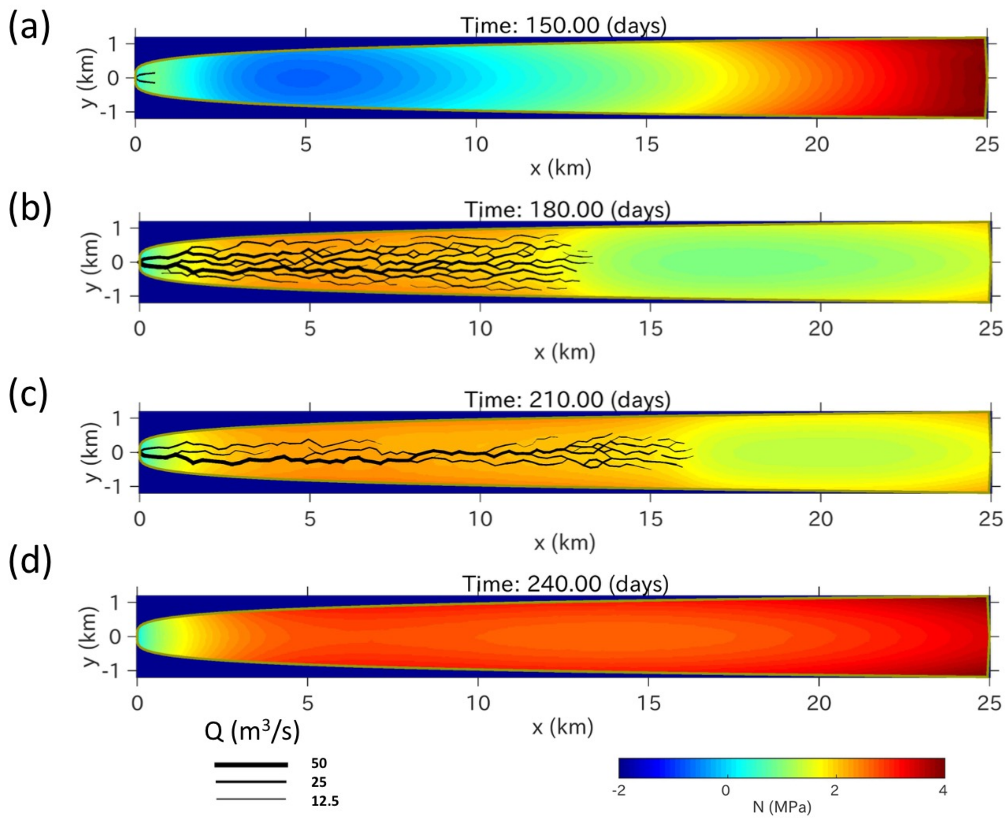

Figure 5-3 Time evolution of the development of the channel system (black line) and the effective pressure N (contour color) with different times.

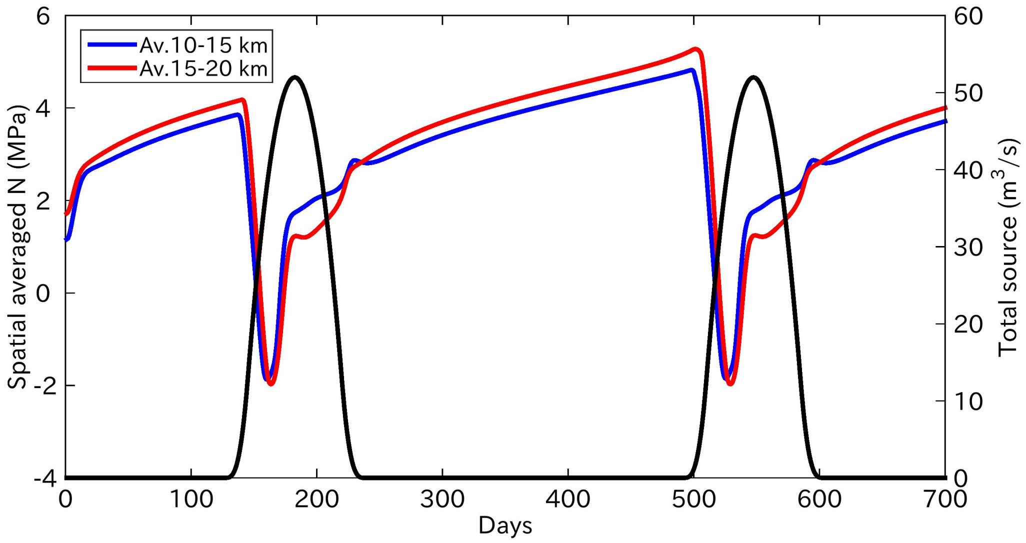

Figure 5-4 Temporal changes in the *N* (blue and red) and seasonal water input (black). The blue and red represent the averaged N over the section between 10 and 15 km, 15 and 20 km, respectively.

However, only parameter changes did not generate any increases of the *N* during winter season. For example, the increase of conductivity tended to decrease the *N*, but we found the large value inadequate because the channel did not develop as water input increased. Thus, we set an additional source in upstream that can extract water. The source with an area of 1 km^2 is set in between 20 and 21 km section (box in Figure 5-5a), and the water input only during some certain days. We ran again the model with those settings.

The results show that the effective pressure *N* decreases and the propagation toward downstream are confirmed after additional water input in 350 days (Fig. 5-5b, c and d), which is consistent with the propagation of acceleration observed on Anderson Glacier (Abe and Furuya, 2015). However, the change is rapid, not continuous, which differs from the observed result (Fig. 5-5).

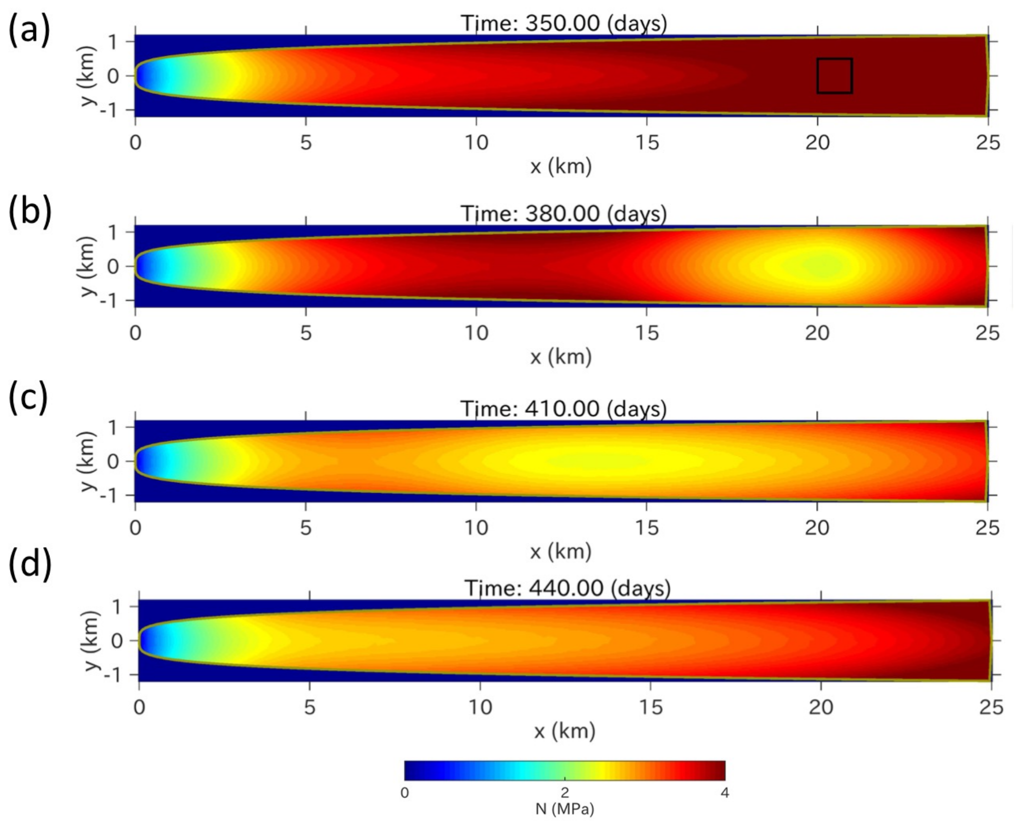

Figure 5-5 Time evolution of the effective pressure *N* during additional water input upstream only in winter with different epoch.

Next, we changed the period and volume of the water input from the additional source. The larger volume of water results in the larger decrease of *N*, which is similar to early summer's behavior (Fig. 5-3, and 5-4) although the winter volume is much smaller than that in Summer (Fig. 5-6). In winter, the total volume of englacial water storage can be smaller than that of seasonal surface meltwater. Thus, we have to consider a mechanism which can decrease *N* with small water volume.

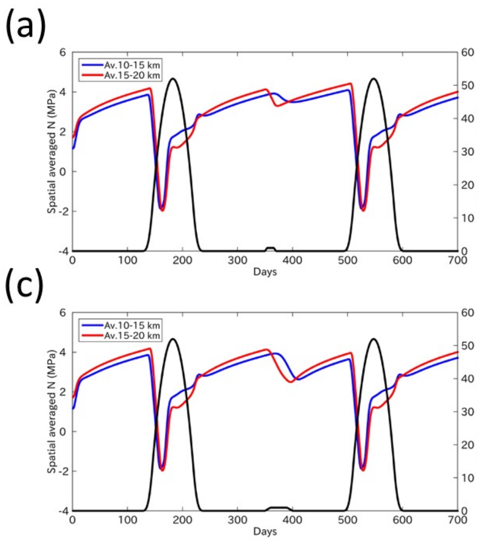

Figure 5-6 Temporal changes in the *N* (blue and red) and seasonal water input (black) including additional input upstream only winter. The volume of water and the input period differs from each other. (c) is derived from the result in Figure 5-5.

The mechanism of decreasing *N* with a small water input at the base may be related to macroscopic porosity in glaciers. In general, the value is only a few percent and it is treated as constant. It has been discussed that basal water pressure is not only proportional to total volume of englacial water but also inversely proportional to the macroscopic porosity (Bartholomaus et al., 2011; Bueler, 2014; Yasuda and Furuya, 2015). Assuming that the meltwater influx itself would be smaller than in summer, it can prevent channels from being developed. Creep closure exactly represents the decrease of the porosity, which may locally generate high basal water pressure. In GlaDS model, the creep related parameter in closing terms is given same constant values in both cavity and channel due to lack of detailed knowledge (Werder et al., 2013). These treatments may be closely related to winter hydrology and glacier dynamics.

Hewitt and Schoof (2017) recently developed two new models to describe the temperature and water-content in ice masses, accounting for the possibility of gravity- and pressure-driven water drainage according to Darcy's law. These models are under a test phase, but it seems to provide more realistic situation.

Moreover, bed topography data under glaciers may be also inevitable. Werder (2016) recently developed a new supercooling threshold formula underlying overdeepening. This threshold is reached when the adverse bed slope terminating an overdeepening is sufficiently large to shut down the efficient, channelized drainage system. He extended that theory by taking into account that downstream water pressure can be below overburden pressure. Supercooling itself prevents development of channels, which may bring cyclic accelerations (Turrin and Foster, 2014). Abe and Furuya (2015) also mentioned the place where the winter speed-up occurred, at the confluence of the tributaries. The confluence is likely to be developed overdeepening (e.g., MacGregor et al., 2000; Anderson et al., 2006). Thus, the detail examinations at confluence are need to reveal basal hydrology under overdeepenings.

5.5 Concluding remarks

In this chapter, we ran numerical glacial hydrology model to explore subglacial condition in winter. The simulated result of assuming winter condition is partly consistent with the winter speed-up (Abe and Furuya, 2015). However, the modeled result is strongly dependent on several parameters and no data were available to better constrain them. There seems to be no model which can completely explain surge generation mechanism to date, and existing physical theories used in present models do not catch up complex observed behaviors in glaciers.

Nowadays, we are able to obtain spatial and temporal changes in ice surface speed derived from satellite images. The surface speed is a result from complex interaction between hydrological environment and basal sliding. In terms of summer speed-up behavior, the response significantly differs in each glacier, and thus the dynamics has not been fully understood. Moreover, it is logistically challenging to acquire in-situ observation data in basal condition such as subglacial water pressure, which can cause difficulty in comparing them with modeling results. Thus, we need to collect both observed and modeled data in a glacier in order to reveal the mechanisms. More various observed data are desirable to constrict modeling results.

Chapter 6

Twelve-year cyclic surging episodes at Donjek Glacier in Yukon, Canada

Paper was published in *The Cryosphere*

Abe, T., M. Furuya, and D. Sakakibara, Twelve-year cyclic surging episodes at Donjek Glacier in Yukon, Canada, *The Cryosphere*, 10(4), 1427-1432, 2016.

6.1 Introduction

During their short (1-15 years) active phase, surge-type glaciers typically speed up by several-fold to over an order-of-magnitude, resulting in significant thickness changes and km-scale terminus advance (Meier and Post, 1969; Raymond, 1987; Harrison and Post, 2003). In their quiescent phase (tens to hundreds of years), they flow slowly or become stagnant. Meanwhile, ice accumulates in the upstream area and the imbalanced flow causes retreating and thinning in the downstream area, which produces a steeper glacier surface in the upstream. This part of the quiescent phase is sometimes called the build-up phase (Dolgoushin and Osipova, 1975; Jiskoot, 2011). As to the cause of the surge, two generation mechanisms have been proposed: the Alaskan-type and the Svalbard-type (e.g., Murray et al., 2003).

In Alaskan temperate glaciers, the active phase is relatively short, lasting a few months to years, and can have a rapid speed-up and slow-down. The Alaskan-type surge often initiates in winter (Raymond, 1987; Harrison and Post, 2003). The initiation mechanism is thought to be a hydrological transition from efficient tunnel-like drainage to inefficient linked-cavity drainage with a corresponding increase in water pressure (Kamb et al., 1985; Harrison and Post, 2003). In contrast, in Svalbard polythermal glaciers, the speed-up is gradual, leading to years-long active surging. For these glaciers, the active-phase duration and the recurrence interval are much longer than those in the temperate Alaskan-type. Moreover, for Svalbard polythermal glaciers, the surge generation mechanism has been considered to be thermal regulation (e.g., Murray et al., 2003). However, recent observations have shown seasonal modulation in ice speed during the years-long active surging, which indicates the importance of the hydrological process, originating from the surface meltwater, for maintaining a multi-year active phase (Yasuda and Furuya, 2015).

Near the border of Alaska and the Yukon, Canada, there are many surge-type glaciers (Meier and Post, 1969; Raymond, 1987; Harrison and Post, 2003). The surge cycles in this area have been examined (e.g., Eisen et al., 2001; 2005; Frappe and Clarke, 2007; Burgess et al., 2012; Bevington and Copland, 2014), but many questions remain about the detailed surging dynamics (Raymond, 1987; Harrison and Post, 2003; Cuffey and Paterson, 2010).

Recent advances in spaceborne remote sensing can provide insight into surging glacier dynamics. In particular, synthetic aperture radar (SAR) images have revealed spatial and temporal changes in ice velocity at surge-type glaciers in Alaska and the Yukon (Burgess et al., 2013a; Abe and Furuya, 2015). The temporal coverage of spaceborne SAR data is still too short to investigate long-term evolution in ice speed, although SAR allows us to image remote areas regardless of weather conditions and acquisition time (i.e. SAR data acquisition can be done both daytime and nighttime). Landsat optical images distributed by the United States Geological Survey (USGS) have been available since 1972. While optical images have their limitations in local weather conditions, they have revealed the long-term changes in terminus positions and velocities of mountain glaciers around the world (e.g., McNabb and Hock, 2014; Sakakibara and Sugiyama, 2014; Sakakibara, 2016).

To reveal the long-term evolution of Donjek Glacier, we use Landsat optical images acquired between 1973 and 2016 to derive the spatial-temporal changes in ice speed (1986-2016) and the terminus areas (1973-2016). As a consequence, we report here my findings of three surging events as well as a likely surging event pre-1985.

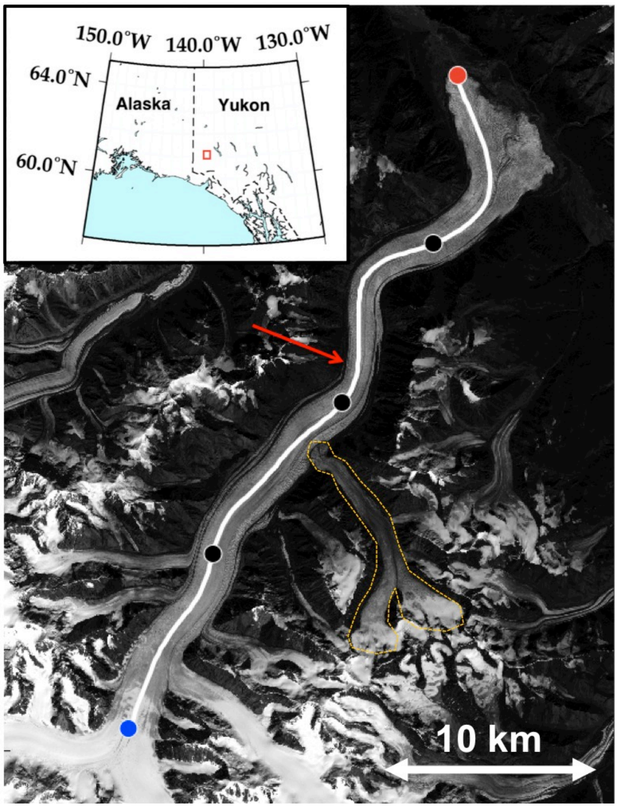

Figure 6-1: Location of Donjek Glacier. Background is a Landsat 8 image acquired on 22 July 2014. White line is the flow line used in Fig. 6-3 and 6-4. The red and blue dots show the start and end points, whereas the black dots mark 10-km intervals. The red arrow indicates a significantly narrower area of the valley and the dotted-orange curves outline the last tributary.

6.2 Donjek Glacier

Donjek Glacier is located in southwest Yukon (Fig. 6-1). Steele, Spring, and Kluane Glaciers are major surge-type glaciers located around Donjek (Clarke and Holdsworth, 2002). The entire length and area of Donjek Glacier are 55 km and 448 km^2, respectively. Donjek Glacier lies at an elevation of 1000-3000 m, and the valley width significantly narrows downstream of 20 km from the terminus. The terminus spreads out as it flows into the river valley to form a small piedmont lobe. Former surges have caused this lobe to expand to the east against the Donjek Ranges, which blocked the flow in the river (e.g., Clarke and Mathews, 1981). Recent airborne laser altimetry revealed that the mass balance of Donjek Glacier was -0.29 m w.e. yr-1 (Larsen et al., 2015). Previous studies mentioned past surging events in 1935, 1961, 1969, and 1978 (Johnson, 1972a; 1972b; Clarke and Holdsworth, 2002). The earliest three events were recognized using aerial photogrammetry and morphological features. However, the details of the observations (e.g., data source and the observation frequency) and even the duration of the active phase are unclear. Moreover, surges since the 1980s are unreported, and the long-term evolution remains uncertain. Donjek's last tributary (Fig. 6-1) is also known as a surge-type glacier that was active in 1974 (Clarke and Holdsworth, 2002), but there is no recent report of this tributary's surge.

6.3 Data processing

We used Landsat optical images, to examine terminus changes from 1973 to 2016 and flow-speed evolution from 1986 to 2016. Because of the lower spatial resolution of the images prior to 1986, we could not derive the velocities between 1973 and 1985, but the images were helpful to examine the terminus changes even in 1970s. These images were acquired by the Landsat 1-5 Multi-Spectral Scanner (MSS), the Landsat 4-5 Thematic Mapper (TM), the Landsat 7 Enhanced Thematic Mapper Plus (ETM+), and the Landsat 8 Operational Land Imager (OLI), all of which are distributed by the USGS (http://landsat.usgs.gov/).

While there are a variety of image matching (i.e. feature tracking) methods to derive glacier surface speed (e.g., Heid and Kääb, 2012), we used the Cross-Correlation in Frequency domain on Orientation images (CCF-O) algorithm (Fitch et al., 2002; Sakakibara, 2016) to derive surface velocity in this study because for Alaskan glaciers, the CCF-O algorithm performs better than the other methods (Heid and Kääb, 2012).

I selected 74 pairs of the Landsat images (Table 6-1) and applied the CCF-O method to the band 4 images (30 m resolution) for Landsat 4 and 5, and the band 8 images (15 m resolution) for Landsat 7 and 8. After co-registration of the two images, we computed the cross-correlation coefficients with a reference chip (30×30 pixels) and a search chip (50×50 pixels) on the orientation images. The step number was set as 6×6 pixels. The distance between the maximum peaks of the two images was regarded as a displacement of glacier.

After performing the CCF-O, the median filters about magnitude and flow direction were performed in each result within areas of 3×3 or 5×5 pixels to reject the outliers and to smooth the results. The velocity errors of ice speed ranged between 0.05 and 0.80 m/d, which was estimated by the mean speed of non-glacier area clipped by the Randolph Glacier Inventory version 4.0 glacial masks (Pfeffer et al., 2014). The error was dependent on the time separations between the image acquisitions, roughly all of which were less than about 4 months. Thus, some pairs could include the seasonal speed-up, but the amplitude was seemed to be much smaller than that in the surging episodes. I also confirmed that the orientations of the displacement vectors were identical to the flow direction of the glacier. However, it was harder to track the surface features in the accumulation area due to its low contrast. Thus, our velocity data indicate the poorer coverage in the upstream region. We averaged the velocity data over the 450 × 450-m^2 area and every 300 m intervals along the flow line set from the terminus (Fig. 6-1).

We also examined the fluctuation of the terminus area associated with the surging events using the false color composite images of bands 4–6 for the Landsat 1–3 MSS, 2–4 for the Landsat 4/5 MSS, 3–5 for the Landsat 5 TM and the Landsat 7 ETM+, and 4–6 for the Landsat 8 OLI. These band combinations take advantage of the clear contrast between ice and rock (McNabb and Hock, 2014). The spatial resolution of a composite image is 60 m for the MSS images and 30 m for the others. We calculated the terminus area changes using a reference line set about 5 km upstream to create a polygon representing the edge of the terminus. Moreover, we investigated the behavior of the tributary and examined the interaction of it to the main stream by the composite images.

Table 6-1: The detail of the Landsat image pairs to derive the velocity field.

Satellite/Sensor	Image1	Image2	Span (day)	Satellite/Sensor	Image1	Image2	Span (day)
Landsat5/TM+	19860716	19860911	57	Landsat7/ETM+	20080830	20081001	32
	19870728	19870829	32		20090427	20090716	80
	19880628	19880806	39		20090716	20090801	16
	19890608	19890827	80		20090801	20090902	32
	19900625	19900812	48		20090902	20090918	16
	19910723	19910925	64		20090918	20091020	32
	19930525	19930728	64		20100601	20100804	64
	19930728	19930813	16		20100804	20100921	48
	19940426	19940715	80		20120419	20120606	48
	19940715	19940816	32		20120606	20120708	32
	19950429	19950515	16		20120816	20120917	32
	19970520	19970815	87		20130321	20130406	16
	19970815	19970925	41				
	19980701	19980928	89	Landsat8/OLI	20130414	20130516	32
	20110806	20111002	57		20130523	20130624	32
					20130624	20130811	48
Landsat7/ETM+	19990705	19990829	55		20130811	20130827	16
	20000504	20000707	64		20130905	20140219	167
	20000730	20001002	64		20140219	20140323	32
	20010327	20010428	32		20140401	20140503	32
	20010421	20010523	32		20140503	20140604	32
	20010523	20010608	16		20140526	20140611	16
	20010608	20010624	16		20140604	20140722	48
	20010701	20010802	32		20140722	20140807	16
	20010802	20010903	32		20140807	20140823	16
	20020307	20020408	32		20140823	20140908	16
	20020408	20020526	48		20140908	20140924	16
	20020526	20020805	71		20141001	20141017	16
	20030411	20030427	16		20141017	20150404	169
	20030427	20030716	80		20150404	20150506	32
	20030716	20030817	32		20150506	20150522	16
	20030817	20031020	64		20150522	20150725	64
	20040413	20040803	112		20150725	20151004	71
	20060505	20060910	128		20151004	20160305	153
	20070609	20070828	80		20160305	20160406	32
	20080424	20080526	32		20160406	20160508	32
	20080526	20080627	32		20160515	20160616	32
	20080627	20080830	64		20160616	20160904	80

6.4 Results

Figure 6-2 shows some samples of the ice speed patterns derived from Landsat images. The results tell us to confirm the normal velocity field, and compare it with that during the active phase. Figure 6-2a, c, and e are the samples associated with surging episodes in 1989, 2001, and 2013, respectively. These panels show the fastest region due to surging is near the terminus. However, the velocity field during the quiescent phase in 1998, 2003, and 2014 are opposite spatial pattern; the speed near the terminus is close to zero, and the upstream portion is fastest, roughly equal to ~1 m/d.

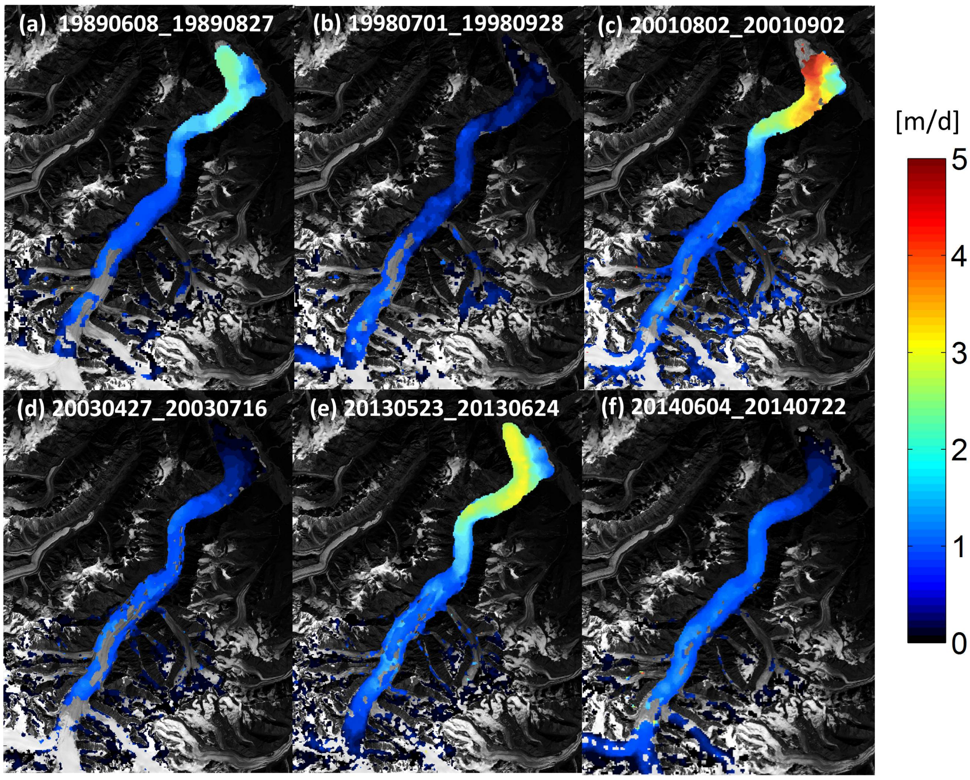

Figure 6-2: Some samples of spatial patterns in ice speed. Please note the color scale is shown as linear scale. The dates in each panel show the acquisition date of the two images used to derive surface speed.

Figure 6-3 indicates the spatial-temporal velocity evolution along the flow line shown in Fig. 6-1 from 1986 to 2014. In 1989, 2001 and 2013, the speed near the terminus appears much greater, by up to 2 m/d, 4.5 m/d, and 3 m/d, respectively, than that during the other years (i.e. quiescent phases, see also Fig. 6-2), which is about 0.5 m/d or less. During the three active phases, the speed-up regions are mostly limited to the ~20-km section from the terminus (see also Fig. 6-2a, c, and e), which we associate below with the shape of the glacier. In terms of seasonal change in ice speed, we can see the variation in the area between 20 and 30 km, with the amplitude of ~0.3 m/d, from 2013 to 2016. This is because the image quality and data frequency of Landsat-8 has been improved, but the amplitude is much smaller than that of surging.

We compare the width of the valley with the velocities associated with the three surging episodes (Fig. 6-4). The initiation of the three surging episodes occurred in the valley at the section between 18 and 22 km from the terminus is about 33% narrower than upstream (Fig. 6-3), which is also an S-shaped valley. Meanwhile, the velocities further upstream do not show any significant temporal changes throughout the analyzed period, maintaining a speed of about 1.0 m/d (Figs. 6-3c and 6-4). Also, the velocity front of ~0.5 m/d (i.e. the boundary between the stagnant and moving part near the terminus) propagates downstream for the 5-year or longer period prior to the 2001 and 2013 active phases (red arrows in Fig. 6-3). The active phase seems to initiate when this front reaches the terminus. In addition, the velocities behind the front clearly indicate a gradual acceleration toward the peak active phases. However, we cannot identify a clear timing of the surge initiation and termination season, which could be due to the multi-year precursory acceleration or a lack of temporal resolution in the available data.

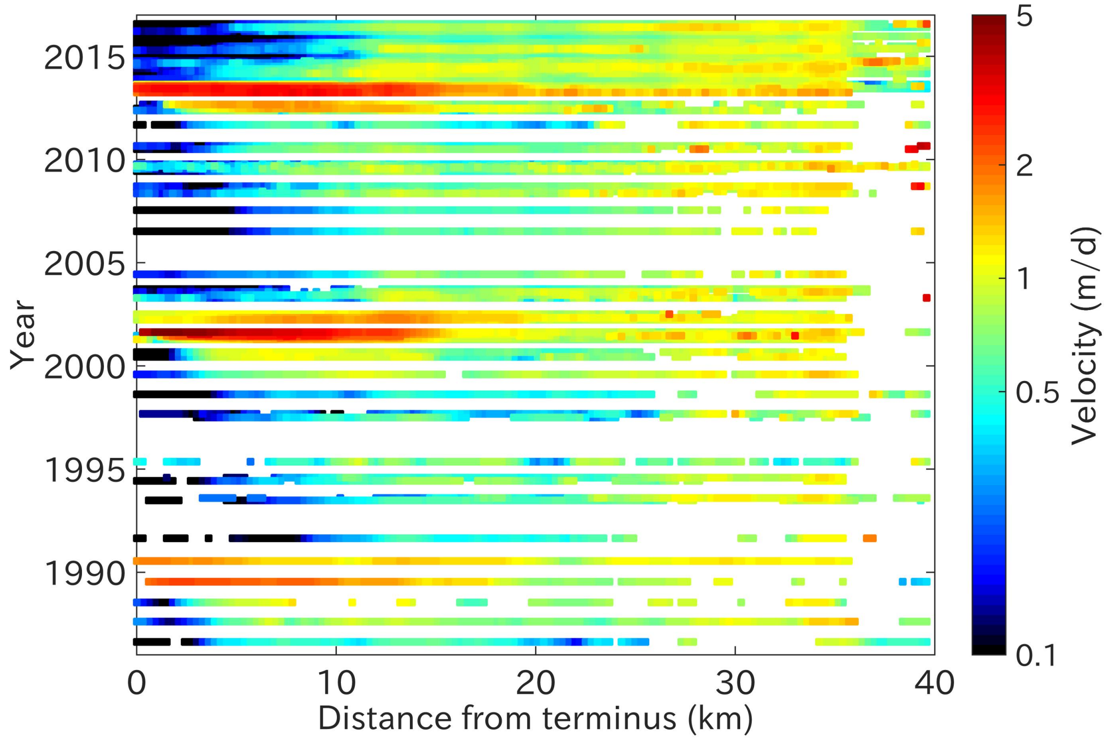

Figure 6-3: Spatial and temporal changes in ice speed along the flow line in Fig. 6-1 between 1986 and 2016. The red arrows indicate the propagation of the velocity front.

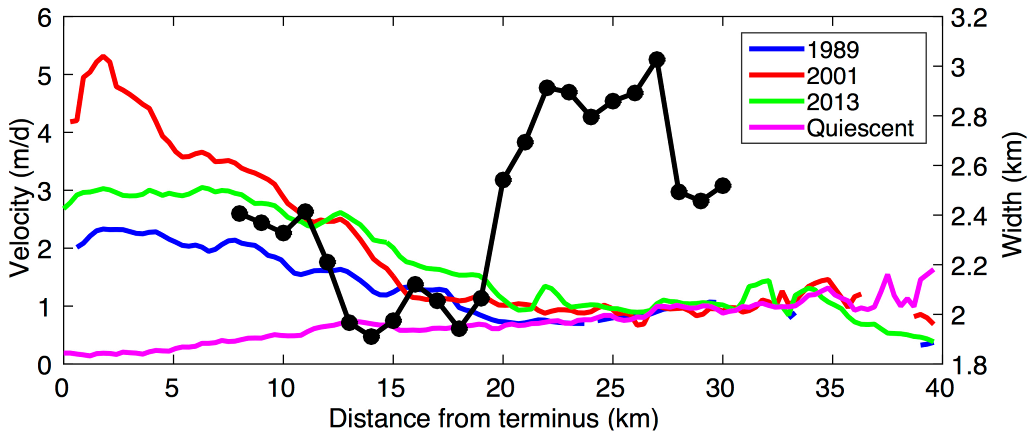

Figure 6-4: Spatial changes in the valley width between 8 and 30 km along the flow-line. The blue, red, and green lines show the ice velocity associated with surging episode in 1989, 2001, and 2003, respectively. The pink line is the averaged velocity between 2003 and 2011 (i.e., the quiescent phase).

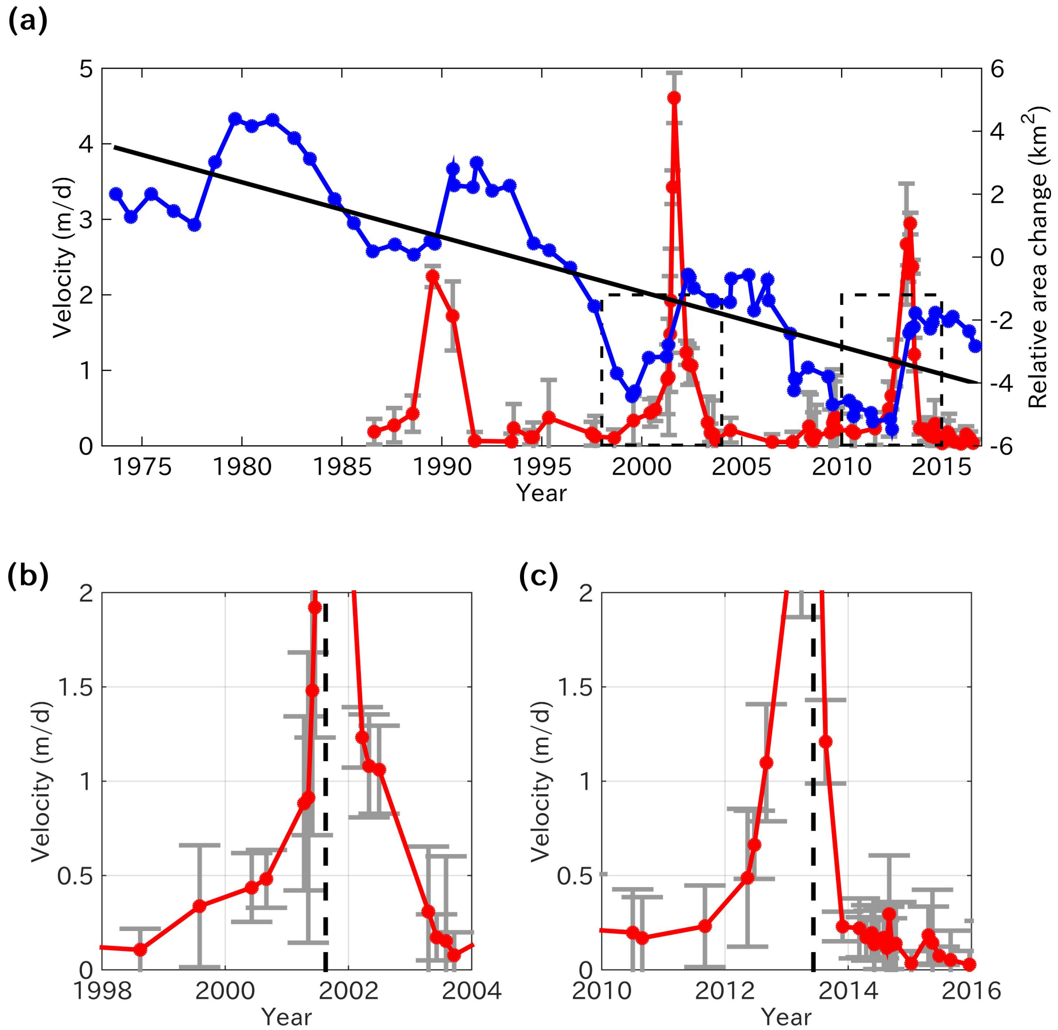

Figure 6-5: Ice speeds and area near the terminus. (a) Temporal changes of the ice speed (red) and the terminus area (blue). The ice speed data are averaged over the section between 0 and 5 km along the flow line shown in Fig. 6-1. The error-bars indicate the mean speed in the non-glacial region. The black line indicates the long-term change of the terminus area. The dotted-line boxes mark the areas shown in (b) and (c). (b) Temporal change of the ice speed associated with the 2001 event. (c) Same as (b) except for the 2013 event. The black-dotted line marks the peak in ice speed during each event.

The red curve in Fig. 6-5 shows the temporal changes of the ice speed averaged over the section between 0 and 5 km from the terminus. This curve has three significant peaks, which correspond to the active phases in 1989, 2001, and 2013 (Figs. 6-3 and 6-4). The peak magnitudes all differ, but the differences are likely due mainly to the coarse temporal sampling of the velocities. In the 2001 event (Fig. 6-5b), the speed starts to gradually increase in late 1998-1999, rapidly increasing in late 2000-2001, and rapidly decreasing in 2003. The evolution of the speed for the 2013 event (Fig. 6-5c) is similar to that for the 2001 event. Namely, the speed starts to gradually increase in late 2011-2012, rapidly increasing in late 2012 and then terminates in late 2013. Although the data do not resolve the exact month or season of the initiation, the duration of the active phase is about 1 year.

The terminus area also changes from 1973 to 2016, with decadal fluctuations superimposed on a gradual decrease. The black line in Fig. 6-5a indicates a long-term rate of decrease of -0.18 km^2/yr, which presumably indicates the negative mass balance trend from recent climate warming (e.g., Luthcke et al., 2013; Larsen et al., 2015). The decadal fluctuations in blue show peaks around 1980, 1991, 2002, and 2014. Comparing those peaks with the speed changes in red, the last three peaks in blue coincide with the last three peaks in the speed data, with a 0-to-2 years-time lag (Fig. 6-5a). These correspondences indicate that the decadal fluctuations in terminus area are attributable to the sudden speed-up of a surge event. During a surge, a significant volume of ice must be rapidly transported to the terminus area, and thus the wax and wane of the terminus area occur with the surge cycle. Although my speed measurements do not go back before 1985, such a surge is likely the reason for the temporal increase of the terminus area around 1980 as well.

There are many looped moraines on the main stream induced by the tributary's surge (Fig. 6-6a). During the period between 1973 and 2016, we observed the two surge events, in 1973-74 (Fig. 6-6b) and 2009-10 (Fig. 6-6e), and couldn't identify any surges between 1974 and 2009.

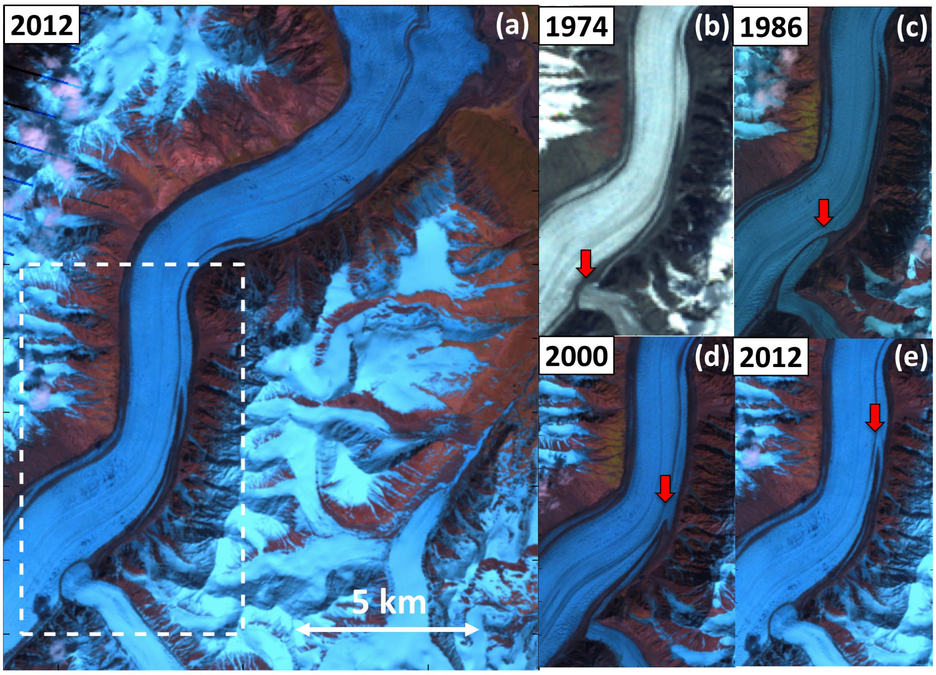

Figure 6-6: Spatial patterns of the looped moraines induced by the tributary surges shown in the Landsat images. (a) The near-terminus region of Donjek Glacier shown in Landsat 7 ETM+ false color composite image acquired on 6 June 2012. The white-dotted box shows the enlarged areas shown in (b)–(e). (b) Snapshot on 19 July 1974 of the moraine movements (red arrow) generated by the 1973–1974 tributary's surge. (c) Same as (b) except 25 July 1986. (d) Same as (b) except 7 July 2000. (e) Same as (b) except 6 June 2012.

6.5 Discussion

Post (1969) developed the first comprehensive map of the distributions of surge-type glaciers near the border of Alaska and Yukon, mostly based on aerial photogrammetry. Donjek Glacier was also identified as a surge-type, presumably from its 1961 surge. However, the timing of past surging events at Donjek Glacier from previous studies includes large uncertainties. Those data sources have very different spatial and temporal coverages than mine, and the active surging was largely judged from morphological observations. For instance, we could not find any descriptions of the activity of the surge at Donjek Glacier in the 1960s. Regarding the 1969 surge, Johnson (1972b) noted that the terminus advance was less than 500 meters, which was much smaller than about 1-km advances of the earlier surges in 1935, 1961, and the recent three surges in 1989, 2001, 2013. However, given the recent observations, we may argue that a mini-surge-like acceleration (so-called pulse) could cause the slight advance of the terminus in 1969, a mini event like the pulse-like events in 1995 and 2009 (Fig. 6-3). In addition, according to Johnson (1972a), there were no observations before 1935. Thus, we cannot say the surge initiated in 1935. Therefore, we do not merge these past events with my findings.

The recurrence intervals between the 1989 and 2001 events and between the 2001 and 2013 events are 12 years (Figs. 6-3 and 6-4a). Although I cannot derive the velocity data before 1985, the similar 12-year fluctuation in terminus area that extends before 1985 strongly suggests that previous surging occurred in the late 1970s. Such a surge is consistent with the previous report of the surge in 1978 (Clarke and Holdsworth, 2002). The 12-year recurrence interval is as short as the latest interval at Lowell Glacier

(Bevington and Copland, 2014). Lowell Glacier experienced five surges between 1948 and 2013, and the surge-cycle recurrence interval (12-20 years) has been shortening over time, which is interpreted as being due to a strongly negative mass balance since the 1970s or earlier (Bevington and Copland, 2014). Variegated Glacier is one of the most famous surge-type glaciers in Alaska, and its surge cycle has been well-studied (Eisen et al., 2001; 2005). Eisen et al. (2001) attributed the variability in the recurrence intervals to the variable annual mass balance. However, in contrast to the Lowell and Variegated Glaciers, whose average recurrence intervals are 15.25 (Bevington and Copland, 2014) and 15 years (Eisen et al., 2005), respectively, the recurrence interval at Donjek Glacier is not only shorter but also apparently less variable over time, which we consider as significant differences despite the three surge-type glaciers sharing a similar climate.

The behavior of Donjek Glacier is similar to Medvezhiy Glacier in Tajikistan (Dolgoushin and Osipova, 1975, Cuffey and Paterson, 2010), in that both have a short recurrence interval (10-14 years) and both have apparent geometrical control of the surging area. Medvezhiy Glacier lies in the West Pamir Mountains, and its surging activity was extensively monitored in the 1960s-70s (Dolgoushin and Osipova, 1975). Medvezhiy Glacier has a wider accumulation area at an elevation of 4600 to 5500 m, but the surges are confined to the 8-km long ice tongue in the narrow valley, separated by a steep ice fall that drops by 800 m per 1 km (Dolgoushin and Osipova, 1975). Although the slope changes on Donjek Glacier are smaller, the significant valley constriction may generate a steep surface slope in the quiescent phase around the narrowing zone due to the mass transport from upstream. Figure 6-7 shows the slope angles along the flow line used in Fig. 6-1 derived from three ASTER DEMs (blue in 28

September 2001, red in 26 May 2002, green in 30 September 2016) and ASTER GDEM (pink). The Black line shows the width of the valley. Although GDEM is composite DEM and we don’t know the exact date, all the three curves indicate peaks around 18.5 and 22 km point. The former point corresponds the initiation point of S-shape valley, and the latter is that of narrowing valley. These indicate that the valley constriction could generate the slope steepening. Moreover, comparing the blue and red curve especially in the section between 18 and 19.5 km, the slope in 2002 (red) is clearly larger than that in 2001 (blue). This is consistent with our suggestion that the ice had been thickened after the peak speed in the 2001 episode. In addition, assuming that ASTER GDEM stands for the condition immediately before the 2013 episodes, the slope in 2016 (green) could show ice thinning due to rapid ice transport in 2013. Thus, the localized ice thickening and the apparent regularity of the recurrence interval may be due to the narrowing zone and rather steady flow speed upstream. Moreover, we consider that the surge is independent from the tributary’s surge. This is because the interval of the tributary’s surge is 36 years, which is much longer than that of the main stream’s.

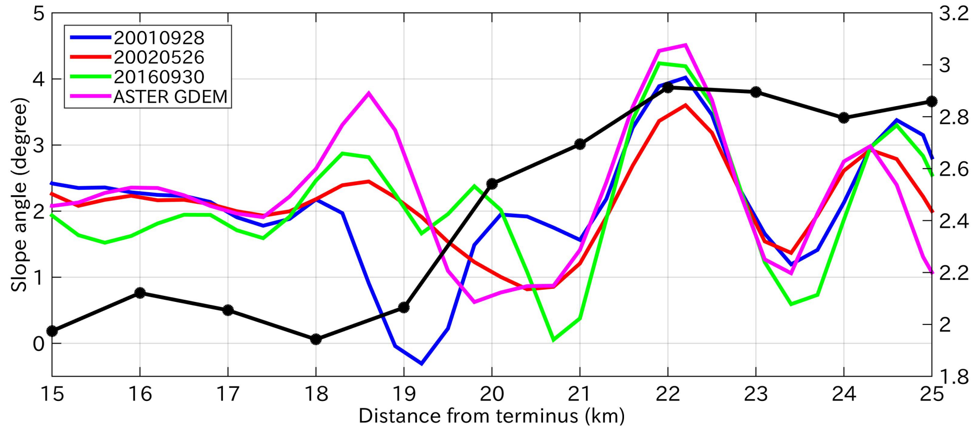

Figure 6-7: Slope angles along the flow line used in Fig. 6-1. The blue, red and green line show the slope angle derived from three ASTER DEMs on 28 September 2001, and 26 May 2002, and 30 September 2016, respectively. The pink line shows the angle derived from ASTER GDEM. The black line shows the width of the valley.

At Medvezhiy Glacier, the observed maximum speed exceeds 100 m/d, and the active phase initiates in winter, lasting about 3 months (Cuffey and Paterson, 2010). At Variegated Glacier, the surge also initiates from fall to winter and the maximum speed is 50 m/d during the 1982-1983 surge (Kamb et al., 1985). At Bering Glacier, a similar behavior (speed exceeding 10 m/d, and winter initiation) is observed in the 2008-2011 surge (Burgess et al., 2012). The recurrence interval is about 18 years. Similar behavior has also been confirmed at Lowell Glacier (Bevington and Copland, 2014). These sudden speed-ups in fall-to-winter and rapid slow-downs in early summer are thought to arise from the hydrological regulation mechanism. The mechanism, which involves a destruction of tunnel-like channels and subsequent change into a linked-cavity system that increases the water pressure, has been proposed based on detailed observations of the 1982-1983 surge at Variegated Glacier (Kamb et al., 1985). Thus, such surges are often termed an Alaskan-type surge. Meanwhile, our observed maximum speed reached at most ~ 5 m/d and we couldn't determine the initiation season. It is likely, however, that I have missed much higher speeds and winter initiation due to the coarse temporal resolution in our velocity data and difficulties for optical image matching caused by the lack of identifiable surface features when the glacier is snow-covered. The 12-year recurrence interval is apparently shorter than that in a Svalbard-type surge, whose cycle is thought to be 50 years or much longer (Murray et al., 2003; Jiskoot, 2011). Moreover, the active duration is much shorter than that of Svalbard-type, and the flow speed seems to have rapidly slowed down after the active phase. The observed multi-year acceleration may include small acceleration events or mini-surges that redistribute thickening and thinning (Raymond and Harrison, 1988; Harrison and Post, 2003) during the build-up phase. Thus, we consider that the surge phase of the two events is about 1 year, and that Donjek Glacier presumably has the Alaskan-type surge.

Based on these findings, we argue that the cyclic surging at Donjek Glacier occurs as follows. In the quiescent phase, ice delivered from the upstream area stores up at the highly narrowed area (Fig. 6-1), causing local thickening. The ice thickening generates a steeper slope (Fig. 6-7) with a corresponding higher driving stress. When the ice thickness reaches a critical value, the glacier starts to speed-up. I do not claim, however, that this driving stress itself is high enough to initiate the surging; that is, the thickening of ice and steeper slope are not the direct cause of surging. Rather, thickened ice upstream is just a pre-condition prior to surging. But as the ice thickness increases, the volume of englacial water storage will also increase, which can supply a greater basal water flux and increase its pressure, thereby allowing the higher speed during the surging event (Lingle and Fatland, 2003; Abe and Furuya, 2015). During the surge, the inefficient subglacial drainage system and the sufficient englacial water volume can maintain higher velocity. After the mass re-distribution terminates, the thickness in the reservoir zone will again increase for the next event.

The next event of Donjek Glacier is likely to occur around 2025. To test the model proposed here, we need detailed observations of not only ice velocities but also the associated geometric and hydrological changes.

6.6 Concluding remarks

We examined the evolutions of the terminus area (1973-2016) and ice speed (1986-2016) at Donjek Glacier in Yukon, Canada, inferred from Landsat-series optical images. The results showed the surging events have been occurring every twelve years (1989, 2001, and 2013), and the interval has been short and constant. The surging area is limited within the ~20km section from the terminus, originating in an area where the flow width significantly narrows downstream. Our results suggest strong control of the valley constriction on the surge dynamics.

Chapter 7

Surge dynamics of Steele Glacier in Yukon, Canada, revealed by multi-satellite images

Paper will be submitted soon

Abe, T., M. Furuya, and D. Sakakibara, Surge dynamics of Steele Glacier in Yukon, Canada: the 2011-2016 surging episode, *in preparation*.

7.1 Introduction

Surge-type glaciers are characterized by quasi-cyclic oscillations between a short active phase defined by rapid ice motion and decades-long quiescent phase with slow ice motion. During the quiescent phase, the lower part of glacier is stagnant or gradually retreats with the ice thinning. During the active phase, it accelerates and thickens significantly, which sometimes causes terminus advance. On the other hands, the upper part of glacier thickens during the quiescent phase, and it thins in the active phase as the ice is transported from upstream to downstream. Surge-type glaciers are distributed in certain areas (e.g., Post, 1969) and some recent studies have been trying to classify them and other normal glaciers in terms of climatic, geometric, and sediment size of bed rock (Sevestre and Benn, 2015; Crompton and Flowers, 2016). Moreover, there is a diversity of the behaviors among surge-type glaciers (Herreid and Truffer, 2016).

Murray et al. (2003) suggested that there are at least two distinct surge mechanisms of Alaskan temperate-type, and Svalbard polythermal-type, inferred from the maximum speed and the period of the active phase. The Alaskan-type surges often abruptly initiate in winter and terminate in summer with a-few-year active phase (e.g., Kamb et al., 1985; Harrison and Post, 2003). On the other hand, the Svalbard-type surges gradually initiate and terminate after a longer active phase than five years (Fowler et al., 2001; Murray et al., 2003). Their maximum flow velocities and recurrence intervals also differ, with the Svalbard-type surge having lower maximum flow velocity and longer recurrence interval (several decades or more). These different behaviors seem to indicate different physical mechanisms, specifically between hydrological regulation for the Alaskan type and thermal regulation for the Svalbard type. However, Yasuda and Furuya (2015) have recently shown seasonal modulation of faster speed in winter during the active surging phase of Svalbard-type at West Kunlun Shan. They suggest the importance of englacially stored water from surface melting in Svalbard-type surge. This indicates there are some similarities in both surge generation mechanisms. Thus, the generation and maintenance mechanisms of glacier surge have not been fully understood.

Near the border of Alaska and Yukon, Canada, there are many surge-type glaciers, of which almost all were identified by Post (1969). Many surge-type glaciers in the area have been studied over a few decades by ground-based and remote sensing observations (Clarke et al., 1984; Kamb et al., 1985, Fatland and Lingle, 1998, Truffer et al., 2000, Eisen et al., 2001; Lingle and Fatland, 2003; Burgess et al., 2012; Bevington and Copland, 2014). However, there remain some questions about the understanding of surge dynamics. First, where does it initiate? In a quiescent phase, ice thickens in the reservoir area and thins in the receiving area, which is generally different from the so-called accumulation and ablation zone (Cuffey and Paterson, 2010). In an active phase, the ice is transported from reservoir area to receiving area through a high basal sliding. What factors can really control the area of surge onset? Second, what keeps such a faster speed during the active phase of a few months to years? Linked-cavity model described by Kamb (1987) has been proposed in order to explain high basal water pressure during the 1982-83 Variegated Glacier's surge. To explain the high speed, however, large amount of water is needed to supply at the base. This theory has also been widely applied to explain seasonal speed-up in early summer because there is enough surface meltwater volume to be supplied into a glacier. On the other hand, there is no meltwater on glacier surface in winter, and it remains unclear what maintains active basal sliding without water input from the surface. Indeed, the last part of the introduction in Kamb (1987) states “The discussion concentrates on the mechanism of surging in spring and summer when relatively large amounts of water are available to the basal water conduit system. The surge mechanism in wintertime can be considered by extending the concepts developed here to conditions of low water flow; this will be done in a subsequent paper”. The origin of water to maintain high speed in winter remains unclear. To address these questions, diverse datasets with high temporal resolution are indispensable. Here we used multi-satellite images to derive ice speed, ice thickness change, moraine movement, focusing on the recent surge at Steele Glacier in Yukon, Canada, and try to answer the questions mentioned above.

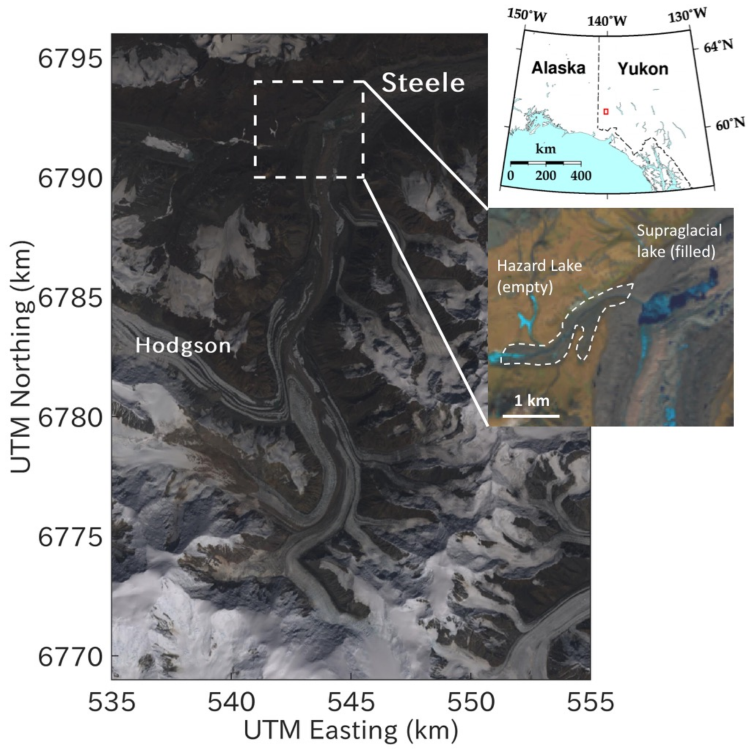

Figure 7-1 Location and entire image of Steele Glacier. Background is the Landsat 8 image acquired on 22 May 2015. The white-dotted box shows the enlarged area shown in the middle-right panel. Middle-right panel: The location of Hazard Lake and the supraglacial lake are shown in the false-color composite image of the Landsat 8 image.

7.2 Steele Glacier

Steele Glacier (the former name is Wolf Creek Glacier) is located in the St. Elias Mountains, near the border between Alaska and Yukon, Canada (Fig. 7-1). Its length is about 40 km (Clarke and Holdsworth, 2002). Steele Glacier is identified as a surge-type glacier by aerial photogrammetry (Post, 1969). The surge of Steele Glacier in 1965-67 drew much scientific attentions (Clarke, 2014) and some studies about the surge have been reported in this glacier (e.g., Bayrock, 1967; Stanley, 1969). The thermal structure in the ice body after the surge of Steele Glacier was examined (Jarvis and Clarke, 1974; Clarke and Jervis, 1976), which implies it is polythermal surge-type glacier. Thus, the thermal control has been considered a surge generation mechanism (Jarvis and Clarke, 1974; 1975; Clarke and Jarvis, 1976). Recent airborne laser altimetry revealed that the mass balance was -0.18 m w.e. yr^{-1} (Larsen et al., 2015). However, the spatial and temporal variations of the ice speed and the ice thickness remain uncertain.

The Hazard Lake is a surge-dammed lake located in the western margin of Steele Glacier (Fig, 7-1), which is filled by damming of Steele's surge. The previous surge in 1965-67 filled the lake and the cyclic drainage events have been studied (Collins and Clarke, 1977; Clarke, 1982). At the present, a supraglacial lake has been formed on Steele Glacier (Fig. 7-1).

Hodgson Glacier, a western tributary of Steele Glacier covering an area of 100 km^2, has been also well-known and often compared with Steele Glacier (Fig. 7-1). During and after the previous surge of Steele Glacier, it also advanced 3 km down the Steele valley (Stanley, 1969). This Hodgson's surge might have been triggered by the Steele's surge (Clarke and Holdsworth, 2002).

7.3 Data and method

In this study, we used SAR and optical images to track the temporal changes in ice speed distribution. Terra/ASTER DEM was used to derive ice thickness changes due to surge event. Moreover, we created false color composite images from Landsat-series images to investigate the spatial patterns of looped moraines. Details of the data processing is described below.

7.3.1 ALOS and Sentinel-1A SAR images

ALOS is Japanese L-band SAR satellite, launched in January 2006 and terminated its operation in May 2011. PALSAR onboard ALOS uses microwave, which is advantageous over optical sensor because it can image the Earth regardless of weather and time. Moreover, L-band penetrates glacier surface and scatters off at internal glacier features, allowing the return signals of SAR to keep coherent between two image acquisitions, even if the glacier surface loses its feature and/or has changed due to heavy snowfall.

Sentinel-1A is European C-band SAR satellite operated under the Copernicus program by ESA, and it was launched in April 2014. The SAR sensor SAR-C is operated with the Terrain Observation by Progressive Scans (TOPS) mode that can cover an wider area of 250×250 km^2 than that of ALOS/PALSAR strip map mode.

We used ALOS/PALSAR raw data acquired from December 2006 to March 2011, and Sentinel-1A/SAR-C SLC data acquired from June 2016 to September 2016. The detail of the dataset is listed in Table 7-1. Gamma software was used to generate SLC images (Wegmüller and Werner, 1997).

Table 7-1: Data sets of SAR images used in this study.

Satellite/Sensor	Path/Frame	Master	Slave	Mode	Bperp (m)	Span (day)
ALOS/PALSAR	243/1220	20061230	20070214	FBS-FBS	1342	46
		20070817	20071002	FBD-FBD	425	46
		20080102	20080217	FBS-FBS	1041	46
		20090104	20090219	FBS-FBS	652	46
		20090822	20091007	FBD-FBD	566	46
		20091007	20100107	FBD-FBS	726	92
		20100107	20100222	FBS-FBS	794	46
		20100825	20101010	FBD-FBD	505	46
	244/1220	20070116	20070303	FBS-FBS	1554	46
		20070903	20071019	FBD-FBD	474	46
		20071019	20080119	FBD-FBS	799	92
		20080905	20081021	FBD-FBD	672	46
		20090908	20091024	FBD-FBD	419	46
		20101027	20110127	FBD-FBS	997	92
		20110127	20110314	FBS-FBS	840	46
Sentinel-1A/SAR-C	123/1	20160629	20160723	IW-IW	104	24
		20160723	20160909	IW-IW	-100	24

FBS: Fine Beam Single polarization mode, FBD: Fine Beam Double polarization mode
IW: Interferometric Wide swath mode

7.3.2 Landsat optical images

Landsat optical images were used to examine the ice speed evolution from 2007 to 2016. Although there were many available images acquired before 2006, we could not derive the velocity field due to the slow speed of ~ 0.4 m/d in the quiescent phase. Thus, we used Landsat 7 Enhanced Thematic Mapper Plus (ETM+), and the Landsat 8 Operational Land Imager (OLI), distributed by the USGS, to derive average velocity field using two images with a time interval of a few months. Since 2013, only Landsat-8 images were used to calculate surface speed because of high quality and image acquisition frequency. Both band 8 panchromatic images of Landsat 7 and 8 were used to calculate surface velocity because of the highest spatial resolution (15 m) in the product.

Table 7-2: Data sets of Landsat image pairs used in this study.

Satellite/Sensor	Image1	Image2	Span (day)	Satellite/Sensor	Image1	Image2	Span (day)
Landsat7/ETM+	20080424	20081001	160	Landsat8/OLI	20140823	20140908	16
	20090427	20091020	176		20141017	20141127	41
	20100516	20100921	128		20150215	20150404	48
	20110627	20110830	64		20150404	20150506	32
					20150506	20150522	16
Landsat8/OLI	20130414	20130516	32		20150529	20150614	16
	20130523	20130624	32		20150709	20150725	16
	20130624	20130811	48		20150902	20151004	32
	20130905	20131108	64		20151004	20151020	16
	20131108	20140203	97		20160218	20160305	16
	20140219	20140323	32		20160305	20160406	32
	20140401	20140503	32		20160406	20160422	16
	20140503	20140604	32		20160422	20160508	16
	20140611	20140713	32		20160515	20160531	16
	20140807	20140823	16		20160531	20160616	16

7.3.3 Terra/ASTER DEMs

ASTER is one of the high-performance optical sensors onboard Terra, which can acquire 15 m-resolution image. Since June 2016, the new ASTER product ASTER-VA including digital elevation model has been downloadable. We can explore the data in METI AIST satellite Data Archive System. We searched the products, including non-cloud-covered images, and selected 4 images on 1 April 2006, 30 August 2011, 28 May 2015, and 3 September 2016.

7.3.4 Feature tracking for deriving ice speed

We selected 15 pairs of ALOS/PALSAR images, 2 pairs of Sentinel-1A images, and 29 pairs of Landsat optical images to derive the glacier velocity (Table 7-1 and 7-2).

The feature tracking method for SAR images used in this chapter basically follows that in Strozzi et al., (2002), Yasuda and Furuya (2013), and that in Chapter 4. We set a search patch of 64 × 192 and 160 × 32 pixels (range × azimuth) with a sampling interval of 4 × 12 pixels and 20 × 4 pixels for ALOS and Sentinel-1A, respectively. The FBD data for ALOS/PALSAR were oversampled in the range direction (i.e., satellite to ground direction) due to the difference of the range dimension so that it is the same as that of the FBS data.

In the feature tracking using SAR data, we corrected for a stereoscopic effect known as an artifact offset over rugged terrain (Strozzi et al., 2002; Kobayashi et al., 2009), which is caused by the separation between satellite orbital paths, and the effect of foreshortening also generates the offsets. We reduced the artifact by applying an elevation-dependent correction, incorporating ASTER GDEM version 2 data with 30-m resolution. We applied the same method followed by Kobayashi et al. (2009) and confirmed that there remained few topography-correlated artifact offsets.

Using both range and azimuth offset field, we derived the surface velocity fields (Fig. 7-2) based on the parallel flow assumption (Joughin et al., 1998). Although this assumption is not entirely correct, we can derive 3D surface velocity field using both range and azimuth offset data. I estimated the measurement error to be 0.02 m/d, from the mean displacement in non-glacial area.

We also processed Landsat images with a similar feature tracking technique. The procedure is the same as that in Chapter 6, using the Cross-Correlation in Frequency domain on Orientation images (CCF-O) algorithm (Fitch et al., 2002; Haug et al., 2010; Sakakibara, 2016). The basic strategy is to calculate cross-correlation coefficients between two images, and the distance of correlation peaks of the two images was considered as a movement of glacier. We set the reference window size as 30×30 pixels, and the search window size as 50×50 pixels with a sampling interval of 6×6 pixels. After implementing the CCF-O, the filtering was performed to remove the outliers and to smooth the results. The velocity error of ice speed is estimated as 0.14 m/d and the mean velocity error both SAR and optical images is 0.1 m/d.

7.3.5 Surface elevation change

We used Terra/ASTER DEMs distributed from MADAS to derive surface elevation change. At first, we removed some outliers on each DEM whose difference are larger than 100 m compared to AW3D30, but the threshold was set 250 m for the image on 2016 due to large elevation changes. Then, the scene offsets between two images were estimated in off-glacial area. After performing the procedure, we calculated surface elevation changes using multi-ASTER DEMs. The errors are ~ 10 m, which is estimated from non-glacial area.

7.3.6 False color composite images

In order to grasp spatial pattern and its temporal evolution of looped moraine, we derived false color composite images from 1973 to 2016, to easily recognize glacier and others. The detail of how to generate the images is described in Chapter 3, which is the same method as used by McNabb and Hock (2014). Using the images, we created animated image sequences. Although this method seems to be less quantitative than that of deriving exact rates of glacier changes, the information of seeing animations of the individual images can provide insight into glacier dynamics (Paul, 2015).

7.4 Results

7.4.1 Ice speed evolution between 2007 and 2016

Using SAR and Landsat optical images, we derived the ice speed evolution of Steele Glacier associated with the recent surging episode. Figure 7-2 shows some examples of the ice velocity fields. Normally, the speed of Steele glacier in 2007 and 2011 were up to 0.4 m/d in a few kilometers upstream from the confluence of Steele and Hodgson Glaciers (Fig. 7-2a and b). The velocity-front defined by the border between the stagnant and moving part is located at 2 km upstream from the confluence. In 2013, the glacier accelerated to the speed of 1 m/d at the front, and the velocity-front advanced by about 5 km (Fig. 7-2c). The speed further increased up to 5 m/d in 2014 (Fig. 7-2d), and the maximum speed was more than 20 m/d in early summer 2015 (Fig. 7-2e). Then, the ice speed decreased at a rate of 2.5 m/d in 2016 (Fig. 7-2f). The traveling distance of the velocity-front was about 19 km comparing the fields in 2007 to that in 2016 (Fig. 7-2a and f).

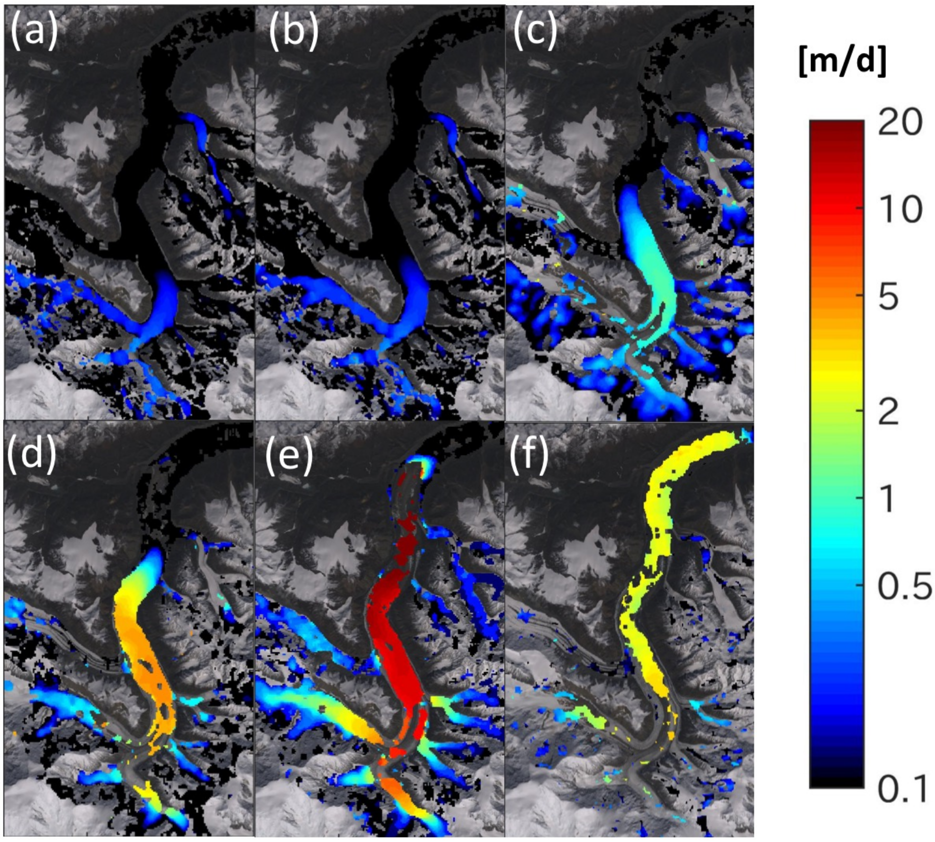

Figure 7-2 Examples of the velocity fields from ALOS/PALSAR, Landsat 8, and Sentinel 1A images. Background is a Landsat 8 image acquired on 4 August 2015. (a) and (b) are derived from ALOS/PALSAR image pairs from 16 January 2007 and 3 March 2007, 27 January 2011 and 14 March 2011, respectively. (c)-(e) are derived from Landsat 8 image pairs from (c) 24 June 2013 and 11 August 2013, (d) 11 June 2014 and 13 July 2014, (e) 29 May 2015 and 14 June 2015. (f) is derived from Sentinel-1A image pair from 29 June 2016 and 23 July 2016, respectively.

The ice speed evolution associated with the surge event is summarized in Figure 7-3. We set the flow-line from the tongue (Fig. 7-3a), and calculated the averaged speed over

7 × 7 pixels every 300 m along the flow-line (Fig. 7-3b). The velocities from 2007 to 2011 were less variable in the upstream region higher than 20 km point, with a speed of ~0.4 m/d, whereas it stagnated downstream. The velocity-front stayed at 22 km point from the terminus. Although we could not derive the speed data between late 2011 and early 2013 because of the termination of ALOS/PALSAR operation and non-availability of Landsat 7 image pairs, the speed in 2013 shows an apparent acceleration near the 20-km section. Then, it further sped-up in 2014 and up to over 20 m/d at the 12-km point in early summer 2015. After the peak, the speed slowed-down to ~1 m/d at the 5-km point in fall 2016. In total, the velocity-front traveled from 22 km to 3 km point between 2011 and 2016 (Fig. 7-3b).

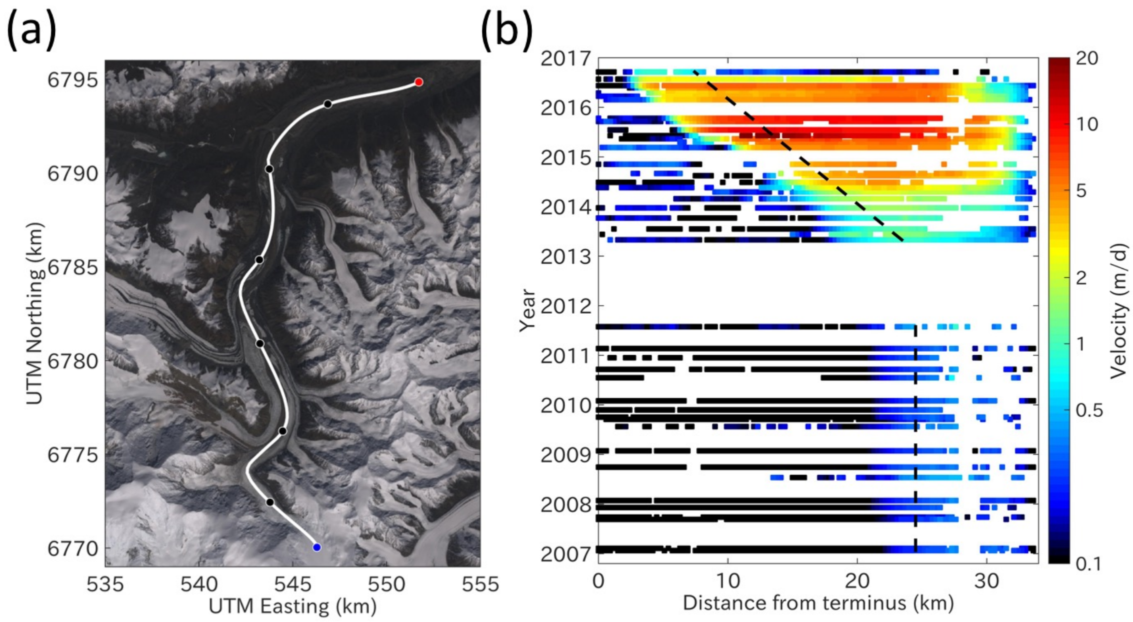

Figure 7-3 (a) Central flowline on Steele Glacier. The red and blue dots show the lower and upper most points, whereas the black dots mark 5-km intervals. The total distance between red and blue dots along the flowline is close to 35 km. (b) Ice speed evolution between 2007 and 2016 along the flow-line shown in (a). The color scale is given in a logarithmic scale. The black-dotted line shows the flowline for Figure 7-4.

Next, we examined the detailed temporal changes in the ice speed (Fig. 7-4), calculating from averaging ice speed data every 300 m along the line given in Fig. 7-3b. This is because the seasonal changes between 2013 and 2016 were observed in the faster velocities than that before 2011, especially over the for a few kilometers' section behind the velocity-front (Fig. 7-3b). As seen in Figure 7-3b, the speed between 2007 and 2011 was almost stable at ~0.4 m/d (Fig. 7-4a), but there were small seasonal speed-ups in each summer (Fig. 7-4b). Although there are no data between late 2011 and early 2013, the speed in 2013 was much faster than that in early 2011 (Fig. 7-4c). The speed, thereafter, accelerated from 2013 to 2014, but the seasonal speed-ups were taking place every early summer in both 2013 and 2014. It reached up to 21.6 m/d in early summer 2015 with a further rapid acceleration. After the peak speed was achieved, the speed rapidly slowed down to 8 m/d in the late summer. In 2016, it further slowed down to less than 1 m/d although the summer speed-up was observed in the early summer.

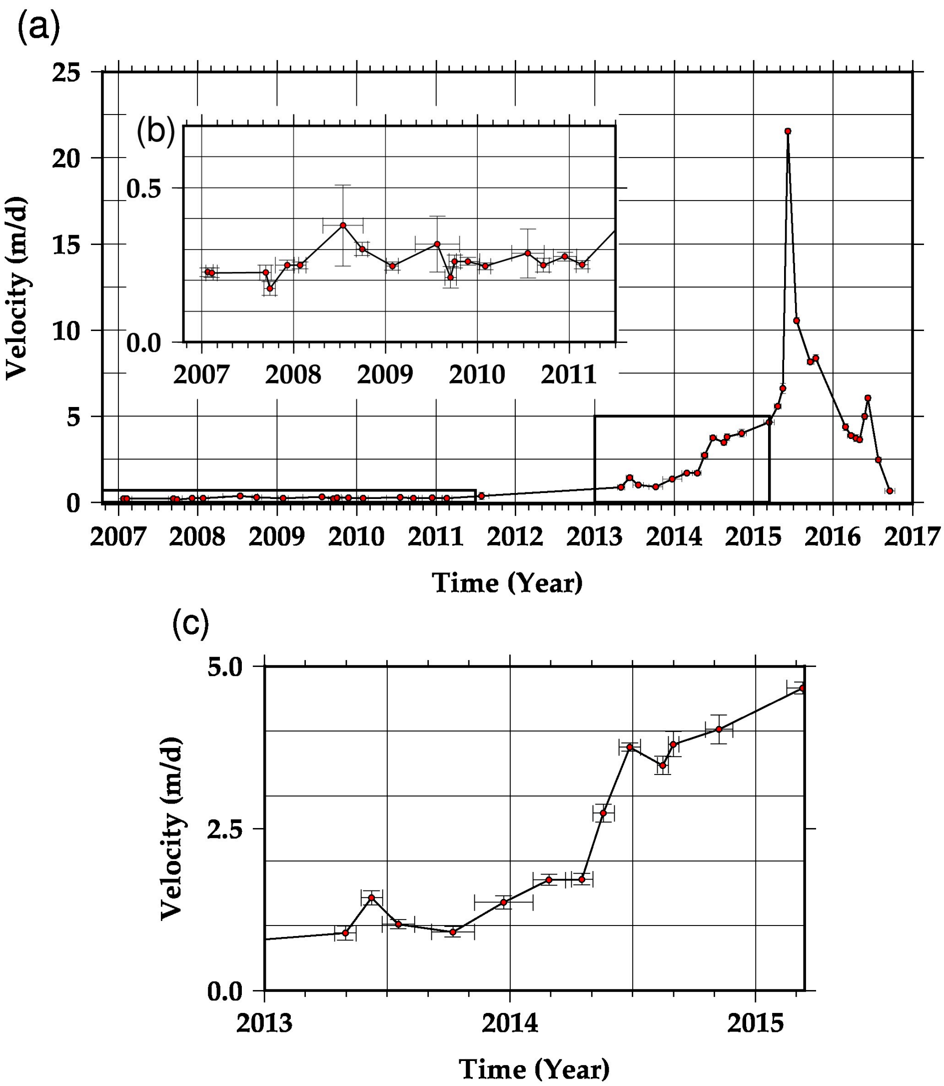

Figure 7-4 Temporal changes in ice speed along the flowline shown in Fig. 7-3b. The horizontal error-bars indicate the interval of the image pairs and the vertical do the mean speed in the non-glacial region. The black-line boxes mark the areas shown in (b) and (c). (b) Temporal change of ice speed in the quiescent phase; 2007-2011, (c) Same as (b) except for the build-up phase; 2013-2014.

7.4.2 Ice thickness changes due to active surging

Figure 7-5 shows the spatial and temporal changes in the ice thickness associated with the surging event, derived from multi-Terra/ASTER DEMs. Between 2006 and 2011, it thickened by ~25 m in the upstream above the confluences between Steele and Hodgson Glaciers, whereas it thinned by ~30 m in the middle and downstream (Fig. 7-5a). Between 2011 and 2015, the ice thickened in the middle section by 80 m (Fig. 7-5b), while thinning in the upstream section by ~65 m (Fig. 7-5b). Between 2015 and 2016, the thickened region moved toward downstream, further thickening by 150 m (Fig. 7-5c), whereas the length of the thickened region seemed to become shorter than previously. Moreover, in the two upstream tributaries, the ice thinning was confirmed. Throughout this surge, Hodgson Glacier did not show any changes in the ice thickness.

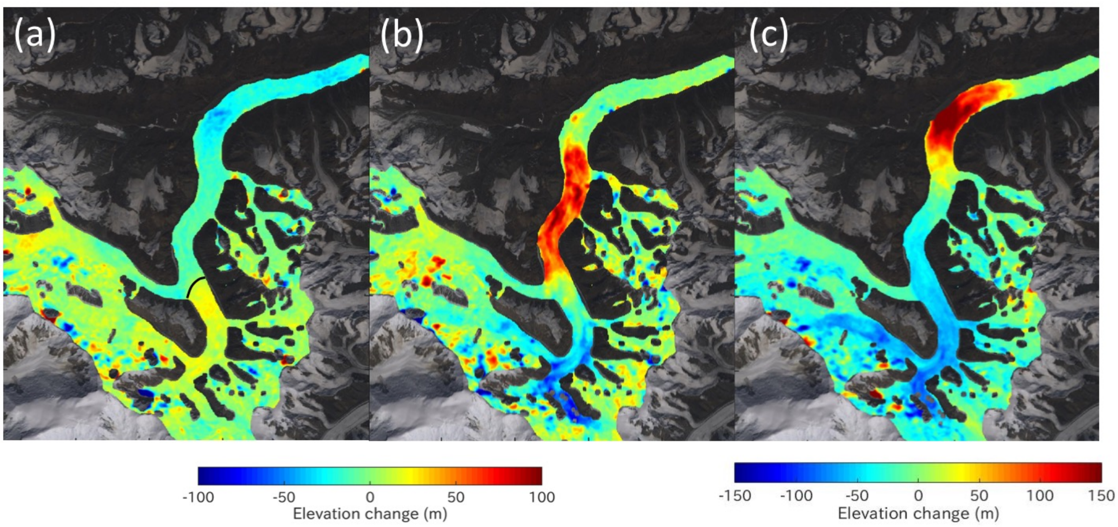

Figure 7-5 Spatial distribution of ice thickness change due to surging episode. The black line indicates the DBL. (a) Spatial patterns of elevation change in the quiescent phase; 2006-2011, (b) Same as (a) except for the build-up phase; 2011-2015, (c) Same as (a) except for the active phase; 2015-2016. Note that the color scales differ from each image.

7.4.3 Spatial and temporal changes of looped moraines

False color composite image sequences based on Landsat-series optical images from 1973 to 2016 clearly show that some looped moraines are present and moved downstream on the Steele Glacier during the four decades (Fig. 7-6a). Comparing the image in 1974 to that in 1997, the looped moraine between Hodgson and Steele Glaciers expanded toward eastern side of Steele Glacier (Fig. 7-6b). In 2014, the ice speed of Steele Glacier accelerated and it pushed the ice body from Hodgson Glacier (Fig. 7-6c). Further speed-up of Steele Glacier pushed and cut the moraines toward downstream (Fig. 7-6e).

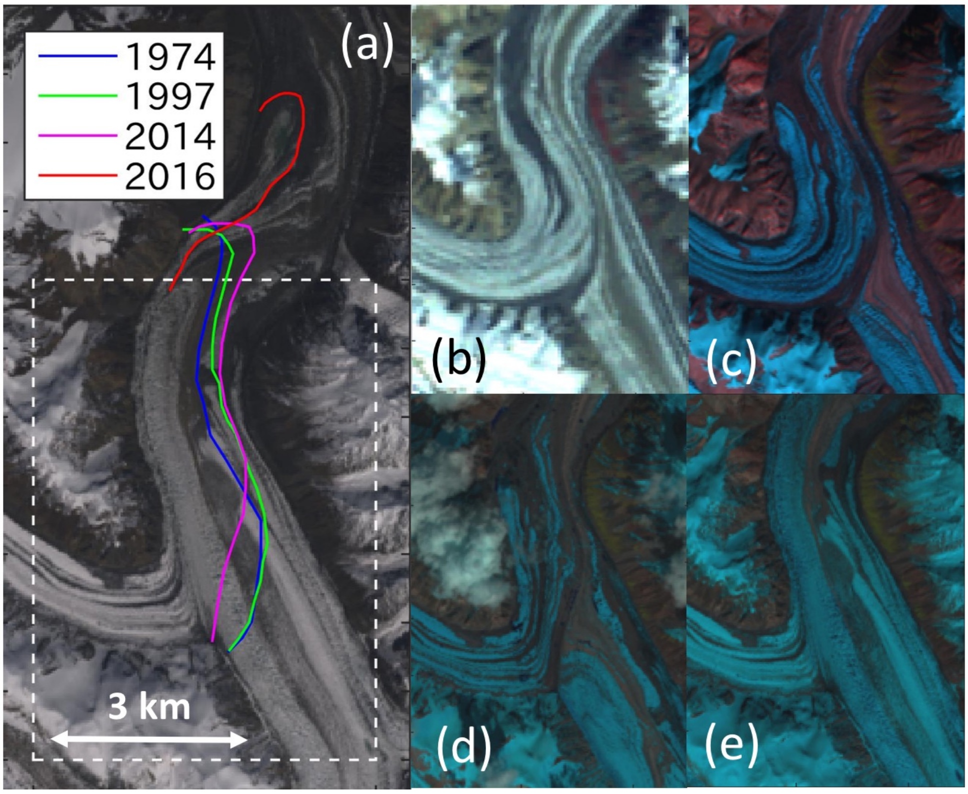

Figure 7-6 (a) Spatial patterns and the temporal changes of looped moraines on Steele Glacier shown on the Landsat true color composite image acquired on 16 June 2016. The white-dotted box shows the enlarged areas shown in (b)-(e). (b) Snapshot on 18 July 1974, (c) Same as (b) except 15 August 1997, (d) Same as (b) except 11 June 2014, (e) Same as (b) except 16 June 2016.

7.4.4 Drainage of supraglacial lake and formation of Hazard Lake

The false color composite images also revealed the formation and drainage of the supraglacial lake on Steele Glacier at the 8-km point from the terminus (Fig. 7-1 and 7-3a). Until the mid 2015, the supraglacial lake has been repeatedly filled and drained (Fig. 7-7a-c). The tunnel outlet from the glacier is shown by the white lines in Figure 7-7a-c following Clarke (1982). When the peak speed was achieved in early summer 2015, the velocity-front arrived at the point (Fig. 7-3b), breaking down the supraglacial lake (Fig. 7-7d, and e). In the late 2015, the Hazard Lake initiated to be filled and continued until June 2016 (Fig. 7-7f). The newly formed outlet is located at the western margin of the glacier (Fig. 7-7f). At September 2016, the lake has been still filled and undrained. The area of the lake is about 1 km^2, which is similar to that formed in the 1965-67 surge (Collins and Clarke, 1977).

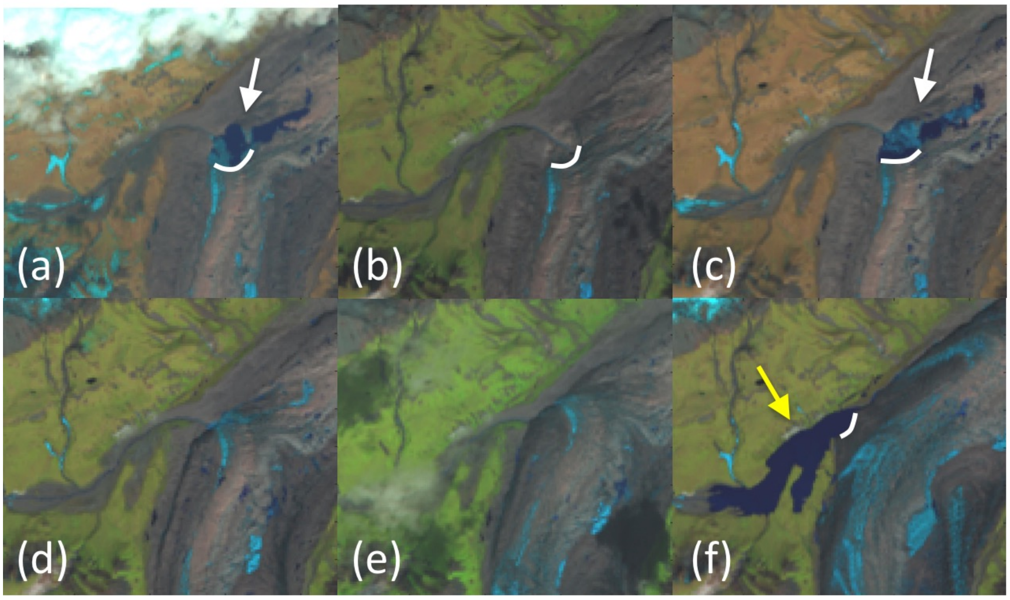

Figure 7-7: Spatial extent of supraglacial lake (white arrows in a and c) and formation of Hazard Lake (yellow arrow in f). The false-color composite images were derived from Lantsat-8 taking on (a) 26 May 2014, (b) 23 August 2014, (c) 22 May 2015, (d) 14 June 2015, (e) 16 July 2015, (f) 16 June 2016. The white lines indicate the outlet tunnel from glacial inside. The Hazard lake is filled in (f).

7.5 Discussion

The previous surge of Steele Glacier in 1965-67 has been reported by some authors (Bayrock, 1967; Stanley, 1969; Clarke and Holdsworth, 2002). Stanley (1969) showed that the surge initiated in late 1965, and a large wavelike-bulge was confirmed moving down by summer 1966. The peak speed was 24 m/d in early 1966. At the beginning of 1968, the speed was dwindling down to 1 m/d. The latest surge in this study has many similarities to this previous episode in 1965-67. The observed peak speed was 23 m/d in early summer 2015, and the speed in late 2016 was down to 1 m/d. Our observed data show the surge initiated about 3-4 years before the speed peak was achieved, that ranges from late 2011 to early 2013 (Fig. 7-3 and 7-4). Although we have no velocity data between late 2011 and early 2013 due to the lack of available data, RADARSAT-2 images showed the upstream speed in February-March 2012 was nearly double as fast as that in January-February 2011 (Waechter, 2013), which suggests that the recent surge initiated in 2011. The previous observations did not seem to capture the detail of pre-surge and the surging behaviors in terms of ice speed, whereas aerial photographs by A. Post showed extensive crevasses that formed during the initial phase of the surge (Stanley, 1969). The spatial and temporal changes in the velocity distribution and ice thickness have much information about the recent surge evolution, which can help us to better understand the surge triggering mechanisms.

The detailed evolutions of ice speed derived from SAR and optical images clearly tell where the surge initiates. Figure 7-3 indicates that the initiation point was the confluence of Steele and Hodgson Glaciers. The downstream area below the confluence was nearly stagnant between 2007 and 2011 (Fig. 7-2a, b and 7-3b). It may suggest that there exists efficient drainage system in this area, or that the speed is slow due to the small thickness. Although the formation and the cyclic drainage events of Hazard Lake have been studied (Collins and Clarke, 1977; Clarke, 1982), the recent status of the supraglacial lake may show the subglacial water comes from upstream through the outlet tunnel (Fig.7-1, and Fig,7-7a-c). Thus, we consider the efficient drainage system exists in this portion.

Based on the ice speed and ice thickness change data, the location of dynamic balance line (DBL) is clearly identified (Fig. 7-5a). The DBL is defined as a border between upstream thickening area and downstream thinning area (Raymond, 1987), which is a key surface expression in basal condition that will control the surge onset and the progression (Burgess et al., 2012). The moraines give us some hints about how to create the DBL. Comparing the Figure 3 in Stanley (1969) to Figure 7-6b, it is clear that Hodgson Glacier overrode on Steele Glacier, i.e. Hodgson Glacier blocked the ice flow of Steele Glacier. Stanley (1969) reported that Hodgson Glacier did not contribute to the Steele Glacier's surge in mid 1966. Late in 1966, however, the Hodgson Glacier began to advance into the main trunk. Moreover, our animated image sequence derived from Landsat images shows that Hodgson Glacier suddenly advanced in 1993-1997, resulting in pushing the main trunk forward by a few hundred meters (Fig. 7-6a and c), which might further block the ice flow of Steele Glacier. Downstream resistance to sliding is a factor of unstable flow at surge-type glaciers (Clarke et al., 1984), and the interaction of tributaries has been thought to be one of the possible restrictions of ice flow (Murray et al., 2003; Jiskoot, 2011). The various factors such as the entrance angle, direction, depth of the tributaries may be the important factors in determining whether a tributary can block a trunk or not (Kargel et al., 2005). Such a circumstance may be applicable to this surge. The Hodgson's block generated the resistance to sliding toward downstream from the confluence, which caused the ice thickening upstream, resulting in creating the DBL (Fig. 7-6a). Similar elevation change and advance of Hodgson Glacier were not observed in the recent surge (Fig. 7-5 and 7-6), which indicates that it was not activated by the Steele's surge.

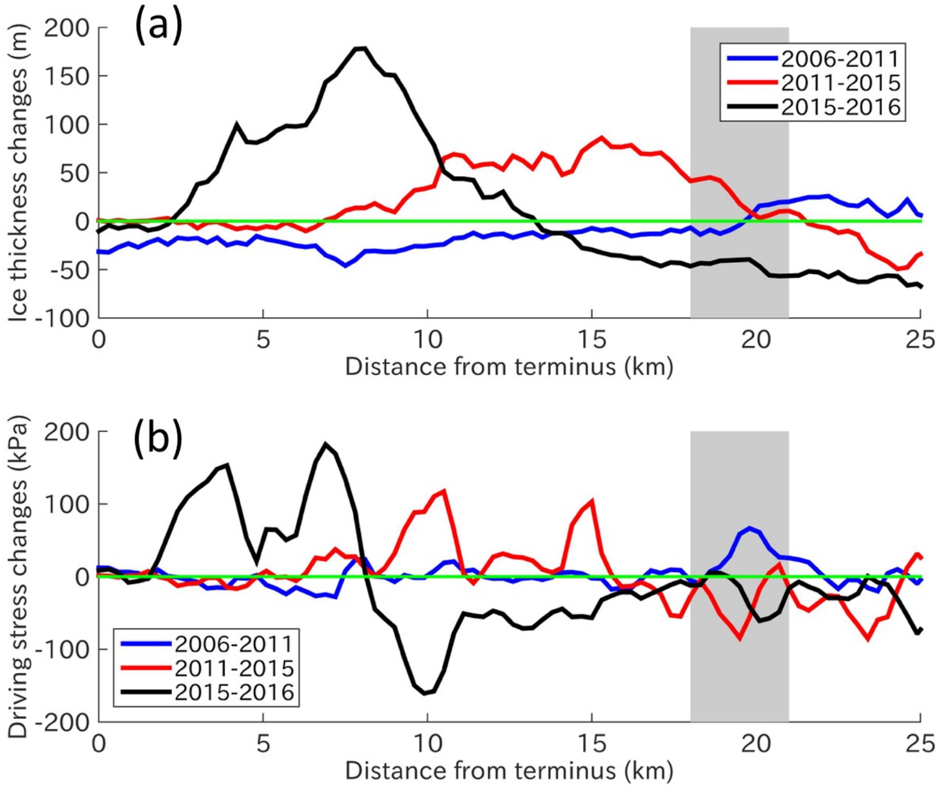

Figure 7-8 (a) Ice thickness and (b) driving stress along the flow-line shown in Fig. 7-3. The gray-shaded area stands for the confluence of Hodgson and Steele Glaciers.

In order to better understand how the glacier evolves from quiescent to active phase, we calculated the driving stress τ_d defined by the following equation (Cuffey and Paterson, 2010),

$$\tau_d = \rho g H \sin \alpha,$$

where ρ is density of ice, and g is gravitational acceleration. H is ice thickness, and α is surface slope. Using surface elevation changes and the surface slopes derived from multi-ASTER DEMs (Fig. 7-8a), we derived the temporal changes in the driving stress during the three periods (Fig. 7-8b). Between 2006 and 2011, the driving stress increased at the 20-km point, which was caused by the ice thickening and the steeper slope around the confluence (Fig. 7-8a). In 2011-15, the high driving stress was created in the middle part because of the large ice transport from upstream with a higher speed and the following ice thickening. In 2016, the high stress portion moved downstream with larger value than that in 2015 (Fig. 7-8b).

Although the driving stress increases between 2006 and 2011 (Fig. 7-8b), the ice speed in the same period is almost stable (Fig. 7-3b, and 7-4). This indicates the driving stress itself is insufficient to cause the observed acceleration in 2011. We speculate that till deformation is one possible mechanism to explain the acceleration, which is often applied to both temperate and polythermal surges (Truffer et al., 2000; Murray et al., 2003; Eisen et al., 2005). Most surging glaciers, not all, are underlain by a deformable bed (Harrison and Post, 2003). Assuming the rheology of coulomb-plastic behavior (Kavanaugh and Clarke, 2006), high basal water pressure is required to deform the subglacial till. The ice thickening in 2006-2011 (Fig. 7-5a and 7-8a) may increase the rate of creep closure, which can restrict the drainage system at the base, generating the high-water pressure. The block of Hodgson Glacier may be also related to the basal drainage constriction. The high basal water pressure can reduce the yield stress and the till deforms at a critical value.

Moreover, large amount of water needs to be supplied at the base. This is because high subglacial water pressure is essential but not sufficient condition for rapid basal sliding (Lingle and Fatland, 2003). Thus, we claim the importance of englacial water storage. As the ice thickness increases, the volume of englacial water storage will also increase, which can supply enough volume of water input in the distributed hydrological system. Lingle and Fatland (2003) suggest that large amount of water can be stored englacially, and can gradually move downward into the subglacial till, which can also reduce the yield stress. However, the origin of the water at the base still remains unclear because pressure melting due to ice thickening and geothermal heat are other alternatives to supply the water at the base.

The existence of till is reasonable to explain the gradual acceleration between 2011 and 2015 (Fig.7-3b and 7-4). This is because the till deformation would contribute both to the destruction of the drainage pathways and to rapid movement (Harrison and Post, 2003). The former increases the basal water pressure, which can enhance the basal sliding. Once the till starts to deform, the affected area has been gradually expanding downstream as well as the speed increases.

However, the rapid acceleration in early-summer 2015 (Fig.7-3b and 7-4) suggest hydrological switch from efficient channel-like drainage system to inefficient distributed drainage system due to the traveling of velocity-front. The timing is consistent with seasonal meltwater input. Large meltwater injection through crevasses goes into the ice body and reaches the distributed drainage system, which can rapidly increase both amount of water in the glacier and the subglacial water pressure. Thus, the speed rapidly increased (Fig. 7-3b and 7-4).

Moreover, seasonal meltwater input from the surface plays a key role for maintaining the high speed throughout an active phase. Figure 7-3b and 7-4 clearly shows summer speed-up every year during the active phase. This reflects the surface meltwater drains through the ice and reaches the bed, which enhances more basal sliding. We consider the opened crevasses on the surface during the active phase can indirectly connect to the base through water pathways. The high driving stress maintaining the distributed linked-cavity system and the seasonal water input from the surface can keep the higher speed during the active phase (Kamb, 1987; Burgess et al., 2012). Especially, the summer speed-up observed during the active phase (Fig. 7-3b and 7-4) can be explained by largest water input in each year. Seasonal meltwater can also be stored inside the ice body, and it is used to keep the high speed in winter even in the absent of surface meltwater.

Despite the significant increase in the "driving stress" near the downstream in 2015-16, the ice speed rapidly decreased after the peak in 2015, which can be explained by the water release from the ice body. At the speed peak in early summer 2015, the tunnel outlet was closed (Fig. 7-7d), which caused large amount of water to be stored in the ice body. Since late 2015, the water had been released from the western margin of Steele Glacier until June 2016, which filled Hazard Lake (Fig. 7-7f). The water discharge resulted in the rapid decrease of the ice speed after the peak (Fig. 7-3b and 7-4). Indeed, in fall 2016, the speed sufficiently slow-down and the surge terminated (Fig. 7-3 and 7-4). This termination is similar to that of the 1982-83 surge at Variegated Glacier (Humphrey and Raymond, 1994).

Here we compare the surge behavior with the previous studies. The multi-year acceleration in 2011-early 2015 coincides with the feature of the Svalbard type surge (Murray et al., 2003). On the other hand, the significant speed-up observed in 2015 and the rapid deceleration after the speed peak is one of the well-known features in Alaskan style (Kamb et al., 1985). Recalling that Steele Glacier is polythermal-type, the surging behavior has been considered as a style of Svalbard-type (Clarke and Jarvis, 1976). The Svalbard-type surge is thought to be controlled by thermal regulation (Fowler et al., 2001; Murray et al., 2003). However, the observation report by Stanley (1969) indicates the style of the previous surge was rather similar to the Alaskan-type surge, which suggests the hydrological regulation by surface meltwater for the surge mechanism. In this latest surge, the rapid acceleration and deceleration show the hydrological control on the surge.

Two styles of surge behavior have been observed so far, and hence the two different mechanisms have been discussed (Murray et al., 2003). These styles are distinguished by the differences in the durations of the active and the quiescent phases, the peak velocities, and the presence or absence of discharge events. Jiskoot and Juhlin (2009) indicates the presence of both Alaskan-type and Svalbard-type surges in the same geographical locations in East Greenland. They suggest the two surge mechanisms postulated by Murray et al (2003) indeed comes from thermal difference in the glaciers. In our study area, Trapridge Glacier, about a few kilometers away from Steele Glacier, has also been well-studied and the surge mechanism has been considered as thermal regulation on the soft bed (Frappé and Clarke, 2007). Such a situation is closely similar to East Greenland. Moreover, the glacier size is significantly different. The length of Trapridge Glacier is only 4 km and the ice thickness is dozens of meters, while the length of Steele Glacier is about 40 km and the thickness is a few hundred meters. These differences may arise the different surge behaviors under the same climatic condition.

Sevestre et al. (2015) conducted the field observations to reveal the thermal structures of six glaciers in Svalbard. They suggest that the surges of the large glaciers cannot be explained by thermal switches. This finding is consistent with that the surge of Trapridge Glacier is controlled by thermal regulation and that Steele Glacier is not. They argue that the processes of enthalpy production and dissipation balance at each glacier govern glacier surging. Enthalpy is defined as an internal energy of glacier and it is a function of ice temperature and water content (Aschwanden et al., 2012). Surge-type glaciers are in the optimal zone, where neither heat conduction nor runoff can effectively discharge enthalpy gains. Thus, dynamic cyclic behavior (i.e. surge) can occur (Sevestre and Benn, 2015). We basically agree with their idea. The amount of meltwater injection into glacier (related to climatic condition) and the thermal structure (related to glacier size) may describe just like different behaviors as Alaskan and Svalbard-type, which has given impression that distinct mechanisms could cause different behaviors (Yasuda and Furuya, 2015).

The basal condition with respect to thermal structure, bed topography and hydrology is so complex, and it is difficult to observe directly. However, surface information about velocity evolution, ice thickness changes, and spatial patterns of looped moraines can give us some hints to better understand what it occurs under the glacier. Ground observations such as thermal structure, ice thickness and basal water pressure are necessary to completely decipher the surge mechanism. New analysis method is also desirable to be developed to examine internal structure of glacier inferred from remote sensing data.

7.6 Concluding remarks

In this chapter, we examined the spatial and temporal changes in ice speed, ice thickness, and looped moraines associated with the recent surge at Steele Glacier in Yukon, Canada. The findings of this study are summarized as follows;

1) Using multi-satellite images combined SAR and Landsat images, the detailed evolution of ice speed associated with the surge were revealed. Further downstream below the confluence of Steele and Hodgson Glaciers, the ice was almost stagnant, while in the upstream the speed was about 0.4 m/d.

2) The DBL is located at the confluence, which was generated from the previous surge at Hodgson glacier immediately after the surge at Steele Glacier. The ice on Hodgson Glacier blocked to the ice flow on Steele Glacier, which made the pre-surge condition such as the thickened ice and the steeper slope.

3) The ice thickening over the confluence during the quiescent phase increases the rate of creep closure, which can increase the basal water pressure in the till. Once the till initiates to deform, the affected area is expanding downstream, which results in the gradual acceleration in 2011-15.

4) The temporal changes in ice speed showed the seasonal speed-ups during the active

phase. This indicates the seasonal surface meltwater goes to the bed and enhances more basal sliding. Especially the rapid acceleration in 2015 was achieved by both summer meltwater input and the hydrological switch from efficient channel-like drainage system to inefficient distributed drainage system. The seasonal meltwater can also be stored englacially, and it is used to maintain the high speed in winter even in the absent of surface meltwater.

5) The rapid decrease of the ice speed was caused by the water release from the glacier inside, which filled Hazard Lake in the western margin of Steele Glacier.

6) Our observed data shows the latest surge has the features of both Alaskan-type and Svalbard-type surges. The surge behaviors can be determined by the glacier size and the amount of water input. This is consistent with the enthalpy balance idea, which also controls whether a glacier is surge-type or not.

Chapter 8

Conclusions and future works

8.1 Conclusions

In this thesis, we examined spatial and temporal variation and discussed dynamics of surge-type glaciers in Yukon, Canada, using SAR and optical images. Here we summarized my study as follows. Then, I would like to propose some future works.

Chapter 4: Winter speed-up of quiescent surge-type glaciers in Yukon, Canada

1) Winter speed-up signals were observed at some surge-type glaciers despite their quiescent phase.
2) The winter speed-up propagated from upstream to downstream, whereas well-known summer speed-up propagates upstream.
3) Given the absence of surface meltwater input in winter, we suggested the presence of water storage near the base that does not directly connect to the surface, yet can promote basal sliding through increased water pressure.

Chapter 5: Basal condition in winter using numerical glacier hydrology model

1) We demonstrated shortly high basal water pressure in early summer, but not in winter with default setting.
2) Additional water input upstream only in winter could reproduce high basal water pressure in winter, but the change rate was transient, which is not consistent with the results in Chapter 4.

3) A new theory of reproducing high basal water pressure with small input are needed to explain the winter speed-up signals.

Chapter 6: Twelve-year cyclic surging episodes at Donjek Glacier in Yukon, Canada

1) Surging episode has occurred every twelve years for forty years, and the next episode is highly likely to initiate in 2025.
2) The surging area is limited only ~ 20 km section from the terminus, originating in an area where the flow width significantly narrows downstream.
3) The valley constriction strongly controls the surge dynamics.

Chapter 7: Surge dynamics of Steele Glacier in Yukon, Canada, revealed by multi-satellite images

1) The detailed evolutions of ice speed, ice thickness, spatial patterns of looped moraines associated with the recent surge at Steele Glacier were detected.
2) Based on ice speed and ice thickness change data, the initiation point of the surge is the confluence between Steele and Hodgson Glaciers. The spatial pattern of the looped moraine indicates the Hodgson Glacier blocked the ice flow on Steele Glacier, which generated the ice thickening and the steepening above the confluence during the quiescent phase.
3) The driving stress changes indicate that the ice thickening and the following steeper

slope near the confluence increased the stress in the quiescent phase. However, the driving stress itself is insufficient to explain the acceleration. The ice thickening increases the rate of creep closure, which causes the high basal water pressure in the till. Once the till initiates to deform, the affected area is expanding downstream, which results in the gradual acceleration in 2011-15. The high driving stress in 2011-15 helps to maintain the distributed hydrological system at the base.

4) The seasonal speed-up during active phase indicates the seasonal surface meltwater could reach the bed, which enhanced basal sliding. Especially the rapid acceleration in 2015 was achieved by both summer meltwater input and the hydrological switch from efficient channel-like drainage system to inefficient distributed drainage system. The seasonal meltwater can also be stored englacially, and it is used to maintain the high speed in winter even in the absent of surface meltwater.

5) The rapid decrease of the ice speed was caused by the water release from the glacier inside, which filled Hazard Lake in the western margin of Steele Glacier.

6) Our observed data shows the latest surge has the features of both Alaskan-type and Svalbard-type surges.

8.2 Future works

While we revealed dynamics of surge-type glaciers in Yukon, showing many results derived from multi-satellite images, there are some rooms for discussing the mechanism. Here we propose possible future works for better understanding surge mechanism.

Satellite image analysis

Recent advances of analyzing satellite images has revolutionized the study of glacier dynamics. In particular, SAR images has much contributions to it. Recent SAR satellites such as Sentinel-1 and ALOS-2 have the revisit interval of within two weeks, which enables us to detect short and small changes in ice speed. This will bring some hints of further understanding glacier dynamics. Moreover, combination both SAR and optical images are very useful to examine detail evolution of ice speed in terms of temporal resolutions. Deriving short-term changes in ice speed and its constant collection are hoped. It is also desirable develop some analysis method to examine internal structure of ice to understand meltwater behavior through glacier.

Ground observation

Glacial hydrology and its impact to glacier dynamics is complex and needed to be clear for further understanding glacier variation. Recent satellite image analysis has impact on deriving surface velocity fields without ground observation. However, there are some parameters which can be acquired only by in-situ observations such as basal water pressure and ice thermal structure through drilling. Thus, ground observations are indispensable to better understand glacier dynamics. In-situ observations on one of surge-type glaciers that we examined in this thesis may bring some new insight into the surge dynamics.

Modeling

Modeling subglacial drainage is also useful to understand what is going on in a glacier. However, it is necessary to have observed results as mentioned above, adding metrological and surface/bed topography data. The present model strongly dependent on the data. When we model some specific phenomena like winter speed-up, such information is essential for revealing what causes the phenomenon. Moreover, new theories may be needed to developed.

References

Abe, T., Earth surface changes detected by synthetic aperture radar and their interpretations: the Iwate-Miyagi inland earthquake and glacier dynamics in Yukon, Canada (in Japanese with English figure captions), *Master thesis in Hokkaido University, Japan*, 2013.

Abe, T., and M. Furuya, Winter speed-up of quiescent surge-type glaciers in Yukon, Canada, *The Cryosphere*, 9(3), 1183-1190, 2015.

Abe, T., and M. Furuya, Dynamics of surge-type glaciers in Alaska-Yukon revealed by Synthetic Aperture Radar (in Japanese), *Seppyo*, 78(6), 425-438, 2016.

Abe, T., M. Furuya, and D. Sakakibara, Brief Communication: Twelve-year cyclic surging episodes at Donjek Glacier in Yukon, Canada. *The Cryosphere*, 10(4), 1427-1432, 2016.

Anderson, R. S., P. Molnar, and M. A. Kessler, Features of glacial valley profiles simply explained, *J. Geophys. Res.*, 111, F01004, doi:10.1029/2005JF000344, 2006.

Aschwanden, A., E. Bueler, C. Khroulev, and H. Blatter, An enthalpy formulation for glaciers and ice sheets, *J. Glaciol.*, 58(209), 441–457, 2012.

Bartholomaus, T. C., R. S. Anderson, and S. P. Anderson, Growth and collapse of the distributed subglacial hydrologic system of Kennicott Glacier, Alaska, USA, and its effects on basal motion, *J. Glaciol.*, 57(206), 985–1002, 2011.

Bartholomew, I., P. Nienow, D. Mair, A. Hubbard, M. A. King, and A. Sole, Seasonal evolution of subglacial drainage and acceleration in a Greenland outlet glacier, *Nat. Geosci.*, 3, 408-411, 2010.

Bayrock, L. A., Catastrophic advance of the Steele Glacier, Yukon, Canada, *Boreal Inst., Univ. Alberta*, Dec., Publ. No.3, 35 pp.

Berthier E, E. Schiefer, G. K. C. Clarke, B. Menounos, and F. Rémy, Contribution of Alaskan glaciers to sea-level rise derived from satellite imagery, *Nature Geosci.*, 3(2), 92–95, 2010.

Bevington, A., and L. Copland, Characteristics of the last five surges of Lowell Glacier, Yukon, Canada, since 1948, *J. Glaciol.*, 60(219), 113-123, 2014.

Bueler, E., Extending the lumped subglacial-englacial hydrology model of Bartholomaus and others (2011), *J. Glaciol.*, 60(222), 808–810, 2014.

Burgess, E. W., R. R. Forster, C. F. Larsen, and M. Braun, Surge dynamics on Bering Glacier, Alaska, in 2008–2011, *The Cryosphere*, 6(6), 1251–1262, 2012.

Burgess, E. W., R. R. Foster, and C. F. Larsen, Flow velocities of Alaskan glaciers, *Nat. Comms.*, 4, 2146, 2013a.

Burgess, E. W., C. F. Larsen, and R. R. Foster, Summer melt regulates winter glacier flow speeds throughout Alaska, *Geophys. Res. Lett.*, 40, 6160–6164, 2013b.

Clarke, G. K. C., Glacier outburst floods from "Hazard Lake," Yukon Territory, and the problem of flood magnitude prediction, *J. Glaciol.*, 28(98), 3–21, 1982.

Clarke, G. K. C., Lumped-elements analysis of subglacial hydraulic circuits, *J. Geophys. Res.*, 101(B8), 17, 547–17, 559, 1996.

Clarke, G. K. C., Subglacial processes. *Ann. Rev. Earth Planet. Sci.*, 33, 247-276, 2005.

Clarke, G. K. C., A short and somewhat personal history of Yukon glacier studies in the twentieth century, *Arctic*, 67(5), 1-21, 2014.

Clarke, G. K. C., and G. T. Jarvis, Post-surge temperatures in Steele Glacier, Yukon Territory, Canada, *J. Glaciol.*, 16(74), 261-268, 1976.

Clarke, G. K. C., and W. H. Matthews, Estimates of the magnitude of glacier outburst floods from Lake Donjek, Yukon Territory, *Canada, Can. J. Earth Sci.*, 18, 1452-1463, 1981.

Clarke, G. K. C., S. G. Collins, and D. E. Thompson, Flow, thermal structure and subglacial conditions of a surge-type glacier, *Can. J. Earth Sci.*, 21, 232–240, 1984.

Clarke, G. K. C., J. P. Schmok, C. S. L. Ommanney, and S. Collins, Characteristics of Surge-Type Glaciers, *J. Geophys. Res.*, 91(B7), 7165–7180, 1986.

Clarke, G. K. C., and G. Holdsworth, Glaciers of the St. Elias Mountains, in Satellite Image Atlas of Glaciers of the World, *USGS Professional Paper 1386-J*, J301-J327, Eds. R. S. Williams, Jr. & J. G. Ferrigno, 2002.

Collins, S. G., and G. K. C. Clarke, History and bathymetry of a surge-dammed lake, *Arctic*, 30(4), 217–224, 1977.

Copland, L., M. J. Sharp, and J. A. Dowdeswell, The distribution and flow characteristics of surge-type glaciers in the Canadian High Arctic, *Ann. Glaciol.*, 36, 73–81, 2003.

Crompton, J. W., and G. E. Flowers, Correlations of suspended sediment size with bedrock lithology and glacier dynamics, *Ann. Glaciol.*, 57(72), 142-150, 2016.

Cuffey, K. M. and W. S. E. Paterson, The Physics of Glaciers 4th edition, *Academic Press*, 2010.

Dolgoushin, L. D., and G. B. Osipova, Glacier surges and the problem of their forecasting, *Int. Assoc. Hydrol. Sci. Pub.*, 104, 292–304, 1975.

Eisen, O., W. D. Harrison, and C. F. Raymond, The surges of Variegated Glacier, Alaska, U.S.A., and their connection to climate and mass balance, *J. Glaciol.*, 47(158), 351-358, 2001.

Eisen, O., W. D. Harrison, C. F. Raymond, K. A. Echelmeyer, G. A. Bender, and J. L. D. Gorda, Variegated Glacier, Alaska, USA: a century of surges, *J. Glaciol.*, 51(174), 399–406, 2005.

Enderlin, E. M., I. M. Howat, S. Jeong, M.-J. Noh, J. H. van Angelen, and M. R. van den Broeke, An improved mass budget for the Greenland ice sheet, *Geophys. Res. Lett.*, 41, 866–872, 2014.

Fatland, D. R. and C. S. Lingle, Analysis of the 1993-95 Bering Glacier (Alaska) surge using differential SAR interferometry, *J. Glaciol.*, 44(148), 532-546, 1998.

Fahnestock, M., T. Scambos, T. Moon, A. Gardner, T. Haran, and M. Klinger, Rapid large-area mapping of ice flow using Landsat 8, *Remote Sens. Environ.*, 185, 84-94, 2016.

Fitch, A. J., A. Kadyrov, W. J. Christmas, and J. Kittler, Orientation Correlation, *in British Machine Vision Conference*, Cardiff, UK, 133-142, 2002.

Flowers, G. E., H. Björnsson, F. Pálsson, and G. K. C. Clarke, A coupled sheet-conduit mechanism for jökulhlaup propagation, *Geophys. Res. Lett.*, 31, L05401, doi:10.1029/2003GL019088, 2004.

Flowers, G. E., N. Roux, S. Pimentel, and C. G. Schoof, Present dynamics and future prognosis of a slowly surging glacier, *The Cryosphere*, 5(1), 299-313, 2011.

Fowler, A., T. Murray, and F. Ng, Thermally controlled glacier surging, *J. Glaciol.*, 47(159), 527–538, 2001.

Fountain, A. G., and J. S. Walder, Water flow through temperate glaciers, *Rev. Geophys.*, 36, 299-328, 1998.

Frappé, T. -P., and G. K. C. Clarke, Slow surge of Trapridge Glacier, Yukon Territory, Canada, *J. Geophys. Res.*, 112, F03S32, 2007.

Goldstein, R. M., H. Engelhardt, B. Kamb, and R. M. Frolich, Satellite radar interferometry for monitoring ice sheet motion: application to an Antarctic ice stream, *Science*, 262, 1525-1530, 1993.

Gomba, G., A. Paizzi, F. De Zan, M. Eineder, and R. Bamler, Toward Operational Compensation of Ionosperic Effects in SAR Interferograms: The Split-Specturm Method, I*EEE Trans. Geosci. Remote Sens.*, 54 (3), 1446–1461, 2016.

Gray, A. L., K. E. Mattar, and P. W. Vachon, InSAR results from the RADARSAT Antarctic Mapping Mission data: estimation of glacier motion using a simple registration procedure, I*n Inter. Geoscience and Remote Sensing Symp.*, IGARSS'98, Seattle, July, 1998.

Harper, J. T., J. H. Bradford, N. F. Humphrey, and T. W. Meierbachtol, Vertical extension of the subglacial drainage system into basal crevasses, *Nature*, 467, 579-582, 2010.

Harrison, W. D. and A. S. Post, How much do we really know about glacier surging? *Ann. Glaciol.*, 36, 1-6, 2003.

Haug, T., A. Kääb, and P. Skvarca, Monitoring ice shelf velocities from repeat MODIS and Landsat data – a method study on the Larsen C ice shelf, Antarctic Peninsula, and 10 other ice shelves around Antarctica, *The Cryosphere*, 4(2), 161-178, 2010.

Heid, T., and A. Kääb, Evaluation of existing image matching methods for deriving glacier surface displacements globally from optical satellite imagery, *Remote Sens. Environ.*, 118, 339–355, 2012.

Herreid, S., and M. Truffer, Automated detection of unstable glacier flow and a spectrum of speedup behavior in the Alaska Range, *J. Geophys. Res. Earth Surf.*, 121, 64-81, 2016.

Hewitt, I. J., Seasonal changes in ice sheet motion due to melt water lubrication. *Earth Planet. Sci. Lett.*, 371–372, 16–25, 2013.

Hewitt, I. and C. Schoof, Models for polythermal ice sheets and glaciers, *The Cryosphere*, doi:10.5194/tc-2016-240, accepted, 2017.

Hoffman, M. J., and S. Price, Feedbacks between coupled subglacial hydrology and glacier dynamics, *J. Geophys. Res. Earth Surf.*, 119, 414-426, 2014.

Humphrey, N. F., and C. F. Raymond, Hydrology, erosion and sediment production in a surging glacier: Variegated Glacier, Alaska, 1982-1983, *J. Glaciol.*, 40(136), 539-552, 1994.

Iken, A., and R. A. Bindschadler, Combined measurements of subglacial water pressure and surface velocity of the Findelengletscher, Switzerland: Conclusions about drainage system and sliding mechanism, *J. Glaciol.*, 32(110), 101-119, 1986.

Iken, A., and M. Truffer, The relationship between subglacial water pressure and velocity of Findelengletscher, Switzerland, during its advance and retreat, *J. Glaciol.*, 43(144), 328–338, 1997.

Jarvis, G. T., and G. K. C. Clarke, Thermal effects of crevassing on Steele Glacier, Yukon Territory, Canada, *J. Glaciol.*, 13(68), 243-254, 1974.

Jarvis, G. T., and G. K. C. Clarke, The thermal regime of Trapridge Glacier and its relevance to glacier surging, *J. Glaciol.*, 14(71), 235-250, 1975.

Jiskoot, H., Glacier surging, in Encyclopedia of snow, ice and glaciers, *Springer*, Dordrecht, The Netherlands, 2011.

Jiskoot, H., P. Boyle, and T. Murray, The incidence of glacier surging in Svalbard: evidence from multivariate statistics, *Comput. Geosci.*, 24(4), 387-399, 1998.

Jiskoot, H., and D. T. Juhlin, Surge of a small East Greenland glacier, 2001–2007, suggests Svalbard-type surge mechanism, *J. Glaciol.*, 55(191), 567–570, 2009.

Johnson, P. G., A possible advanced hypsithermal position of the Donjek Glacier, *Arctic*, 25, 302–305, 1972a.

Johnson, P. G., The morphological effects of surges of the Donjek Glacier, St. Elias Mountains, Yukon Territory, Canada, *J. Glaciol.*, 11(62), 227-234, 1972b.

Joughin, I. R., R. Kwok, and M. A. Fahnestock, Interferometric estimation of three-dimensional ice-flow using ascending and descending passes, *IEEE Trans. Geosci. Remote Sens.*, 36 (1), 25–37, 1998.

Joughin, I., L. Gray, R. Bindschadler, S. Price, D. Morse, C. Hulbe, K. Mattar, and C. Werner, Tributaries of West Antarctic ice streams revealed by RADARSAT interferometry, *Science*, 286, 283-286, 1999.

Joughin, I., W. Abdalati, and M. Fahnestock, Large fluctuations in speed on Greenland's Jakobshavn Isbræ glacier, *Nature*, 432, 608–610, 2004.

Joughin, I., S. B. Das, M. A. King, B. E. Smith, I. M. Howat, and T. Moon, Seasonal speed-up along the western flank of the Greenland Ice Sheet, *Science*, 320(5877), 781-783, 2008.

Joughin, I., B. E. Smith, and W. Abdalati, Glaciological advances made with interferometric synthetic aperture radar, *J. Glaciol.*, 56(200), 1026-1042, 2010.

Kamb, B., Glacier surge mechanism based on linked cavity configuration of the basal water conduit system, *J. Geophys. Res.*, 92(B9), 9083–9100, 1987.

Kamb, B., and H. Engelhardt, Waves of accelerated motion in a glacier approaching surge: the mini-surges of Variegated Glacier, Alaska, U.S.A., *J. Glaciol.*, 33(113), 27-46, 1987.

Kamb, B., C. F. Raymond, W. D. Harrison, H. Engelhardt, K. A. Echelmeyer, N. Humphrey, M. M. Brugman, and T. Pfeffer, Glacier Surge Mechanism: 1982-1983 Surge of Variegated Glacier, Alaska, *Science*, 227(4686), 469-479, 1985.

Kargel, J. S., M. J. Abrams, M. P. Bishop, A. Bush, G. Hamilton, H. Jiskoot, A. Kääb, H. H. Kieffer, E. M. Lee, F. Paul, F. Rau, B. Raup, J. F. Shroder, D. Soltesz, D. Stainforth, L. Stearns, and R Wessels, Multispectral imaging contribuions to Global Land Ice Measurements from Space, *Remote Sens. Environ.*, 99(1–2), 187–219, 2005.

Kavanaugh, J. L., and G. K. C. Clarke, Discrimination of the flow law for subglacial sediment using in situ measurements and an interpretation model, *J. Geophys. Res.*, 111, F01002, 2006.

Kessler, M. A., and R. S. Anderson, Testing a numerical glacial hydrological model using spring speed-up events and outburst floods, *Geophys. Res. Lett.*, 31, L18503, 2004.

Kinoshita, Y., M. Shimada, and M. Furuya, InSAR observation and numerical modeling of the water vapor signal during a heavy rain: A case study of the 2008 Seino event, central Japan, *Geophys. Res. Lett.*, 40, 4740-4744, 2013.

Kobayashi, T., Y. Takada, M. Furuya, and M. Murakami, Locations and types of ruptures involved in the 2008 Sichuan earthquake inferred from SAR image matching, *Geophys. Res. Lett.*, 36, L07302, 2009.

Kobayashi, T., Y. Morishita, and H. Yarai, Detailed crustal deformation and fault rupture of the 2015 Gorkha earthquake, Nepal, revealed from ScanSAR-based interferograms of ALOS-2. Earth

Planets Space, 67:201, doi:10.1186/s40623-015-0359-z, 2015.

Larsen, C. F., E. Burgess, A. A. Arendt, S. O'Neel, A. J. Johnson, and C. Kienholz, Surface melt dominates Alaska glacier mass balance, *Geophys. Res. Lett.*, 42, 5902-5908, 2015.

Lingle, C. S., and D. R. Fatland, Does englacial water storage drive temperate glacier surges?. *Ann. Glaciol.*, 36(1), 14–20, 2003.

Luckman, A., T. Murray, and T. Strozzi, Satellite flow evolution throughout a glacier surge measured by satellite radar interferometry, *Geophys. Res. Lett.*, 29(23), 2095, 2002.

Luthcke, S. B., T. J. Sabaka, B. D. Loomis, A. A. Arendt, J. J. McCarthy, and J. Camp, Antarctica, Greenland and Gulf of Alaska land-ice evolution from an iterated GRACE global mascon solution, *J. Glaciol.*, 59(216), 613–631, 2013.

MacGregor, K. R., R. S. Anderson, S. P. Anderson, and E. D. Waddington, Numerical simulations of glacial-valley longitudinal profile evolution, *Geology*, 28, 1031–1034, 2000.

MacGregor, K. R., C. A. Riihimaki, and R. S. Anderson, Spatial and temporal evolution of rapid basal sliding on Bench Glacier, Alaska, USA, *J. Glaciol.*, 51(172), 49-63, 2005.

Machguth, H., and M. Huss, The length of the world's glaciers – a new approach for the global calculation of center lines, *The Cryosphere*, 8(5), 1741-1755, 2014.

Massonnet, D., M. Rossi, C. Carmona, F. Adragna, G. Pletzer, K. Feigl, and T. Rabaute, The displacement field of the Landers earthquake mapped by radar interferometry, *Nature*, 364, 138-142, 1993.

McNabb, R. W. and R. Hock, Alaska tidewater glacier terminus positions, 1948–2012, *J. Geophys. Res. Earth Surf.*, 119, 153–167, 2014.

Meier, M. F. and A. Post, What are glacier surges?, *Can. J. Earth Sci.*, 6(4), 807–817, 1969.

Michel, R., J.-P. Avouac, and J. Taboury, Measuring ground displacements from SAR amplitude images: application to the landers earthquake, *Geophys. Res. Lett.*, 26(7), 875-878, 1999.

Moon, T., I. Joughin, B. Smith, and I. Howat, 21st-Century Evolution of Greenland Outlet Glacier Velocities, *Science*, 336, 576-578, 2012.

Moon, T., I. Joughin, B. Smith, M. R. van den Broeke, W. J. van de Berg, B. Noël, and M. Usher, Distinct patterns of seasonal Greenland glacier velocity, *Geophys. Res. Lett.*, 41, 7209-7216, 2014.

Moon, T., I. Joughin, and B. Smith, Seasonal to multiyear variability of glacier surface velocity, terminus position, and sea ice/ice mélange in northwest Greenland, *J. Geophys. Res. Earth Surf.*, 120, 818–833, 2015.

Moreira, A., G. Krieger, I. Hajnsek, K. Papathanassiou, M. Younis, P. Lopez-Dekker, S. Huber, M. Villano, M. Pardini, M. Eineder, F. De Zan and A. Parizzi, Tandem-L: A Highly Innovative Bistatic SAR Mission for Global Observation of Dynamic Processes on the Earth's Surface, *IEEE Geoscience and Remote Sensing Magazine*, 3, 8-23, 2015.

Mouginot, J., and E. Rignot, Ice motion of the Patagonian Icefields of South America: 1984–2014, *Geophys. Res. Lett.*, 42, 1441–1449, 2015.

Murray, T., T. Strozzi, A. Luckman, H. Jiskoot, and P. Christakos, Is there a single surge mechanism? Contrasts in dynamics between glacier surges in Svalbard and other regions, *J. Geophys. Res.*, 108(B5), 2237, 2003.

Muto, M. and M. Furuya, Surface velocities and ice-front positions of eight major glaciers in the Southern Patagonian Ice Field, South America, from 2002 to 2011. *Remote Sens. Environ.*, 139, 50–59, 2013.

Nagler, T., H. Rott, M. Hetzenecker, J. Wuite, and P. Potin, The Sentinel-1 Mission: New Opportunities for Ice Sheet Observations, *Remote Sens.*, 7, 9371-9389, 2015.

Ouchi, K., Fundamental of Synthetic Aperture Radar for Remote Sensing (in Japanese) 2nd edition, *Tokyo Denki University Press*, 2009.

Ozawa, T., K. Doi, and K. Shibuya, Detection of Ice Flow and Deformation of the Antarctic Ice Sheet using JERS-1 SAR Interferometry (in Japanese with abstract and figure captions in English), *J. Geod. Soc. Jpn.*, 46(1), 43-52, 2000.

Paul, F., Revealing glacier flow and surge dynamics from animated satellite image sequences: examples from the Karakoram, *The Cryosphere*, 9(6), 2201-2214, 2015.

Pfeffer, W. T., A. A. Arendt, A. Bliss, T. Bolch, J. G. Cogley, A. S. Gardner, J. -O. Hagen, R. Hock, G. Kaser, C. Kienholz, E. S. Miles, G. Moholdt, N. Mölg, F. Paul, V. Radić, P. Rastner, B. H. Raup, J. Rich, M. J. Sharp, and the Randolph consortium: The Randolph Glacier Inventory: a globally complete inventory of glaciers, *J. Glaciol.*, 60(221), 537–552, 2014.

Post, A., Distribution of surging glaciers in western North America, *J. Glaciol.*, 8(53), 229-240, 1969.

Pritchard, H. D., R. J. Arthern, D. G. Vaughan, and L. A. Edwards, Extensive dynamic thinning on the margins of the Greenland and Antarctic ice sheets, *Nature*, 461(7266), 971–975, 2009.

Quincey, D. J., M. Braun, N. F. Glasser, M. P. Bishop, K. Hewitt, and A. Luckman, Karakoram glacier surge dynamics, *Geophys. Res. Lett.*, 38, L18504, 2011.

Radić, V., and R. Hock, Regionally differentiated contribution of mountain glaciers and ice caps to future sea-level rise, *Nat. Geosci.*, 4, 91-94, 2011.

Raymond, C. F., How do glaciers surge? A review, *J. Geophys. Res.*, 92(B9), 9121-9134, 1987.

Raymond, C. F., and W. D. Harrison, Evolution of Variegated Glacier, Alaska, U.S.A., prior to its surge, *J. Glaciol.*, 34(117),154-169, 1988.

Raymond, C, F., R. J. Benedict, W. D. Harrison, K. A. Echelmeyer, and N. Strum, Hydrological discharges and motion of Fels and Black Rapid Glaciers, Alaska, U.S.A.: implications for the structure of their drainage systems, *J. Glaciol.*, 41(138), 290-304, 1995.

Rignot, E., K. C. Jezek and H. G. Sohn, Ice flow dynamics of the Greenland ice sheet from SAR interferometry, *Geophys. Res. Lett.*, 22(5), 575-578, 1995.

Rignot, E., K. Echelmeyer, and W. Krabill, Penetration depth of interferometric synthetic-aperture radar signals in snow and ice, *Geophys. Res. Lett.*, 28(18), 3501–3504, 2001.

Rignot, E., J. Mouginot, and B. Scheuchi, Ice Flow of the Antarctic Ice Sheet, *Science*, 333, 1427-1430, 2011.

Rignot, E. and J. Mouginot, Ice flow in Greenland for the International Polar Year 2008–2009, *Geophys. Res. Lett.*, 39, L11501, 2012.

Rosenau, R., M. Scheinert, and R. Dietrich, A processing system to monitor Greenland outlet glacier velocity variations at decadal and seasonal time scales utilizing the Landsat imagery, *Remote Sens. Environ.*, 169, 1-19, 2015.

Röthlisberger, H., Water pressure in intra- and subglacial channels, *J. Glaciol.*, 11(62), 177–203, 1972.

Sakakibara, D., Ice front variations and velocity changes of calving glaciers in the Southern Patagonia Icefield and northwestern Greenland, *Ph.D. thesis in Hokkaido University, Japan*, 2016.

Sakakibara, D., and S. Sugiyama, Ice-front variations and speed changes of calving glaciers in the Southern Patagonia Icefield from 1984 to 2011, *J. Geophys. Res. Earth Surf.*, 119, 2541-2554, 2014.

Schoof, C., Ice-sheet acceleration driven by melt supply variability, *Nature*, 468, 803-806, 2010.

Schoof, C., C. A. Rada, N. J. Wilson, G. E. Flowers, and M. Haseloff, Oscillatory subglacial drainage in the absence of surface melt, *The Cryosphere*, 8(3), 959-976, 2014.

Seeber, G., Satellite Geodesy, 2nd edition, *DeGruyter*, Berlin, Germany, 2003.

Sevestre, H., and D. I. Benn, Climatic and geometric controls on the global distribution of surge-type glaciers: implications for a unifying model of surging, *J. Glaciol.*, 61(228), 646-662, 2015.

Sevestre, H., D. Benn, N. R. J. Hulton, and K. Bælum, Thermal structure of Svalbard glaciers and implications for thermal switch models of glacier surging, *J. Geophys. Res. Earth Surf.*, 120, 2220-2236, 2015.

Sole, A., P. Nienow, I. Bartholomew, D. Mair, T. Cowton, A. Tedstone, and M. A. King, Winter motion mediates dynamic response of the Greenland Ice Sheet to warmer summers, *Geophys. Res. Lett.*, 40, 3940-3944, 2013.

Stanley, A. D., Observations of the surge of Steele Glacier, Yukon Territory, Canada, *Can. J. Earth Sci.*, 6(4), 819–830, 1969.

Stevens, L. A., M. D. Behn, S. B. Das, I. Joughin, B. P. Y. Noël, M. R. van den Broeke, and T. Herring, Greenland Ice Sheet flow response to runoff variability, *Geophys. Res. Lett.*, 43, doi:10.1002/2016GL070414, 2016.

Strozzi, T., A. Luckman, T. Murray, U. Wegmüller, and C. L. Werner, Glacier Motion Estimation Using SAR Offset-Tracking Procedures, *IEEE. Trans. Geosci. Remote Sens.*, 40(11), 2384-2391, 2002.

Sundal, A. V., A. Shepherd, P. Nienow, E. Hanna, S. Palmer, and P. Huybrechts, Melt-induced speed-up of Greenland ice sheet offset by efficient subglacial drainage, *Nature*, 469, 521-524, 2011.

Tedstone, A. J., P. W. Nienow, N. Gourmelen, A. Dehecq, D. Goldberg, and E. Hanna, Decadal slowdown of a land-terminating sector of the Greenland Ice Sheet despite warming, *Nature*, 526(7575), 692–695, 2015.

Turrin, J. B. and R. R. Forster, A conceptual model of cyclical glacier flow in overdeepenings, *The Cryosphere Discuss.*, 8, 4463-4495, 2014.

Truffer, M., W. D. Harrison, and K. A. Echelmeyer, Glacier motion dominated by processes deep in underlying till, *J. Glaciol.*, 46(153), 213–221, 2000.

van den Broeke, M. R., J. L. Bamber, J. Ettema, E. Rignot, E. J. O. Schrama, W. J. van de Berg, E. van Meijgaard, I. Velicogna, and B. Wouters, Partitioning recent Greenland mass loss, *Science*, 326, 984–986, 2009.

van der Veen, C. J., Fracture mechanics approach to penetration of bottom crevasses on glaciers, *Cold Reg. Sci. Technol.*, 27, 213-223, 1998.

Waechter, A., Regional Assessment of Glacier Motion in Kluane National Park, Yukon Territory, *Master thesis in University of Ottawa, Canada*, 2013.

Werder, M. A., The hydrology of subglacial overdeepenings: A new supercooling threshold formula, *Geophys. Res. Lett.*, 43, 2045-2052, 2016.

Werder, M. A., I. J. Hewitt, C. G. Schoof, and G. E. Flowers, Modeling channelized and distributed subglacial drainage in two dimensions, *J. Geophys. Res. Earth Surf.*, 118, 2140–2158, 2013.

Wegmüller, U., and C. L. Werner, Gamma SAR processor and interferometry software, *in Proc. of the 3rd ERS Symposium, European Space Agency Special Publication*, ESA SP-414, Florence, Italy, 14–21 March, 1686–1692,1997.

Yasuda, T. and M. Furuya, Short-term Glacier Velocity Changes at West Kunlun Shan, Northwest Tibet, Detected by Synthetic Aperture Radar Data, *Remote Sens. Environ.*, 128, 87-106, 2013.

Yasuda, T. and M. Furuya, Dynamics of surge-type glaciers in West Kunlun Shan, Northwestern Tibet, *J. Geophys. Res. Earth Surf.*, 120, 2393-2405, 2015.

Zwally, H. J., W. Abdalati, T. Herring, K. Larson, J. Saba, and K. Steffen, Surface melt-induced acceleration of Greenland ice-sheet flow, *Science*, 297, 218–222, 2002.